2

Formulations sans maillage pour l'acoustique faiblement couplée

L'erreur ne devient pas vérité parce qu'elle se propage et se multiplie ; la vérité ne devient pas erreur parce que nul ne la voit.

(Gandhi)

2.1 Qu'est-ce qu'une méthode sans maillage ?

La simulation des problèmes physiques décrits par des systèmes d'équations différentielles ou aux dérivées partielles est traditionnellement effectuée à l'aide de méthodes de résolution numérique de type éléments finis ou différences finies. Dans ces méthodes, le domaine spatial est discrétisé par des maillages dont la fonction est de définir un lien topologique entre les nœuds, support de l'interpolation des variables inconnues. Une méthode sans maillage procède en général des mêmes ingrédients que les méthodes traditionnelles (approximation, intégration, résolution d'un système d'équations linéaires) mais s'affranchit d'une définition du maillage ; la discrétisation se base alors sur un nuage de nœuds uniquement.

La définition minimale d'une méthode sans maillage (*meshfree* ou *meshless*) est qu'elle ne nécessite pas la génération *a priori* d'un maillage pour la construction de l'interpolation. Cette définition minimale a souvent été critiquée car une méthode réellement sans maillage (*truly meshless*) ne devrait jamais faire appel à un maillage, ni pour les étapes d'interpolation, ni pour les étapes d'intégration numérique. La réalité des méthodes disponibles aujourd'hui dans la littérature est évidemment beaucoup plus complexe. Toujours en essayant d'esquisser une classification (arbitraire), on pourrait proposer trois familles de méthodes.

1. *Les méthodes basées sur la* ***discrétisation de la forme faible*** (type Galerkin). Au sein de cette famille, on peut encore distinguer deux grandes approches : celle se basant sur une méthode de moindres carrés mobiles (à coefficients variables – *Moving Least Squares* MLS) et la deuxième sur une méthode de partionnement de l'unité (*Partition of Unity Method* PUM).[1]

    - *MLS* : initialement exploitée par Nayrolles *et al.* sous le nom de méthodes des éléments diffus (Diffuse Element Method DEM) [NAY92], la méthode des moindres carrés mobiles

[1] Ces deux approches ne s'excluant pas nécessairement l'une l'autre.

a ensuite largement popularisée par T. Belytschko *et al.* sous le nom d'*Element-Free Galerkin Method* EFGM [BEL94],

- *PUM* : initialement proposée par I. Babuška *et al.* [BAB97b] sous cette dénomination, mais aussi par J.T. Oden dans une version hp (*hp-clouds*) [ODE96], cette méthode est aujourd'hui largement étudiée par T. Strouboulis *et al.* sous le nom de méthode des éléments finis généralisée (*Generalized Finite Element Method* GFEM) [STR00, STR01a, STR01b].

2. *Les méthodes basées sur la* ***discrétisation de la forme forte***. Basée souvent sur des méthodes particulaires avec des variables lagrangiennes, cette classe de méthodes est historiquement une des première tentatives sans maillage avec la méthode SPH (Smooth Particle Hydrodynamics) [LUC77]. Plus récemment, E. Oñate *et al.* ont proposé la méthode des points finis (Finite Point Method FPM) [ONA96] très similaire à une méthode nettement antérieure due à Orkisz *et al.* [LIS80]. La méthode RKPM (Reproducing Kernel Particle Method), proposée par W.K. Liu [LIU93, LIU95], peut être vue comme une généralisation de la méthode SPH et a été ensuite également formulée pour des formes faibles.

3. *Les approches utilisant la* ***discrétisation de formes faibles locales***. Celles-ci sont basées soit sur une approximation de type Petrov-Galerkin (Meshless local Petrov-Galerkin method MLPG) [ATL98], sur une interpolation par collocation (Point Interpolation Method PIM) [LIU01], voire sur une approche MLS (Boundary node methods) [MUK97].

La suite de ce mémoire s'intéressera plus particulièrement aux formulations basées sur une discrétisation de la forme faible de type Galerkin, soit EFGM pour l'acoustique seule (Chapitre 2), soit PUM pour le couplage aux vibrations structurales (Chapitre 3).

Trois inconvénients propres à ce genre de méthodes sans maillage seront plus particulièrement analysés dans la suite.

1. ***L'intégration numérique.*** D'une part, l'absence de maillage prive les méthodes sans maillage d'une grille d'intégration. D'autre part, les fonctions à intégrer sont souvent d'ordre élevé, voire non rationnelles.

2. ***Le traitement des conditions aux limites de type Dirichlet***. Les méthodes d'approximation de type MLS impliquent que la fonction interpolée ne passe pas nécessairement par les valeurs nodales. Dans ce cas, les conditions aux limites de type Dirichlet, ou la continuité d'éléments non coplanaires dans des structures de type coques, nécessitent des traitements particuliers.

3. ***Le temps de calcul***. A nombre d'inconnues égal, les méthodes sans maillage sont évidemment plus lentes que la méthode des éléments finis. Dans la suite, nous essayerons toujours de faire des comparaisons à précision égale. Dans ce cas, les méthodes sans maillage se révèlent souvent plus performantes.

2.2 La méthode EFGM à base polynomiale

La méthode EFGM proposée par T. Belytschko [BEL94] est basée sur une *méthode des moindres carrés mobiles* avec base polynomiale. Considérons une fonction $g(\boldsymbol{x})$: $\Omega \to \mathbb{R}$ à approcher à partir de valeurs nodales g_I définies en les points $\mathbf{x}_I \in \Omega$ ($I = 1,...,n$). En chaque point $\mathbf{x}^* \in \Omega$, une approximation $L^{(\boldsymbol{x}^*)}g$ de g est définie à partir d'une base $\boldsymbol{P}(\boldsymbol{x})$ de dimension m. A titre d'exemples, une telle base peut être définie dans un espace à deux dimensions par :

$$\begin{aligned} \boldsymbol{P}^t(\boldsymbol{x}) &= \{1, x, y\} && (m=3, \text{ base linéaire géométrie 2D}) \\ \boldsymbol{P}^t(\boldsymbol{x}) &= \left\{1, x, y, x^2, xy, y^2\right\} && (m=6, \text{ base quadratique géométrie 2D}) \end{aligned} \tag{2.1}$$

L'approximation g est choisie comme une combinaison linéaire des termes polynomiaux de la base

$$L^{(\boldsymbol{x}^*)}g = \boldsymbol{P}^t\boldsymbol{a}^* \tag{2.2}$$

et les coefficients $\boldsymbol{a}^*$ sont déterminés par la minimisation d'une norme L^2 discrète pondérée

$$\min_{\boldsymbol{a}^*} \sum_{I=1}^{N} w_I(\boldsymbol{x}^*)\left(\boldsymbol{P}^t(\boldsymbol{x}_I)\boldsymbol{a}^* - g_I\right)^2 \tag{2.3}$$

où $w_I(\boldsymbol{x})$ est la fonction poids, elle est nulle partout sauf sur un domaine d'influence centré au nœud I. Cette minimisation est la différence essentielle avec la méthode des éléments finis qui procède par minimisation d'une norme discrète pondérée par une constante sur le support des fonctions de forme et à coefficients $\boldsymbol{a}^*$ constants. (2.3) apparaît donc comme une généralisation de la méthode des éléments finis.

Les fonctions d'interpolation de la méthode EFGM se déduisent de la minimisation (2.3). On démontre dans l'article ci-après qu'elles valent

$$\boldsymbol{N}(\boldsymbol{x}) = \boldsymbol{P}^t(\boldsymbol{x})\boldsymbol{A}^{-1}(\boldsymbol{x})\boldsymbol{B}(\boldsymbol{x}) \tag{2.4}$$

avec

$$\boldsymbol{A}(\boldsymbol{x}) = \sum_{I=1}^{N} w_I(\boldsymbol{x})\boldsymbol{P}(\boldsymbol{x}_I)\boldsymbol{P}^t(\boldsymbol{x}_I) \tag{2.5}$$

$$\boldsymbol{B}(\boldsymbol{x}) = \left[w_I(\boldsymbol{x})\boldsymbol{P}(\boldsymbol{x}_I),...,w_n(\boldsymbol{x})\boldsymbol{P}(\boldsymbol{x}_n)\right] \tag{2.6}$$

où N est le nombre de nœuds influençant le point x et n le nombre de nœuds de la grille. Quelle que soit la base $\boldsymbol{P}(\boldsymbol{x})$, les fonctions d'interpolation $\boldsymbol{N}(\boldsymbol{x})$ sont non rationnelles. L'article qui suit exploite cette première idée : une fonction d'interpolation non rationnelle permet de mieux capturer les solutions ondulatoires que les fonctions polynomiales. Comme il s'agit de la première formulation EFGM proposée pour l'acoustique, l'article s'intéresse à étudier l'influence

des principaux paramètres de la méthode (choix de la base, taille des domaines d'influence, intégration numérique) sur l'erreur de pollution.

L'article suivant est une reproduction de Ph. Bouillard, S. Suleau, *'Element-free Galerkin method for Helmholtz problems: formulation and numerical assessment of the pollution effect'*, Comput. Methods Appl. Mech. Eng. 162 (1998) 317-335.

ELSEVIER

Comput. Methods Appl. Mech. Eng. 162 (1998) 317-335

Computer methods in applied mechanics and engineering

Element-Free Galerkin solutions for Helmholtz problems: formulation and numerical assessment of the pollution effect

Ph. Bouillard[a,*] , S. Suleau[b]

[a] *Department of Continuum Mechanics, CP 194/5 Université Libre de Bruxelles, Av. F. D. Roosevelt 50, 1050 Brussels, Belgium*

[b] *Department of Analytical Mechanics, CP 165 Université Libre de Bruxelles, Av. F. D. Roosevelt 50, 1050 Brussels, Belgium*

Received 8 october 1997 ; revised 26 november 1997

Abstract

The Element-Free Galerkin Method (EFGM), a particular case of the meshless methods, is examined in its application to acoustic wave propagation addressed by the Helmholtz equation. Dispersion and pollution effects, two problems encountered by the classical numerical methods, are reviewed. Numerical tests on two-dimensional problems focus on the parameters governing the formulation of the EFGM. They also demonstrate that the EFGM is affected by dispersion and pollution effects as well as FEM, but these effects are rather low, showing that the EFGM is a promising method.

1. Introduction

The simulation of the elastic and acoustic wave propagation, addressed by the Helmholtz equation $\Delta p + k^2 p = 0$ (where k is the wave number) is today a field of intense developments, because the acoustic performance of a product is required either by some legal rules or by a sales argument (improve the users comfort).

Numerical methods have been developed in order to compute approximate solutions for coupled (vibro-acoustics) or uncoupled problems, on finite or infinite domains. The most popular methods are the standard Galerkin Finite Element Method coupled to Wave Envelope Elements [1] or to a DtN mapping [2] for infinite medium, and the Boundary Element Method (variational or by collocation, see [3]). Both methods have their specificities: while the FEM requires important human resources for pre-processing tasks (mesh generation), the BEM leads to high computational times because the matrix arising in this formulation is full and non symmetric. There is thus still a need for finding a compromise between easy pre-processing tasks and reduction of global computational times. In this paper, we will focus on a meshless method: the Element-Free Galerkin Method (EFGM, see [4]).

Meshless techniques have known relatively few developments until recent years, contrary to finite element, finite volume or finite difference methods which have been subject to intensive research for more than 25 years. Their first formulation is due to L. B. Lucy in 1977 [5] but the use of moving least square

* Corresponding author

approximations, introduced by B. Nayroles *et al*. in 1992 [6] has brought a decisive enhancement. Here we focus on the EFGM, a new trend in meshless methods, which has been surveyed by T. Belytschko and co-workers [3] who also contributed to the improvement of the method. Recently also, the convergence of moving least square-based methods has been theoretically established [7-8].

The resurgence of interest in meshless methods is mainly due to some bottlenecks encountered by the Finite Element Method. For instance, the FEM is not adapted to fracture analysis [9-10], the reason being that evolutive meshes have to be defined to follow crack propagation, and the connectivity conditions to be fulfilled by the finite elements make this task difficult and time consuming. The latter remark is reinforced by the fact that the major changes in the mesh have to be done near the end of the crack, i.e. where the mesh is the finest. With EFGM, no connectivity conditions have to be satisfied, so that nodes can easily be added or removed. For a survey of recent developments of EFGM, see [11].

Our idea here is to extend the field of application of the EFGM to acoustic problems, hoping that it could partially solve some problems encountered by the other methods for the numerical computation of waves, due to specific singularities of the Helmholtz operator [12-15].

In the case of FEM, a phase lag between the computed and the exact wave, growing with the wave number, arises from a numerical pollution related to the dispersive character of the discrete medium (i.e. the computed wave does not propagate at the speed of sound). While pollution and dispersion are well known for the *hp* version of the FEM thanks to the work of F. Ihlenburg *et al*. [12-14], theoretical results are not yet available for the EFGM and this paper presents a numerical assessment of both phenomena in order to demonstrate how they affect the EFGM solutions.

The paper is organized as follows. Section 2 presents the theoretical formulation of the acoustic wave propagation, introducing the strong and the variational forms. Dispersion and pollution effects encountered by the FEM are outlined in Section 3. Section 4 introduces the EFGM applied to acoustics and the mathematical background of the EFGM based on the moving least square method. Numerical tests are described in Section 5.

2. Acoustic wave propagation

2.1. Strong form of the general acoustic problem

The strong formulation of the acoustic wave propagation is addressed by the fundamental equations of continuum mechanics. It is easily derived that, assuming that the fields of pressure, specific mass and velocities are small harmonic perturbations around a steady uniform state,

$$p' = pe^{j\omega t} \qquad \rho' = \rho e^{j\omega t} \qquad \mathbf{v}' = \mathbf{v}e^{j\omega t} \tag{1}$$

the spatial distribution of the complex pressure perturbation must satisfy a Helmholtz equation

$$\Delta p + k^2 p = 0 \tag{2}$$

with appropriate boundary conditions. k denotes the wave number and is defined by the ratio between the angular frequency ω and the speed of sound c

$$k = \frac{\omega}{c} \tag{3}$$

The gradient of pressure is linked to the velocity by the equation of motion which can be written as

$$j\rho ck\mathbf{v} + \nabla p = 0 \tag{4}$$

For interior problems, three sets of boundary conditions are considered ($\bar{\bullet}$ denotes a prescribed value):

Dirichlet boundary conditions on Γ_D

$$p = \bar{p} \tag{5}$$

Neumann boundary conditions on Γ_N

$$v_n = \bar{v}_n \quad \text{or} \quad \boldsymbol{n}^t \boldsymbol{\nabla} p = -j\rho ck\bar{v}_n \tag{6}$$

Robin boundary conditions on Γ_R

$$v_n = A_n p \quad \text{or} \quad \boldsymbol{n}^t \boldsymbol{\nabla} p = -j\rho ckA_n p \tag{7}$$

where v_n is the normal component of the velocity standing for the excitation by the vibrating panels, $\boldsymbol{n}$ is the exterior unit normal vector and A_n is the admittance coefficient modelling the structural damping.

For exterior problems, the Sommerfeld condition implies that there is no reflection at infinity and is usually cast on a fictitious sphere of radius *R* by a DtN mapping [2]. Here, it is assumed that such a mapping has been done and we focus on the computation of the waves either for interior problems or for exterior problems inside the fictitious sphere.

2.2. Variational form of the general acoustic problem

Consider the sesquilinear form $a(p,w): H_D \times H_0 \to \mathbb{C}$

$$a(p,\tilde{w}) = \int_\Omega \left(\partial_i p \partial_i \tilde{w} - k^2 p\tilde{w} \right) d\Omega + \int_{\Gamma_R} j\rho ckA_n p\tilde{w} d\Gamma \tag{8}$$

where $\tilde{\ }$ denotes a complex conjugate. H_D^1 is the space of kinematically admissible trial functions *p* and H_0^1 is the space of kinematically homogeneous test functions *w*

$$H_D^1(\Omega) = \left\{ p \in H^1(\Omega) \mid p = \bar{p}\, on\, \Gamma_D \right\} \tag{9}$$

$$H_0^1(\Omega) = \left\{ w \in H^1(\Omega) \mid w = 0\, on\, \Gamma_D \right\} \tag{10}$$

Defining the functional

$$\Pi = \frac{1}{2} a(p,\tilde{p}) - \varphi(\tilde{p}) \tag{11}$$

with

$$\varphi(\tilde{p}) = -\int_{\Gamma_N} j\rho ck\bar{v}_n \tilde{p} d\Gamma \tag{12}$$

the variational formulation can be expressed as

$$\text{Find } p \in H_D^1(\Omega) \mid \delta\Pi = 0 \quad \forall \delta p \in H_0^1 \tag{13}$$

In order to formulate the Element-Free Galerkin Method (Section 4), it is necessary to slightly modify variational form (13) by introducing Dirichlet boundary conditions (5) with Lagrange multipliers $\lambda \in H^0(\Omega)$ leading to the functional

$$\Pi^* = \Pi + \int_{\Gamma_D} \lambda(\tilde{p} - \tilde{\bar{p}}) d\Gamma \tag{14}$$

and the variational form can be reformulated as

$$\text{Find } p \in H^1 \mid \delta\Pi^* = 0 \quad \forall \delta p \in H_0^1, \delta\lambda \in H^0 \tag{15}$$

The variation $\delta\Pi^*$ is expressed by

$$\delta\Pi^* = \int_\Omega \left(\partial_i p \partial_i \delta\tilde{p} - k^2 p \delta\tilde{p}\right) d\Omega + \int_{\Gamma_R} j\rho ckA_n p\delta\tilde{p} d\Gamma + \int_{\Gamma_N} j\rho ck\bar{v}_n \delta\tilde{p} d\Gamma + \int_{\Gamma_D} \delta\lambda(\tilde{p} - \tilde{\bar{p}}) d\Gamma + \int_{\Gamma_D} \lambda\delta\tilde{p} d\Gamma \tag{16}$$

Existence and uniqueness of the solution of problem (13) can be established from the inf-sup condition. On a one dimensional problem, it can be proved that the Babuška-Brezzi constant is of order k^{-1} [12] i.e. there is a decreasing stability for increasing wave numbers.

2.3. Model problems

In Section 5, numerical tests will be performed on two model problems. They will be solved both with a general two-dimensional formulation even if model problem 1 is one dimensional.

Let L be a characteristic length of the studied domain. Assuming that x and y are the Cartesian two-dimensional coordinates, non dimensional coordinates are defined by

$$\xi = x/L \qquad \eta = y/L \tag{17}$$

and the equations of the following sections are also expressed as a function of the non dimensional wave number

$$\kappa = kL \tag{18}$$

2.3.1 *Model problem 1 (Fig. 1)*

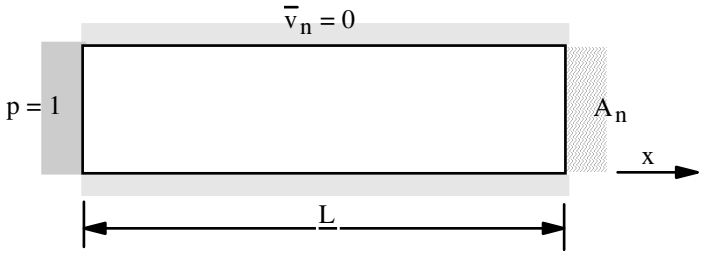

Fig. 1. Model problem 1.

The first model problem is a tube of length L. Dirichlet boundary conditions are prescribed on one end of the tube, while the other end is submitted to Robin conditions. In the particular case of

$$\rho c A_n = -1 \tag{19}$$

the strong form of the acoustic problem is

$$\frac{d^2 p}{d\xi^2} + \kappa^2 p = 0 \quad \text{in } \Omega(0 \le \xi \le 1) \qquad p(0) = 0 \qquad \left.\frac{dp}{d\xi}\right|_1 - j\kappa p(1) = 0 \tag{20}$$

and the analytical solution is a one dimensional propagating wave, i.e. this model problem is equivalent to an exterior problem with the Robin boundary condition standing for the Sommerfeld condition. This solution is expressed by

$$p(\xi) = \cos(\kappa\xi) + j\sin(\kappa\xi) \tag{21}$$

2.3.2 *Model problem 2 (Fig. 2)*

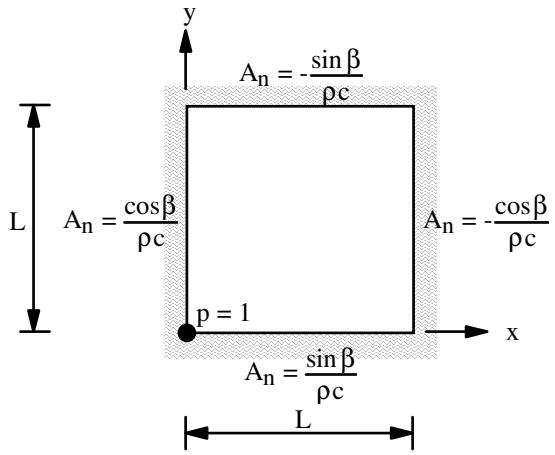

Fig. 2. Model problem 2.

This two-dimensional problem considers a square domain; L is the length of its side. Robin boundary conditions are defined on all four sides as shown in Fig. 2. The pressure is prescribed at one of the corners.

The strong form of this problem is expressed, in its non dimensional form, by the Helmholtz equation

$$\frac{\partial^2 p}{\partial \xi^2} + \frac{\partial^2 p}{\partial \eta^2} + \kappa^2 p = 0 \quad \text{in } \Omega(0 \le \xi \le 1; 0 \le \eta \le 1) \tag{22}$$

with the Dirichlet boundary condition

$$p(0,0) = 0 \tag{23}$$

and the Robin boundary conditions

$$\begin{cases} -\dfrac{\partial p}{\partial \xi} + j\kappa p \cos\beta = 0 \quad on(\xi = 0, \eta) \\ \dfrac{\partial p}{\partial \xi} - j\kappa p \cos\beta = 0 \quad on(\xi = 1, \eta) \\ -\dfrac{\partial p}{\partial \eta} + j\kappa p \sin\beta = 0 \quad on(\xi, \eta = 0) \\ \dfrac{\partial p}{\partial \eta} - j\kappa p \sin\beta = 0 \quad on(\xi, \eta = 1) \end{cases} \tag{24}$$

This two-dimensional problem corresponds to a plane wave propagating along a direction inclined with an angle β on axis x. The analytical solution is

$$p = \cos\left[\kappa(\xi\cos\beta + \eta\sin\beta)\right] + j\sin\left[\kappa(\xi\cos\beta + \eta\sin\beta)\right] \tag{25}$$

3. Dispersion and pollution effect for the FEM

3.1. Dispersion

Before formulating the approximation by the EFGM, let us briefly recall the main phenomena that arise for the numerical solution computed with a standard Galerkin Finite Element Method.

The discrete form of the acoustic problem will require the definition of a characteristic dimension h of the subspaces used in the discrete model (i.e. the element size in the FEM). This size can be expressed in a non dimensional form

$$\hbar = h/L \tag{26}$$

A medium is called non dispersive when the wave propagation speed

$$c = \frac{\omega}{k} \tag{27}$$

is equal to the speed of sound c, and is thus independant of the frequency. It is well known today [14] that the numerical waves are dispersive, i.e. they propagate with a speed different from the speed of sound

$$c^h = \frac{\omega}{k^h} \neq c \tag{28}$$

where index h stands for the discrete solution. For linear elements (p=1), it can be proved on a one dimensional problem [14] that

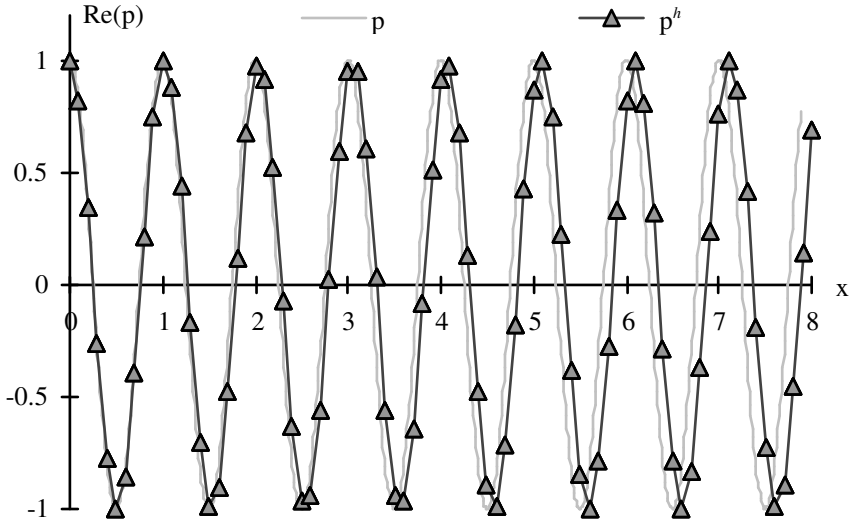

Fig. 3. Model problem 1 (p=1, L=8m, h=0·1m, k=6·28m^{-1}, κ=50·3): dispersion of the finite element wave *vs*. exact wave.

$$k^h = k - \frac{k^3 h^2}{24} + o(k^5 h^4) \tag{29}$$

showing that the numerical wave number is lower than the exact wave number. It results in a phase shift between the exact and the finite element waves as illustrated in Fig. 3 for model problem 1 (tube of length L = 8m with a meshsize of 0·1m (p=1)).

3.2. Pollution effect

Acoustic finite element users usually believe that keeping κh constant is sufficient to ensure an acceptable accuracy level. Due to specific singularities of the Helmholtz operator, this criterion is not reliable. Consider again the standard finite element solution p^h of model problem 1 and define the discretization error in the H^1 semi-norm

$$\left|p-p^h\right|_1^2 = \int_\Omega \left(\tilde{\boldsymbol{v}}-\tilde{\boldsymbol{v}}^h\right)^t \left(\boldsymbol{v}-\boldsymbol{v}^h\right) d\Omega \tag{30}$$

F. Ihlenburg *et al*. proved [12-13] that the error can be split into two terms: the first one is the approximation error (the difference between the exact wave and its interpolant) and the second one is the pollution term (the difference between the interpolant and the finite element wave). This latter is clearly influenced by phase shift (29) but also by the error on the amplitude of the wave. The general estimate for the relative error in H^1 semi-norm for the *hp* version of the finite element method is

$$\frac{\left|p-p^h\right|_1}{\left|p\right|_1} \le C_1\theta + C_2\kappa\theta^2 \tag{31}$$

where $\theta = (\hbar\kappa / p)^p$ is the scale of the finite element mesh. Meshes such that $\kappa\theta^2$ is kept constant ensure that the pollution error is under control and that the asymptotic behaviour is reached. Meshes such that θ is constant are said to be in the preasymptotic range since they ensure a constant resolution of the wave (i.e. "rule of the thumb").

Estimate (31) shows the advantage of the *hp* method, as compared to the traditional *h* method, since the magnitude of the scale decreases when *p* grows. Hence, the pollution error by large κ is smaller for *p=2,3,4* compared to the *h* version with *p*=1. Better than piecewise polynomial interpolation, we present in this paper an original application of the Element-Free Galerkin Method, developed by T. Belytschko *et al*. [4], to the numerical computation of waves. Section 4 will show that this method is based on non rational interpolation functions which seem to be more suited for computing waves.

4. Element-Free Galerkin Method for acoustics

4.1. Discrete variational form

A standard Galerkin procedure is used to obtain the discrete equations corresponding to the variational formulation (Eq. (15)). The choice of the trial and the test functions is restricted to the discrete subspace $V^1 \in H^1$, corresponding to

$$p^h = \sum_{i=1}^{n} N_i p_i = \boldsymbol{N}\boldsymbol{p} \tag{32}$$

where $\boldsymbol{p}$ is a set of n nodal values for the pressure field, and the N_i are the shape functions defined in Section 4.2. It can be already noticed that the shape functions will be chosen non rational, in opposition to the usual shape functions of the standard Finite Element Method. In the same way, the discrete Lagrange multipliers are interpolated by

$$\lambda^h = \boldsymbol{\aleph}\boldsymbol{\Lambda} \tag{33}$$

where $\boldsymbol{\aleph}$ is a polynomial interpolant and the variations of p^h and λ^h are obtained from (32) and (33)

$$\delta p^h = \boldsymbol{N}\delta\boldsymbol{p} \tag{34}$$

$$\delta\lambda^h = \aleph\,\delta\boldsymbol{\Lambda} \tag{35}$$

With these particular choices of trial functions, the variational formulation (15) leads to the following linear algebraic system of equations

$$\begin{bmatrix} \boldsymbol{K} + j\rho ck\boldsymbol{C} - c^2k^2\boldsymbol{M} & \boldsymbol{K}_{p\lambda} \\ \boldsymbol{K}_{p\lambda}^t & 0 \end{bmatrix} \begin{Bmatrix} \boldsymbol{p} \\ \boldsymbol{\Lambda} \end{Bmatrix} = \begin{Bmatrix} -j\rho ck\boldsymbol{f} \\ \boldsymbol{b} \end{Bmatrix} \tag{36}$$

where $\boldsymbol{K}$ is called the stiffness matrix

$$\boldsymbol{K} = \int_\Omega (\boldsymbol{\nabla N})^t (\boldsymbol{\nabla N})\, d\Omega \tag{37}$$

$\boldsymbol{C}$ stands for the damping matrix modelling Robin boundary conditions (7)

$$\boldsymbol{C} = \int_{\Gamma_R} \boldsymbol{N}^t \boldsymbol{N} A_n\, d\Gamma \tag{38}$$

and $\boldsymbol{M}$ is the mass matrix

$$\boldsymbol{M} = \frac{1}{c^2} \int_\Omega \boldsymbol{N}^t \boldsymbol{N}\, d\Omega \tag{39}$$

The right-hand side of (36) contains the prescribed normal velocities (Eq. (6))

$$\boldsymbol{f} = \int_{\Gamma_N} \boldsymbol{N}^t \bar{v}_n\, d\Gamma \tag{40}$$

The formulation of the Dirichlet boundary conditions with Lagrange multipliers appears in the linear system through the $\boldsymbol{K}_{p\lambda}$ matrix coupling the unknowns $\boldsymbol{p}$ and $\boldsymbol{\Lambda}$. In the right-hand side, $\boldsymbol{b}$ is the projection of the prescribed pressure on the shape functions.

$$\boldsymbol{K}_{p\lambda} = \int_{\Gamma_D} \boldsymbol{N}^t \aleph\, d\Gamma \tag{41}$$

$$\boldsymbol{b} = \int_{\Gamma_D} \aleph^t \bar{p}\, d\Gamma \tag{42}$$

4.2. Mathematical background of the Moving Least Square Method

The shape functions introduced in (32) are still to be defined and are obviously the main characteristic of the Element-Free Galerkin Method (EFGM). Here, they are constructed by using the Moving Least Square Method (MLSM) first studied by P. Lancaster *et al*. [16] in the case of surfaces generated from arrays of nodal values. They have later been applied to structural analysis by B. Nayroles *et al*. [6] and T. Belytschko *et al*. [4, 11].

The construction of the shape functions proceeds as follows. Consider a function $g(\boldsymbol{x})$: $\Omega \to \mathbb{R}$ to be approximated from given values g_I at nodes $\boldsymbol{x}_I \in \Omega$ ($I = 1,...,n$). At each point $\boldsymbol{x}^* \in \Omega$, an approximation $L^{(\boldsymbol{x}^*)}g$ of g is defined, using a basis $\boldsymbol{P}(\boldsymbol{x})$ of dimension m. Examples of usual bases are

$$\begin{aligned} &\boldsymbol{P}^t(\boldsymbol{x}) = \{1, x, y\} && (m=3, \text{ linear basis for 2D problems}) \\ &\boldsymbol{P}^t(\boldsymbol{x}) = \{1, x, y, x^2, xy, y^2\} && (m=6, \text{ quadratic basis for 2D problems}) \end{aligned} \tag{43}$$

The approximation of g is chosen as a linear combination of the basis monomials

$$L^{(\boldsymbol{x}^*)}g = \boldsymbol{P}^t \boldsymbol{a}^* \tag{44}$$

and the array of coefficients $\boldsymbol{a}^*$ is determined by minimizing the L^2 discrete weighted norm

$$\min_{\boldsymbol{a}^*} \sum_{I=1}^{N} w_I(\boldsymbol{x}^*)\left(\boldsymbol{P}^t(\boldsymbol{x}_I)\boldsymbol{a}^* - g_I\right)^2 \tag{45}$$

where $w_I(\boldsymbol{x})$ is a weight function associated to node I. It is important to emphasize that coefficients $\boldsymbol{a}^*$ are not constant as in the FEM. Eq. (45) leads to (46) for the coefficients of the linear combination of Eq. (44)

$$\boldsymbol{a}^* = \boldsymbol{A}^{-1}(\boldsymbol{x})\boldsymbol{B}(\boldsymbol{x})\boldsymbol{g} \tag{46}$$

where $\boldsymbol{g}$ is the array of the nodal values g_I and

$$\boldsymbol{A}(\boldsymbol{x}) = \sum_{I=1}^{N} w_I(\boldsymbol{x})\boldsymbol{P}(\boldsymbol{x}_I)\boldsymbol{P}^t(\boldsymbol{x}_I) \tag{47}$$

$$\boldsymbol{B}(\boldsymbol{x}) = \left[w_I(\boldsymbol{x})\boldsymbol{P}(\boldsymbol{x}_I), \ldots, w_n(\boldsymbol{x})\boldsymbol{P}(\boldsymbol{x}_n)\right] \tag{48}$$

The moving least square approximation is defined by

$$g^h(\boldsymbol{x}) = L^{(\boldsymbol{x})} g \tag{49}$$

and, combining Eqs. (44), (46) and (49), leads to

$$g^h(\boldsymbol{x}) = \boldsymbol{N}(\boldsymbol{x})\boldsymbol{g} \tag{50}$$

where the shape functions are defined by

$$\boldsymbol{N}(\boldsymbol{x}) = \boldsymbol{P}^t(\boldsymbol{x})\boldsymbol{A}^{-1}(\boldsymbol{x})\boldsymbol{B}(\boldsymbol{x}) \tag{51}$$

In the Element-Free Galerkin Method applied to acoustics, these shape functions are used to approximate the pressure field. The weight function associated to a node is defined on a domain of influence of this node. This weight is positive inside its support and decreases when the distance to the node increases. The domains of influence connect the nodes, i.e. they play the role of the support of the shape functions.

4.3. Numerical integration

In the EFGM, linear system (36) requires the computation of integrals (Eqs. (37)-(42)). It can not, as it is the case in the FEM, be taken advantage of a mesh to perform those integrations and an artificial grid independent from the node distribution has to be defined, covering domain Ω (Fig. 4) as support for Gauss quadrature formulas. As it can be seen on Fig. 4, some of the cells are cut by the boundary and the contribution of the Gauss points located outside Ω is set to zero.

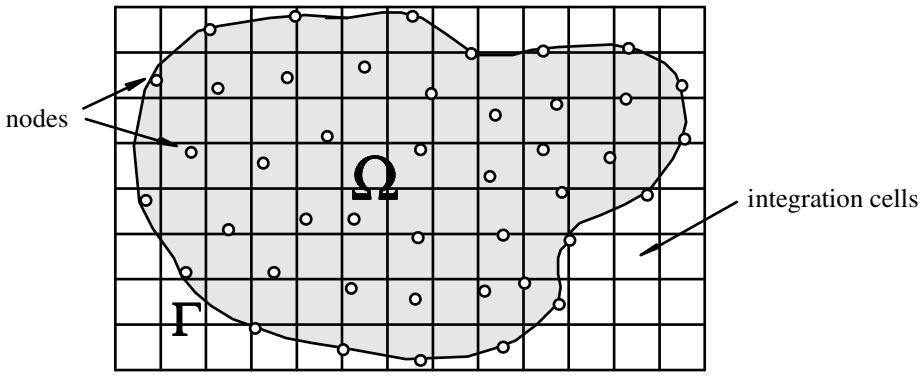

Fig. 4. Grid for numerical integration.

4.4. Properties of the MLSM

The first important property of the MLSM is that a shape function associated to a node is not equal to unity at this node, and is not zero at the other nodes

$$N_I(\boldsymbol{x}_j) \neq \delta_{Ij} \tag{52}$$

meaning that the approximations $g^h(x_I)$ computed from (49) are not equal to the nodal values g_I. This is the reason why Lagrange multipliers are used in variational formulation (15) to prescribe the Dirichlet boundary conditions.

The second property is the consistency of the MLSM as it can be shown that the shape functions reproduce exactly all the functions within the span of the basis $\boldsymbol{P}(\boldsymbol{x})$. In particular,

$$\sum_{I=1}^{n} N_I(\boldsymbol{x}) = 1 \quad \forall \boldsymbol{x} \in \Omega \tag{53}$$

reason why this method is a particular case of the Partition of Unity Method (PUM) [7].

The pressure field obtained with the EFGM has a higher order of continuity than the solution of finite element formulations. C. A. Duarte [8] proves that, if the basis functions $P_i(i=1,...,m) \in C^r(\Omega)$ and the weight functions $w_I(I=1,...,n) \in C^s(\Omega)$, then the MLSM approximation defined by Eq. (49) $\in C^{\min(r,s)}(\Omega)$.

A necessary condition to ensure the regularity of matrix $\boldsymbol{A}(\boldsymbol{x})$ (Eq. (47)) [17-18] is that each point of Ω should be located within at least m domains of influence, where m is the size of the basis $\boldsymbol{P}(\boldsymbol{x})$, meaning that

$$\boldsymbol{x} \in \bigcap_{j=1}^{l} support(w_j) \quad \forall \boldsymbol{x} \in \Omega \quad and \quad l \geq m \tag{54}$$

implying a theoretical minimal size for the domains of influence. The numerical tests of Section 5.2 will show that this condition (54) is not sufficient: domains larger than this minimum have to be considered.

4.5. Important parameters of the MLSM

Several parameters have been introduced in the formulation of the Element-Free Galerkin Method: size of the domains of influence, polynomial basis, weight functions. Their influence on the accuracy of the solutions is numerically investigated in Section 5.

4.5.1 Domains of influence

Only circular domains of influence are considered here. The domains of influence ensure the connection between the nodes and their size is an important parameter: in addition to condition (54), it can be shown [18] that it also influences the accuracy of the solution.

4.5.2 Polynomial basis

In this paper, we will consider polynomial bases, such as presented in Eq. (43). Note that the particular case $m = 1$ corresponding to the basis $\boldsymbol{P}^t(\boldsymbol{x}) = \{1\}$ is known as Shephard interpolant [17]. Its advantage is that matrix $\boldsymbol{A}(\boldsymbol{x})$ (47) is reduced to a 1*1 size, resulting in a lower cost in the computation of the shape functions (Eq. (51)). This particular basis will be examined in the numerical tests.

4.5.3 Weight functions

Two classes of weight functions have been considered (Fig. 5), where d_I is the distance between sample point $\boldsymbol{x}$ and node $\boldsymbol{x}_I$, and D_I is the radius of the domain of influence of node I:

exponential weight function:

$$w(\boldsymbol{x}-\boldsymbol{x}_I) = w(d_I) = \frac{e^{-(2d_I/D_I)^2} - e^{-4}}{1-e^{-4}} \tag{55}$$

cosine weight function:

$$w(\boldsymbol{x}-\boldsymbol{x}_I) = w(d_I) = \frac{1+\cos(\pi d_I/D_I)}{2} \tag{56}$$

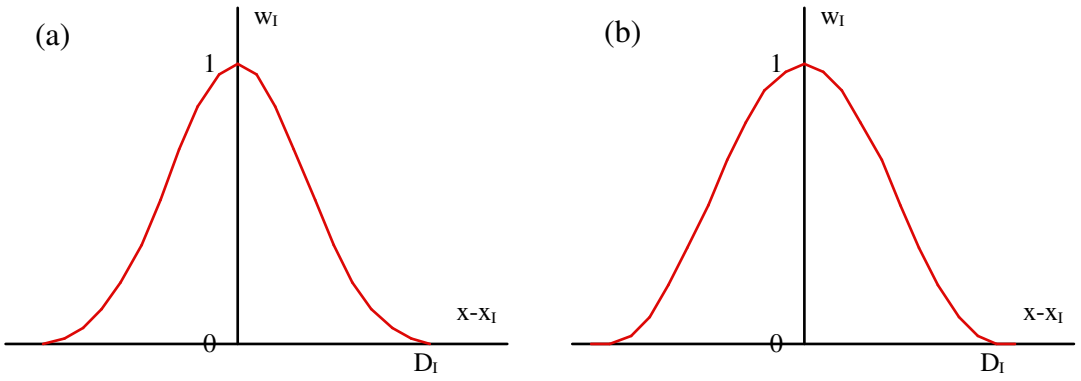

Fig. 5. Weight functions used: (a) exponential; (b) cosine.

According to Duarte [17] as mentioned in Section 4.4, we can deduce the order of continuity of the MLSM approximation (50). The cosine weight function $\in C^1$ while the exponential weight function $\in C^0$ since its normal derivative is discontinuous along the boundary of the domain of influence. When using a polynomial basis which is obviously C^∞, the exponential weight function will give a C^0 approximation while the use of the cosine weight function will result in a C^1 continuity.

5. Numerical tests

5.1. Introduction

This section will present numerical tests on the model problems defined in Section 2.3. The outline of the shape functions (51) will be first discussed in a particular case. Next, the influence of parameters of the MLSM approximation will be examined in Sections 5.2 and 5.3. In Sections 5.4 and 5.6, the dispersion and pollution effects will be highlighted on one dimensional model problem 1. Section 5.7 will examine the behaviour of the Element-Free Galerkin Method on two-dimensional problem 2. Finally, a criterion to control the error will be presented in Section 5.8.

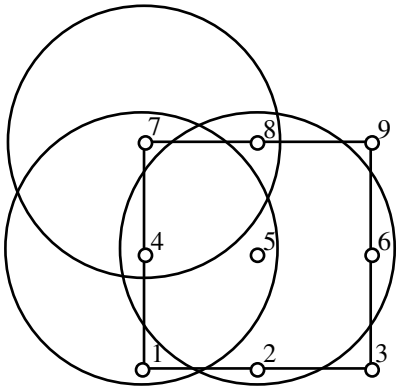

Fig. 6. Square discretized by 9 nodes and some domains of influence.

5.2. Outline of the shape functions

Before considering EFGM numerical tests in acoustics, let us focus on the MLSM non rational shape functions defined by Eq. (51), in the particular case represented in Fig. 6: a square domain discretized by nine nodes.

The shape functions have been computed using the exponential weight (55) and a linear basis (43) and represented on Fig. 7 for three nodes: (a) the middle of a side (node 4), (b) the center of the square (node 5) and (c) a vertex (node 7).

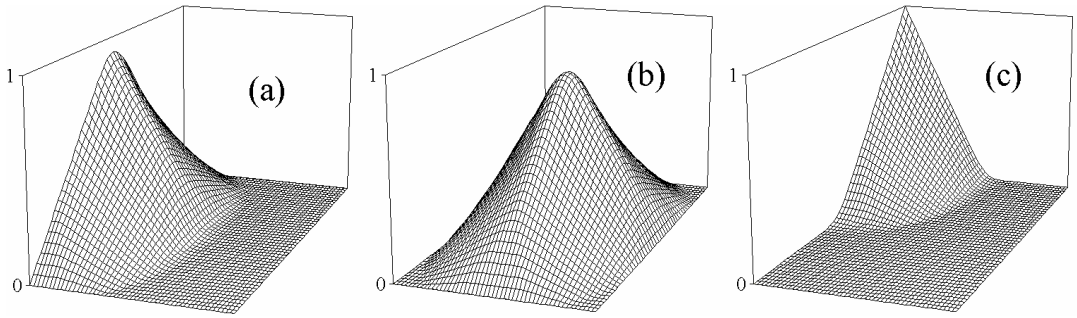

Fig. 7. MLSM shape functions.

We can observe that the shape functions are not equal to unity at nodes (52), meaning that a MLSM approximation (Eq. (50)) built across the square using those shape functions and computed at nodes will not be equal to the corresponding nodal values.

5.3. Size of the domains of influence and choice of weight functions

Model problem 1 is considered in order to show the influence of the size of the EFGM domains of influence. The nodal distribution is regular (33 nodes, Fig. 8), the length of the tube is equal to 1m and the distance between nodes is h=0·1m. A linear basis is used in our tests and the domains of influence are circular.

Assertion (54) shows there is a theoretical minimum radius $D_{I,min}$ for the domains of influence. For a two-dimensional problem and a linear basis (m=3), each point of the domain Ω has to be part of at least 3 domains of influence (Eq. (54)). Applied to the regular nodal distribution, this condition gives us $D_{I,\min} = \sqrt{5/4}h = 1.12h$. Some of the minimal domains corresponding to the nodes coloured in black are shown on Fig. 8.

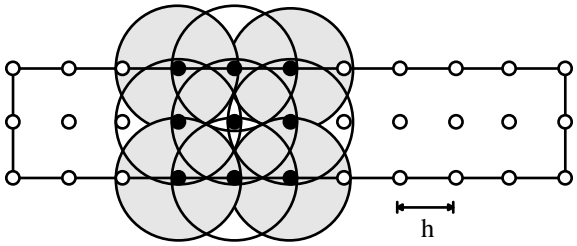

Fig. 8. Distribution of nodes and minimal size for some domains of influence (linear basis).

The EFGM solutions were computed for two frequencies (500 Hz (κ=12·57) and 750 Hz (κ=18·85)) for different domain sizes expressed as a function of parameter α defined by

$$D_I = \alpha D_{I,\min} \qquad \text{with } \alpha \geq 1 \tag{57}$$

The relative error in the H^1 semi-norm (30) is presented as a function of α in Fig. 9 for the exponential weight function (55) and in Fig. 10 for the cosine weight function (56).

These graphs show that the theoretical minimal size corresponding to α=1 is a necessary but not sufficient condition. Furthermore, it seems impossible to point out a unique optimal value for α, but we can observe that the range $1.5 \leq \alpha \leq 3.0$ gives better results than other values of α. We also have to keep in mind that increasing the size of domains of influence, meaning connecting more nodes, leads to a more dense matrix for system (36) and a higher computational time for its resolution.

The comparison of Fig. 9 and Fig. 10 shows that the results are more accurate for the exponential weight function (55).

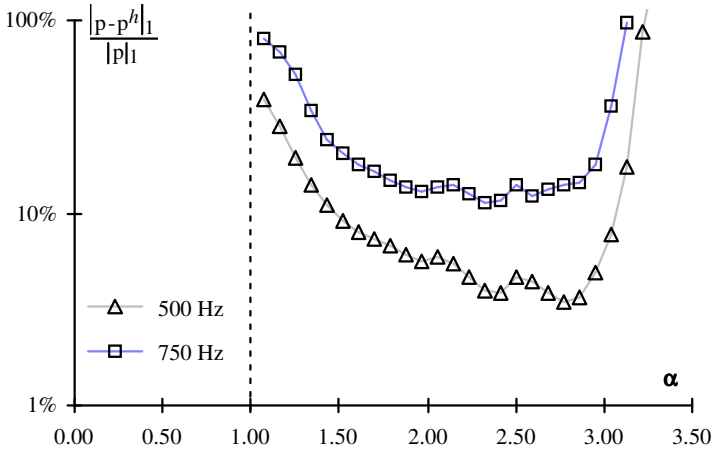

Fig. 9. Relative error in H^1 semi-norm as a function of parameter α (exponential weight function).

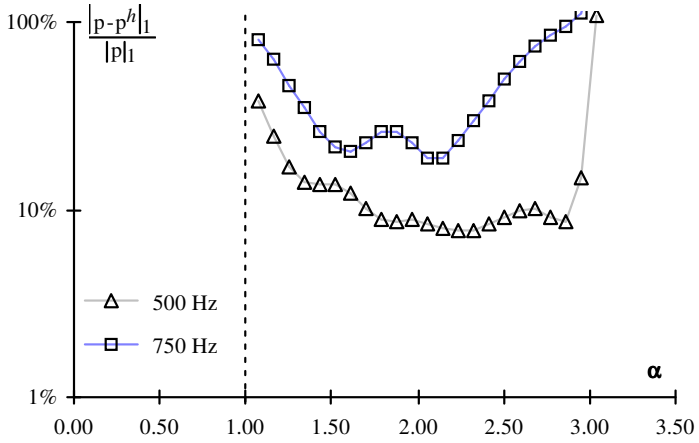

Fig. 10. Relative error in H^1 semi-norm as a function of parameter α (cosine weight function).

5.4. Polynomial basis

Polynomial bases were introduced in Section 4.2 (Eq. 43) and we would expect an increasing accuracy for higher order bases. However, higher computational times are involved as matrix $\boldsymbol{A}(\boldsymbol{x})$ (36) of size $m*m$ (where m is the dimension of the basis) has to be inverted at each integration point. We will compare here the low-cost Shephard basis $\boldsymbol{P}^t(\boldsymbol{x}) = \{1\}$ to the linear polynomial basis $\boldsymbol{P}^t(\boldsymbol{x}) = \{1, x, y\}$ considering convergence analyses (Fig. 11) in the H^1 semi-norm for model problem 1 at two frequencies (40 Hz (κ=1·005) and 1000 Hz (κ=25·13)).

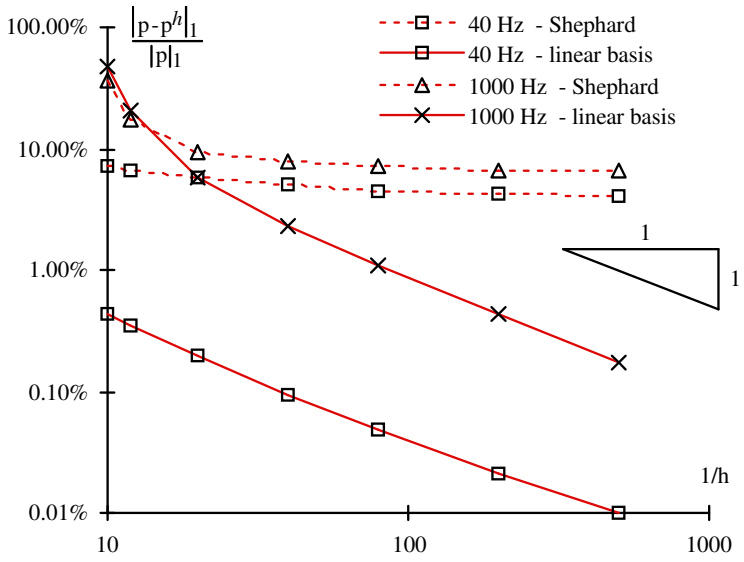

Fig. 11. Convergence for constant and linear bases in H^1 semi-norm.

We can conclude from Fig. 11 that the Shephard basis has a very low rate of convergence while the linear basis has a convergence rate slightly larger than unity.

From the two preceding subsections, we can now choose our parameters for the following tests. The exponential weight function (55) will be preferred to the cosine one (56), and a linear basis will be used, because it seems to ensure a good compromise between accuracy and computational time. The size of the domains of influence (52) will be characterized by $1.5 \leq \alpha \leq 3.0$.

5.5. Dispersion

Model problem 1 is considered in order to show the dispersion phenomenon of the EFGM applied to acoustics. The studied case is the same as in Section 5.3 with a linear basis (43), an exponential weight function (55) and domains of influence of radius 1·7 h, corresponding to α=1·52 (some of them are shown on Fig. 12). This problem has been solved for different values of frequency (250 Hz (κ=6·28), 500 Hz (κ=12·57) and 750 Hz (κ=18·85)), a length of 1 m and a meshsize of 0·1 m.

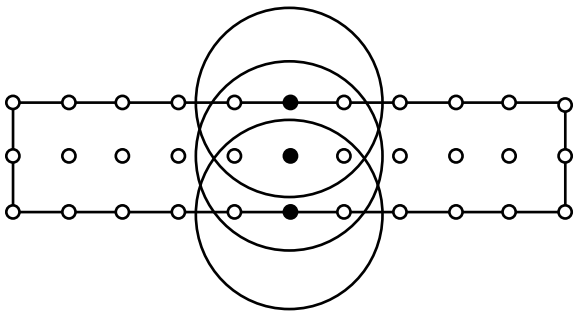

Fig. 12. Distribution of nodes and typical domains of influence.

The distributions of the real part of the pressure are represented on Figs. 13-15 comparing the EFGM and exact (Eq. (22)) solutions. The graphs show that the phase lag between the exact and numerical solutions increases with the frequency (and thus, with the wave number). This means that the EFGM solution is affected by the dispersion phenomenon.

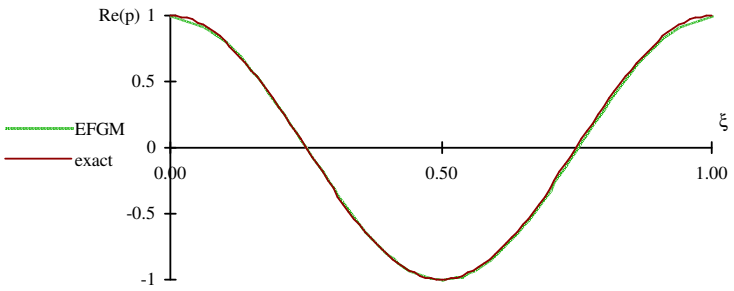

Fig. 13. Model problem 1: spatial distribution of real part of the pressure at 250 Hz (κ=6·28).

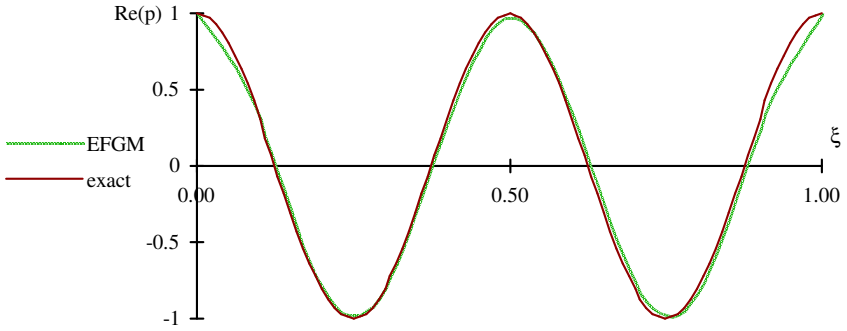

Fig. 14. Model problem 1: spatial distribution of real part of the pressure at 500 Hz (κ=12·57).

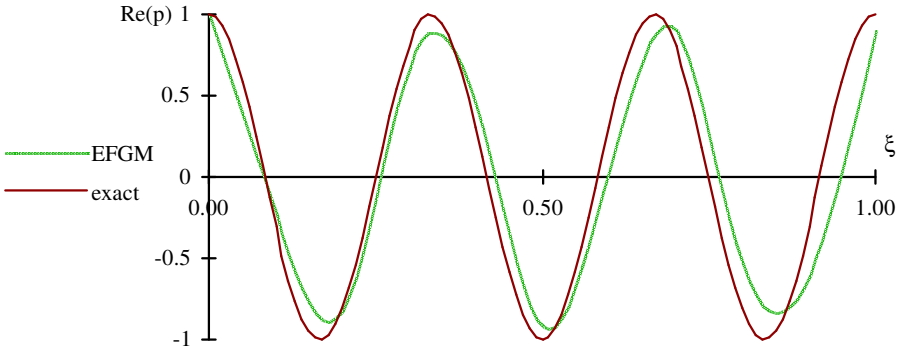

Fig. 15. Model problem 1: spatial distribution of real part of the pressure at 750 Hz (κ=18·85).

5.6. Pollution

The pollution effect presented in Section 3.2 is numerically illustrated with model problem 1 and convergence curves have been computed for several frequency values. The EFGM parameters are the same as previously: a linear basis (43), exponential weight functions (55) and a radius of 1·7 h are used. The values are presented in relative H^1 semi-norm on Fig. 16 in function of the node spacing.

Figure 16 clearly shows two different behaviours: at low non dimensional κ (e.g. 40 Hz, κ=1·005), the convergence is smooth and the solutions have reached their asymptotic behaviour. However, for high frequencies (e.g. > 1000 Hz), there is a pre-asymptotic behaviour for the coarse meshes showing that the influence of pollution increases with the frequency.

In fact, these behaviours are governed by the pollution effect depending on the non dimensional wave number which is a function of a characteristic dimension of the domain Ω. In order to confirm this assertion, tests have been made on model problem 1 with constant values of k and h, and increasing values of length *L*. The evolution of the relative error in semi-norm H^1 is given on Fig. 17, in function of *L* showing that, due to pollution, the relative error increases with the length of the tube, and that k is not the only parameter that influences the pollution effect, the length of the tube has to be taken into account. Note that the same effect can be observed more drastically for the FEM [15].

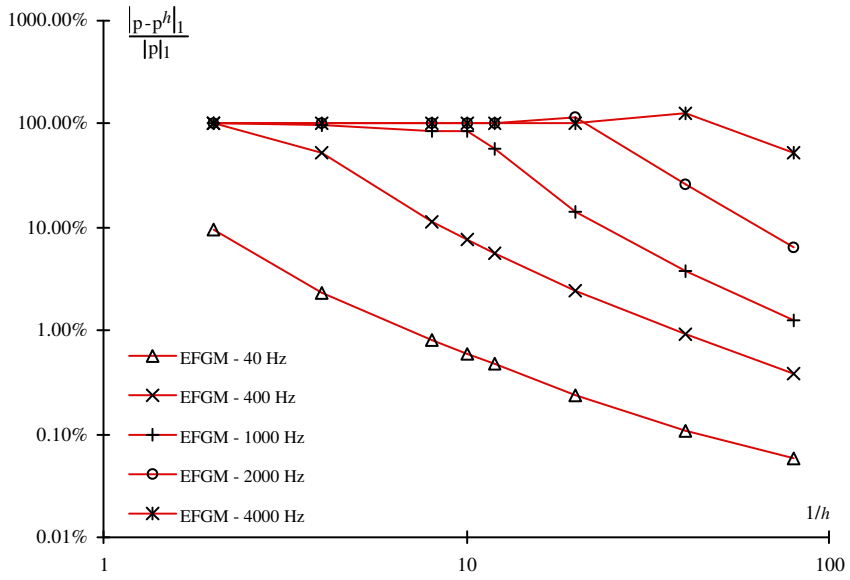

Fig. 16. Convergence in relative H^1 semi-norm.

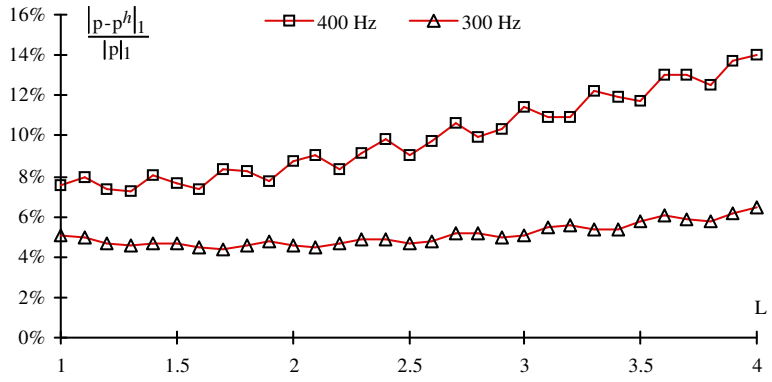

Fig. 17. Relative H^1 semi-norm error as a function of the length L of the tube.

5.7. Behaviour of EFGM for two-dimensional problems

This section will present results for model problem 2 (Section 2.3). The nodal distribution is regular (121 nodes, Fig.18), the side *L* of the square has been chosen equal to 1 m and the node spacing is h=0·1 m. Domains of influence are characterized by α=1·8.

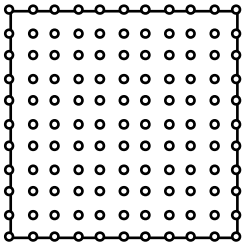

Fig. 18. Distribution of nodes for model problem 2.

We consider the following test: the β angle introduced in the Robin boundary conditions (24) is considered as a variable parameter and the relative error in the H^1 semi-norm is computed as a function of this angle. EFGM results are represented on Fig. 19 for three frequencies: 100 Hz (κ=2·51), 300 Hz (κ=7·54) and 500 Hz (κ=12·57).

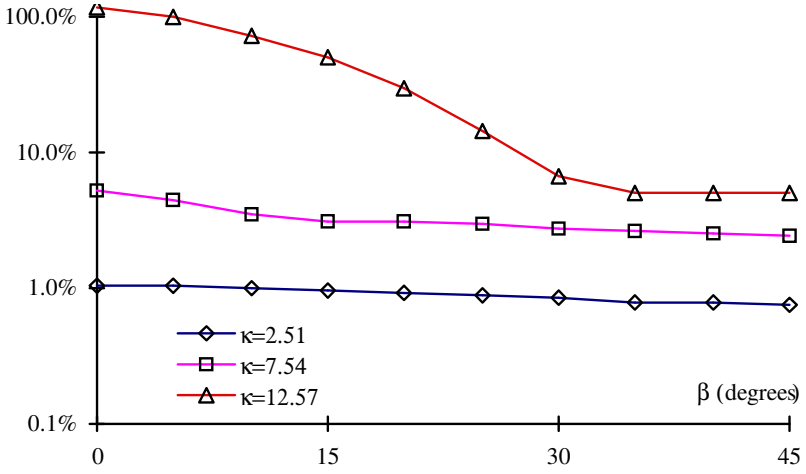

Fig. 19. Relative error in H^1 semi-norm as a function of β.

The error has a minimum for β=45°. This is explained by the fact that the set of shape functions has an x-y symmetry in both cases as well as solution (25) for a value of β=45°.

This test demonstrates the good behaviour of the EFGM on two-dimensional problems. For reasonable frequencies, the error is rather small (a maximum of 5% error for the first two frequencies). In order to obtain similar errors with classical methods, it would be necessary to use a more refined mesh.

We also would like to focus here on a great advantage of the method. The MLSM approximation of Eq. (50) used by the EFGM does not require any post-processing or further approximation in order to plot the results. They can be output as is to represent the iso-curves of pressure and speed. The distribution of pressure and speed v_x for model problem 2 are represented at Figs. 20 and 21.

The distribution of error in absolute value ($\left|\mathrm{Re}(p-p^h)\right|$ and $\left|\mathrm{Re}(v_x-v_x^h)\right|$) corresponding to those two graphs are given at Figs. 22 and 23. Most of the error is concentrated along the boundaries. Figure 23 also highlights that the distribution of speed is slightly discontinuous (according to Section 4.5, because of the use of an exponential weight function), the error having a small jump while crossing the border of a domain of influence.

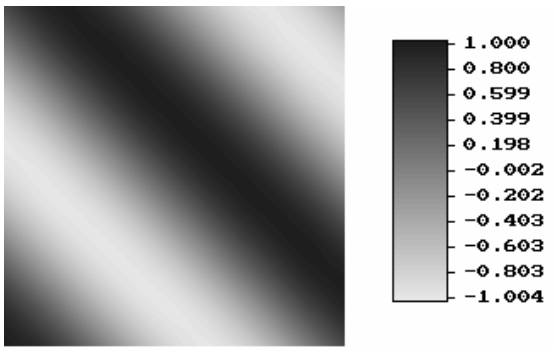

Fig. 20. Model problem 2 (β=45°, 300 Hz, κ=7·54): real part of the pressure.

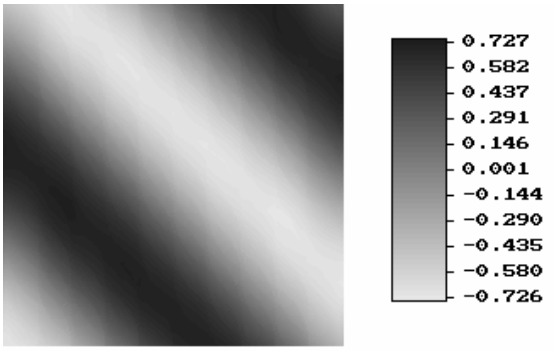

Fig. 21. Model problem 2 (β=45°, 300 Hz, κ=7·54): real part of the speed v_x.

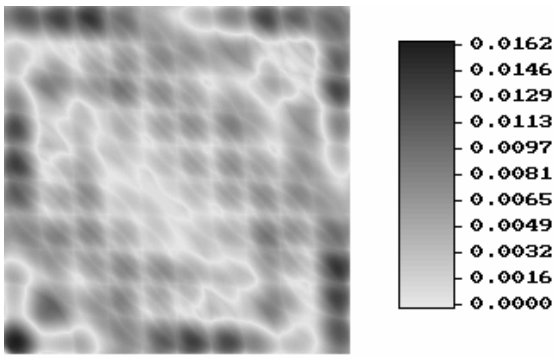

Fig. 22. Distribution of the error on $Re(p)$.

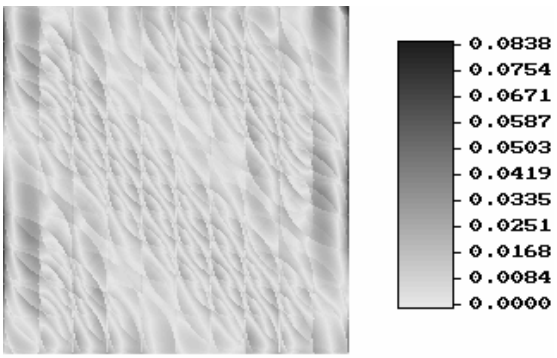

Fig. 23. Distribution of the error on $Re(v_x)$.

5.8. Control of the pollution error

Section 3.2 has introduced the pollution effect in the case of the Finite Element Method. With linear elements (p=1), estimate (31) for the relative error in H^1 semi-norm becomes:

$$\frac{\left|p - p^h\right|_1}{\left|p\right|_1} \leq C_1 \kappa\hbar + C_2 \kappa^3 \hbar^2 \tag{58}$$

meaning that the error must be controlled considering both $\kappa\hbar$ and $\kappa^3\hbar^2$. If the H^1 error is computed on a range of meshes with varying h and κh kept constant, the upper bound of the error (58) will increase linearly with κ. On the other hand, if $\kappa^3\hbar^2$ is kept constant, this error will be controlled. Results of such a test on model problem 1 (Section 2.3) using p=1 elements are shown on Fig. 24. When keeping κh constant, the error increases linearly with κ=1/h, for the low values of 1/h The reason is that most of the error is determined by the phase lag between the numerical and the exact solutions, increasing with 1/h . Once the phase shift is equal to one wave length, the numerical wave coincides with the exact one on a portion of Ω, giving a lower error although the solution is not more accurate. The graph also shows that the error is controlled by keeping $\kappa^3\hbar^2$ constant.

A theoretical upper bound of the relative error in H^1 semi-norm equivalent to (58) has not yet been found for the Element-Free Galerkin Method, but the same test is performed with the EFGM and the results are presented at Fig. 24.

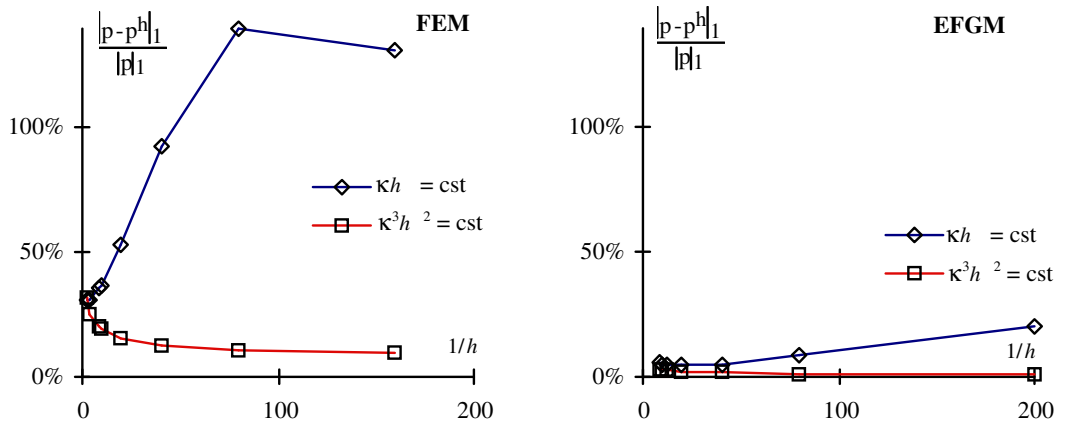

Fig. 24. Evolution of the relative error in H^1 semi-norm as a function of $1/h$ keeping $\kappa\hbar$ constant and $\kappa^3\hbar^2$ constant.

Figure 24 demonstrates numerically that the relative error in H^1 semi-norm in the EFGM has the same behaviour as in the FEM and must be controlled by keeping $\kappa^3\hbar^2$ constant; a criterion based on $\kappa\hbar$ constant seems to be not sufficient, even if the accuracy is significantly better with the EFGM.

6. Concluding remarks

This paper presents an original formulation and implementation of the Element-Free Galerkin Method for solving harmonic forced response of acoustic problems. The general advantages of the EFGM are well known: no mesh has to be generated, reducing the pre-processing tasks to the single generation of a node cloud.

The EFGM formulation involves many parameters (weight functions, domains of influence, function bases) and their influence on the accuracy of the solution has been studied in this paper.

In the particular case of acoustic problems, this paper has shown that the dispersion and pollution phenomena affect the EFGM and FEM solutions in a similar way. However, for identical node distributions, i.e. identical numbers of degrees of freedom, the EFGM results are significantly more accurate than the FEM solutions.

In fact, identical node distributions do not imply the same computational effort : the generation of system matrices are more expensive for EFGM than for FEM and the nodal connectivities are different leading to slightly different CPU resolution times. Up to now, the comparison of EFGM and FEM solutions did not consider the computational times and more detailed and systematic investigations will be presented in a next paper where the dispersion and pollution effects for both methods will be related to the respective computational times. However, it can be pointed out that the pre- and post-processing tasks are significantly reduced for EFGM compared to FEM since the nodes can be arbitrarily distributed and are not to be connected by a mesh.

It can already be expected from further numerical investigations that EFGM applied to acoustics allows a better control of the dispersion and pollution errors thanks to the easy control of the shape functions and nodal distributions. The EFGM is thus a promising method and will be subject to intense developments in the near future.

References

[1] R. J. Astley, G. J. Macaulay and J.-P. Coyette, 'Mapped wave envelope elements for acoustical radiation and scattering', *Journal of Sound and Vibration*, 170/1 (1994) 97-118.

[2] I. Harari, K. Grosh, T. J. R. Hughes, M. Malhotra, P. M. Pinsky, J. R. Stewart, L. L. Thompson, 'Recent Developments in Finite Element Methods for Structural Acoustics', *Arch. of Comp. Meth. Eng.*, 3 (1996) 131-311.

[3] J.-P. Coyette and J. Van de Peer, 'Acoustic Boundary Elements', *Advanced Techniques in Applied and Numerical Acoustics (ISAAC 5)*, VIII, KU Leuven, Belgium (1994) 1-31.
[4] T. Belytschko, Y. Y. Lu and L. Gu, 'Element-Free Galerkin Methods', *Int. j. numer. methods eng.*, 37 (1994) 229-256.
[5] L. B. Lucy, 'A numerical approach to the testing of fission hypothesis', *The Astronomical Journal*, 82 (1977) 1013-1024.
[6] B. Nayroles, G. Touzot and P. Villon, 'Generalizing the finite element method: diffuse approximation and diffuse elements', *Comput. Mech.*, 10 (1992) 307-318 .
[7] I. Babuska and J. M. Melenk, 'The Partition of Unity Method', *Int. j. numer. methods eng.*, 40 (1997) 727-758.
[8] C. A. Duarte and J. T. Oden, '*hp* Clouds - an *hp* meshless method', *Numerical Methods for Partial Differential Equations*, (1996), 1-34.
[9] T. Belytschko and M. Tabbara, 'Dynamic Fracture Using Element-Free Galerkin Methods', *Int. j. numer. methods eng.*, 39 (1996) 923-938.
[10] J.P. Ponthot and T. Belytschko, 'Arbitrary lagrangian eulerian formulation for element-free Galerkin method', submitted for publication in *Comput. Methods Appl. Mech. Eng.*
[11] T. Belytschko, Y. Krongauz, D. Organ, M. Fleming and P. Krysl, 'Meshless methods: An overview and recent developments', *Comput. Methods Appl. Mech. Eng.*, 139 (1996) 3-47
[12] F. Ihlenburg and I. Babuska, 'Finite Element Solution of the Helmholtz Equation with High Wave Number. Part 1: The *h*-Version of the FEM', *Computers Math. Applic.,* 38/9 (1995) 9-37.
[13] F. Ihlenburg and I. Babuska, 'Finite Element Solution of the Helmholtz Equation with High Wave Number. Part 2: The *hp*-Version of the FEM', *SIAM Numer. Anal.*, 34/1 (1997) 315-358.
[14] F. Ihlenburg and I. Babuska, 'Dispersion Analysis and Error Estimation of Galerkin Finite Element Methods for the Helmholtz Equation', *Int. j. numer. methods eng.*, 38 (1995) 3745-3774.
[15] Ph. Bouillard and F. Ihlenburg , 'Error estimation and adaptivity for the finite element solution in acoustics', *Workshop on 'New Advances in Adaptive Computational Methods in Mechanics'*, P. Ladevèze and J.T. Oden (Eds), to be published, Elsevier (1997).
[16] P. Lancaster and K. Salkauskas, 'Surfaces generated by moving least squares methods', *Math. Comput.*, 37 (1981) 141-158.
[17] C. A. Duarte, 'A Review of Some Meshless Methods to Solve Partial Differential Equations', *TICAM Report 95-06* (1995)
[18] Ph. Bouillard, P. Saint-Georges and S. Suleau, 'Méthodes d'interpolation nodale en élastostatique', *Proceedings of the 4th Belgian National Congress on Theoretical and Applied Mechanics*, Leuven, Belgium (1997) 409-412.

2.3 Analyse de dispersion

La méthode EFGM à base polynomiale proposée dans l'article précédent avait pour but de minimiser l'erreur de dispersion en ayant recours à des fonctions d'interpolation non rationnelles. En ce sens, cette approche peut être vue comme une méthode d'ordre élevé. Afin de montrer les avantages de cette approche sur les autres méthodes de minimisation de la dispersion, il nous a paru intéressant de mener rigoureusement une analyse de dispersion de cette approche pour le cas bidimensionnel. Celle-ci consiste à calculer le nombre d'onde correspondant à la solution numérique et à le comparer au nombre d'onde du problème continu. Les principes de l'analyse de dispersion sont présentés à une dimension ci-après. Sa généralisation à deux et trois dimensions sont décrits dans [DER99] et dans l'article qui suit.

Considérons l'équation d'onde unidimensionnelle

$$\frac{d^2p}{dt^2} - c^2 \frac{d^2p}{dx^2} = 0 \tag{2.7}$$

pour laquelle nous cherchons une solution harmonique du type $p(x,t) = p(x)e^{j\omega t}$. La variation spatiale *p(x)* est solution de l'équation de Helmholtz

$$\frac{d^2p}{dx^2} + k^2 p = 0 \tag{2.8}$$

Avec des conditions aux limites judicieuses, la solution correspond à la propagation d'une onde non amortie

$$p(x) = p_0 e^{jkx} \tag{2.9}$$

Dans ce cas, l'équation d'onde (2.7) a donc pour solution générale une onde du type

$$p(x,t) = p_0 e^{j(kx+\omega t)} \tag{2.10}$$

qui se propage à la vitesse

$$\frac{\omega}{k} = c \tag{2.11}$$

Cette vitesse est égale à la vitesse du son et est indépendante de la fréquence d'excitation : le milieu est dit *non dispersif*. Ce n'est pas le cas des ondes éléments finis qui sont du type

$$p^h(x,t) = p_0 e^{j(k^h x+\omega t)} \tag{2.12}$$

où k^h dépend de la fréquence d'excitation. Les ondes éléments finis ont donc une vitesse de propagation

$$\frac{\omega}{k^h} = c^h \neq c \tag{2.13}$$

qui diffère de la vitesse du son et qui détruit le caractère non dispersif des ondes satisfaisant à l'équation de Helmholtz. En fait, le nombre d'onde éléments finis est une fonction non linéaire du nombre d'onde exact. Une méthode d'analyse de dispersion a été élaborée par F. Ihlenburg *et al.* [IHL95b], mais on en trouve déjà l'idée dans [HAR91].

Pour comprendre la méthode, considérons les matrices de rigidité ***K*** et de masse ***M*** au niveau élémentaire. Pour un élément de longueur *h*, les fonctions de forme sont données par (figure 2-1)

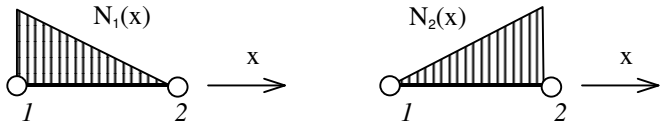

Figure 2-1: Fonctions de forme linéaires pour un élément unidimensionnel

Le système assemblé (1-11) peut alors s'écrire pour la partie acoustique seule en l'absence d'amortissement structural (***C***=0)

$$\begin{bmatrix} S(kh) & R(kh) & 0 & \cdots & \cdots & 0 \\ R(kh) & 2S(kh) & R(kh) & & & 0 \\ 0 & & \cdots & & & \vdots \\ \vdots & & & \cdots & \cdots & 0 \\ 0 & & & R(kh) & 2S(kh) & R(kh) \\ 0 & \cdots & \cdots & 0 & R(kh) & S(kh) \end{bmatrix} \boldsymbol{p}^h = h\boldsymbol{f} \tag{2.14}$$

où,

$$S(kh) = (1 - \frac{k^3 h^2}{3}) \text{ et } R(kh) = (-1 - \frac{k^2 h^2}{6}) \tag{2.15}$$

L'équation correspondant au nœud *n* peut être isolée. Le second membre étant nul si le nœud *n* n'appartient pas à la frontière. On cherche des solutions de type $p_n^h = e^{\alpha^h x_n}$. Ce qui aboutit à une équation du type

$$R(kh) + 2S(kh)\lambda + R(kh)\lambda^2 = 0 \tag{2.16}$$

où $\lambda = e^{\alpha^h h}$ pour un maillage régulier. La résolution de cette équation fournit le nombre d'onde k^h.

Cette méthode peut être généralisée à deux ou trois dimensions. Les équations qui en résultent sont plus compliquées mais peuvent être résolues numériquement [DER99]. L'article qui suit généralise la méthode d'analyse de dispersion à la méthode sans maillage EFGM à base polynomiale et compare celle-ci aux méthodes GLS, QSFEM et *p*.

L'article est un reprint de S. Suleau, A. Deraemaeker, Ph. Bouillard, 'Dispersion and pollution of meshless solutions for the Helmholtz equation', Comput. Methods Appl. Mech. Eng. 190 (2000) 639-657.

ELSEVIER

Comput. Methods Appl. Mech. Eng. 190 (2000) 639-657

Computer methods in applied mechanics and engineering

Dispersion and pollution of meshless solutions for the Helmholtz equation

Stéphane Suleau, Arnaud Deraemaeker, Philippe Bouillard*

Department of Continuum Mechanics, Université Libre de Bruxelles, CP 194/5 Av. F. D. Roosevelt 50, 1050 Brussels, Belgium

Received 14 June 1999

Abstract

It is well known today that the standard finite element method (FEM) is unreliable to compute approximate solutions of the Helmholtz equation for high wavenumbers due to the pollution effect, consisting mainly of the dispersion, i.e. the numerical wavelength is longer than the exact one. Unless highly refined meshes are used, FEM solutions lead to unacceptable solutions in terms of precision, while the use of very refined meshed increases the cost in terms of computational times. The paper presents an application of the Element-Free Galerkin Method (EFGM) and focuses on the dispersion analysis in two dimensions. It shows that it is possible to choose the parameters of the method in order to minimize the dispersion and to get extremely good results in comparison with the stabilized FEM. Moreover, the present meshless formulation is not restricted to regular distribution of nodes and a simple but real-life problem is investigated in order to show the improvement in the accuracy of the numerical results w.r. FEM results.

Keywords: Acoustics; Helmholtz equation; dispersion error; Element-Free Galerkin Method; meshless method

1. Introduction

The numerical solution of the Helmholtz equation, governing the wave propagation, is one of the main problems that has not yet been properly addressed because of the spurious phenomena inherent to this differential operator. In one dimension, the solutions are oscillatory of type $\sin(kx)$ where k is the wavenumber. The major aspects of the numerical solution are the approximation error and the pollution effect.

The discretization error can be split into the approximation error and the pollution error, [1] i.e. the error on the phase (dispersion error) and on the amplitude; for a summary of the pollution effect and demonstrations on industrial examples, see Reference [2]. The numerical wave is of dispersive character, i.e. the numerical wave propagates with a phase velocity ω/k^h different from the speed of sound c; for a theoretical analysis for the finite element method, see e.g. Reference [3].

Several authors have suggested methods to stabilize the finite element method: the Galerkin Least Square (GLS) [5] consists of a modification of the variational problem in order to minimize the dispersion, the Quasi-Stabilized Finite Element Method (QSFEM) [6] modifies the system matrix with the same goal and more recently a Residual-Free Finite Element Method (RFFEM) [7] was implemented for

* Corresponding author.
E-mail address: pbouilla@smc.ulb.ac.be (P. Bouillard)

the Helmholtz equation, etc. However, none of these methods eliminates the dispersion in a general two-dimensional case, see Reference [15] for a complete analysis.

Everybody seems nevertheless to agree that it is very advantageous to use a set of plane wave solutions of the homogenized Helmholtz equation as the local function basis. A natural and very efficient way to achieve this is to use a meshless formulation. I. Babuška and J. Melenk [8] suggest the partition of unity method while, in the present paper, the Element-Free Galerkin Method (EFGM) is investigated and seems particularly suited for that purpose.

The EFGM is based on the Moving Least Square Approximation (MSLA), first introduced by Lancaster *et al.* [9] in the field of surface and function smoothing. Recently, it has been extensively investigated by T. Belystchko et al. in the fields of elasticity and crack propagation problems [10-11]. The main advantages of the formulation are well known (no connections by nodes, easy pre- and postprocessing tasks). For the particular case of the Helmholtz equation, we also take advantage of the fact that the shape functions are non rational (see Reference [12]) and the local basis can naturally contain terms which are solution of the Helmholtz equation.

The paper is organized as follows. Sections 2 and 3 present the strong and variational forms of the acoustic problem. In section 4, the EFGM shape functions are defined and the method is applied to acoustics. Section 5 focuses on the dispersion effect and details the theory to compute the dispersion error. Section 6 presents numerical results obtained with polynomial and frequency dependent function bases, the latter leading to the exact solution of the problem for some directions of propagation of a plane wave. Section 7 gives the numerical comparison with the most popular stabilized finite element solutions showing that EFGM is very close to QSFEM in terms of precision of the solution. Finally, tests on a 2D real-life problem are reported in Section 8 showing the improvement in terms of accuracy on the numerical solution.

2. Strong formulation of the acoustic problem

The topics described in Sections 2 and 3 refer to strong and variational formulations of the harmonic forced response of the acoustic problem. They are recalls from Reference [16].

Consider the fluid inside a domain Ω with boundary Γ, let c be the speed of sound inside this medium and ρ the specific mass of the fluid. If p' denotes the field of acoustic pressure (small perturbations around a steady uniform state), the equation of wave propagation (1) is derived from the fundamental equations of continuum mechanics.

$$\Delta p' = \frac{1}{c^2}\frac{\partial^2 p'}{\partial t^2} \tag{1}$$

If the phenomena are assumed to be steady harmonic,

$$p' = p\exp(j\omega t) \tag{2}$$

where ω is the angular frequency, the spatial distribution p of the acoustic pressure (which is a complex variable) inside Ω, is solution of Helmholtz equation

$$\Delta p + k^2 p = 0 \tag{3}$$

where wavenumber k is defined by the ratio between the angular frequency and the speed of sound

$$k = \frac{\omega}{c} \tag{4}$$

Another important quantity of the acoustic analysis is the particle velocity $\boldsymbol{v}$ linked to the gradient of the acoustic pressure through the equation of motion

$$j\rho ck\boldsymbol{v} + \boldsymbol{\nabla} p = 0 \tag{5}$$

In order to completely define the acoustic problem, Helmholtz Equation (3) has to be associated with boundary conditions on Γ. The boundary is split into three parts

$$\Gamma = \Gamma_D \cup \Gamma_N \cup \Gamma_R \tag{6}$$

corresponding to different types of boundary conditions:

- Dirichlet boundary conditions (the acoustic pressure is prescribed)

$$p = \overline{p} \quad \text{on } \Gamma_D \tag{7}$$

- Neumann boundary conditions (the normal component of the velocity is prescribed)

$$v_n = \overline{v}_n \quad \text{or} \quad \boldsymbol{n}^t \boldsymbol{\nabla} p = -j\rho ck\overline{v}_n \quad \text{on } \Gamma_N \tag{8}$$

- Robin boundary conditions

$$v_n = A_n p \quad \text{or} \quad \boldsymbol{n}^t \boldsymbol{\nabla} p = -j\rho ckA_n p \quad \text{on } \Gamma_R \tag{9}$$

where A_n is the admittance coefficient modelling the structural damping.

Neumann boundary conditions correspond to vibrating panels while Robin boundary conditions correspond to absorbant panels. Conditions (7)-(9) have been defined for interior and exterior problems. For an infinite medium, the boundary condition at infinity is reduced by a DtN mapping on a fictitious sphere around the studied domain of the medium, leading to a boundary condition similar to (9).

3. Variational formulation of the acoustic problem

The variational formulation corresponding to the strong form presented in Section 2 is well known and in the following, only the main aspects will be emphasized. For more details, see Reference [12].
The space of admissible trial functions p is defined as

$$H_D^1(\Omega) = \left\{ p \in H^1(\Omega) \mid p = \overline{p} \, on \, \Gamma_D \right\} \tag{10}$$

and the space of homogeneous test functions w is

$$H_0^1(\Omega) = \left\{ w \in H^1(\Omega) \mid w = 0 \, on \, \Gamma_D \right\} \tag{11}$$

Both of them are subspaces of $H^1(\Omega)$, the Sobolev space of functions square-integrable together with their first derivatives. We define the functional Π

$$\Pi = \frac{1}{2} a(p, \tilde{p}) - \varphi(\tilde{p}) \tag{12}$$

with

$$a(p, \tilde{p}) : H_D^1 \times H_D^1 \to \square \;\Big|\; a(p, \tilde{p}) = \int_\Omega \left(\partial_i p \partial_i \tilde{p} - k^2 p\tilde{p} \right) d\Omega + \int_{\Gamma_R} j\rho ckA_n p\tilde{p} d\Gamma \tag{13}$$

$$\varphi(\tilde{p}) : H_D^1 \to \square \;\Big|\; \varphi(\tilde{p}) = -\int_{\Gamma_N} j\rho ck\overline{v}_n \tilde{p} d\Gamma \tag{14}$$

where the notation $\tilde{\bullet}$ stands for the complex conjugate.

The variational form corresponding to Helmholtz Equation (3) and boundary conditions (7)-(9) is expressed by

$$\text{Find } p \in H_D^1(\Omega) \mid \delta\Pi = 0 \quad \forall \delta p \in H_0^1 \tag{15}$$

It will be shown in Section 4 that, in the case of the Element-Free Galerkin Method, the approximation does not interpolate the nodal values. The variational formulation has to be modified accordingly to take into account Dirichlet boundary conditions (7) by introducing Lagrange multipliers λ in functional (12)

$$\Pi^* = \Pi + \int_{\Gamma_D} \lambda(\tilde{p} - \tilde{\tilde{p}}) d\Gamma \tag{16}$$

and variational form (15) is reformulated as

$$\text{Find } p \in H^1 \mid \delta\Pi^* = 0 \quad \forall \delta p \in H_0^1, \delta\lambda \in H^0 \tag{17}$$

Note that Dirichlet boundary conditions and their treatment by Lagrange multipliers have only been mentioned for completeness. In real-life acoustic problems, this kind of boundary conditions rarely appears. It is also interesting to mention that other and more recent techniques than Lagrange multipliers exist in order to take into account Dirichlet boundary conditions for EFGM [11].

4. Element-free Galerkin method applied to acoustics

4.1. Element-Free shape functions: the Moving Least Square Approximation

A complete report on the construction of the shape functions defining the EFGM can be found in many papers [10, 11, 12]. This paragraph gives only a brief overview of the main steps in the particular case of 2D problems.

The MLSA is defined on a cloud of n nodes, which are not connected by elements as it is required for the Finite Element Method (FEM). The nodes are located at $\boldsymbol{x}_I = (x_I, y_I)$ inside Ω ($I = 1,\ldots,n$). For each node I, we define a domain of influence characterized by a typical dimension size $d_{infl,I}$ (for two-dimensional problems, the domain is a disc of radius $d_{infl,I}$ or a square of half lengthside $d_{infl,I}$). These domains are defined to connect the nodes: two nodes are connected if their domains of influence intersect (see Fig. 1).

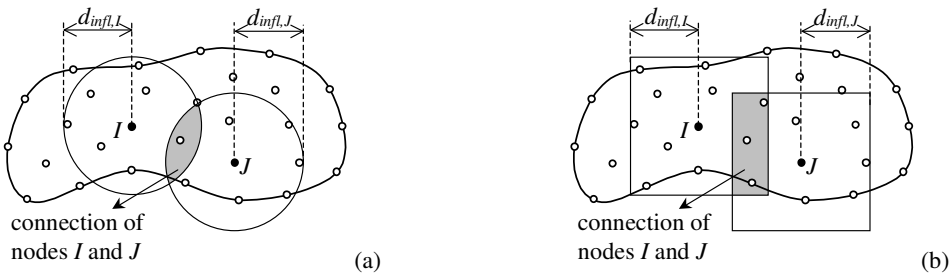

Fig. 1. Domains of influence and connection of nodes: (a) circular domains (b) square domains.

We also define a weight function w_I for each node, which is representative of the influence of the node $\boldsymbol{x}_I$ at a given point $\boldsymbol{x} = (x,y)$. This function is equal to unity at the node, decreasing when the distance to the node increases and zero outside the domain of influence of the node. For all the computations reported in this paper, we have used an exponential weight function, that can be defined either on a square domain of influence as the product of two one-dimensional weight functions

$$\begin{aligned} w(x,y) &= \frac{e^{-(2\frac{x-x_I}{d_{infl,I}})^2} - e^{-4}}{1-e^{-4}} \frac{e^{-(2\frac{y-y_I}{d_{infl,I}})^2} - e^{-4}}{1-e^{-4}} \quad (x \le d_{infl,I} \text{ and } y \le d_{infl,I}) \\ &= 0 \qquad\qquad (x >_{infl,I} \text{ or } y > d_{infl,I}) \end{aligned} \tag{18}$$

or on a circular domain as a function of d, the distance between point $\boldsymbol{x}$ and node $\boldsymbol{x}_I$

$$w(x,y) = \frac{e^{-(2\frac{d}{d_{infl,I}})^2} - e^{-4}}{1-e^{-4}} \quad (d \le d_{infl,I}) \qquad = 0 \quad (d >_{infl,I}) \tag{19}$$

The construction of the MLSA and the corresponding shape functions is based on the choice of a basis $\boldsymbol{P}(\boldsymbol{x})$ (dimension m) of functions which, in the case of 2D polynomials, are

$$\boldsymbol{P}^t(\boldsymbol{x}) = \boldsymbol{P}^t(x,y) = \{1, x, y\} \quad \text{(linear basis, } m = 3) \tag{20}$$

$$\boldsymbol{P}^t(\boldsymbol{x}) = \boldsymbol{P}^t(x,y) = \left\{1, x, y, x^2, xy, y^2\right\} \quad \text{(quadratic basis, } m = 6) \tag{21}$$

Polynomial bases are not the only choice: non-polynomial bases can also be chosen, as it will be seen in section 6, introducing for instance functions better suited for solving the Helmholtz equation.

The unknown p^h (acoustic pressure, the upper h stands for numerical solution) of the problem is built from

$$p^h(\boldsymbol{x}) = \boldsymbol{P}^t(\boldsymbol{x})\boldsymbol{a}(\boldsymbol{x}) \tag{22}$$

where the $\boldsymbol{a}(\boldsymbol{x})$ coefficients are non constant and are determined by minimizing a given norm (see References [10, 11]), leading to

$$\boldsymbol{a}(\boldsymbol{x}) = \boldsymbol{A}^{-1}(\boldsymbol{x})\boldsymbol{B}(\boldsymbol{x})\boldsymbol{p} \tag{23}$$

where $\boldsymbol{p}$ is the array of the nodal values p_I. $\boldsymbol{A}(\boldsymbol{x})$ and $\boldsymbol{B}(\boldsymbol{x})$ are the matrices defined by

$$\boldsymbol{A}(\boldsymbol{x}) = \sum_{I=1}^{N} w_I(\boldsymbol{x})\boldsymbol{P}(\boldsymbol{x}_I)\boldsymbol{P}^t(\boldsymbol{x}_I) \tag{24}$$

$$\boldsymbol{B}(\boldsymbol{x}) = \left[w_I(\boldsymbol{x})\boldsymbol{P}(\boldsymbol{x}_I), ..., w_n(\boldsymbol{x})\boldsymbol{P}(\boldsymbol{x}_n)\right] \tag{25}$$

where n is the number of nodes. Equation (22) can then be written as

$$p^h(\boldsymbol{x}) = \boldsymbol{N}(\boldsymbol{x})\boldsymbol{p} \tag{26}$$

where $\boldsymbol{N}(\boldsymbol{x})$ contains the shape functions and is defined by

$$\boldsymbol{N}(\boldsymbol{x}) = \boldsymbol{P}^t(\boldsymbol{x})\boldsymbol{A}^{-1}(\boldsymbol{x})\boldsymbol{B}(\boldsymbol{x}) \tag{27}$$

At this point, we have to underline the fact that the $m*m$ matrix $\boldsymbol{A}(\boldsymbol{x})$ is the sum of matrices of rank 1. As $w_I(\boldsymbol{x})$ is zero for all the nodes that do not influence point $\boldsymbol{x}$, $\boldsymbol{A}(\boldsymbol{x})$ is the sum of only $n'(\boldsymbol{x})$ matrices of rank 1, where $n'(\boldsymbol{x})$ is the number of nodes influencing $\boldsymbol{x}$. The rank of $\boldsymbol{A}(\boldsymbol{x})$ must be equal to m since (27) needs the computation of $\boldsymbol{A}^{-1}(\boldsymbol{x})$. This leads to the necessary (but not sufficient) condition of existence of the MLSA: $n'(\boldsymbol{x}) \ge m$, i.e. each point of Ω has to be influenced by at least as many nodes as there are functions in the basis $\boldsymbol{P}(\boldsymbol{x})$. The shape functions defined by (27) have the following properties:

- The approximation is consistent with respect to the functions of the basis, i.e. each of these functions can be exactly reproduced by the approximation. In particular, if the constant term 1 is part of the basis, we have

$$\sum_{I=1}^{n} N_I(\boldsymbol{x}) = 1 \quad \forall\, \boldsymbol{x} \in \Omega \tag{28}$$

- The approximation does not interpolate the nodal values

$$N_I(x_J) \neq \delta_{IJ} \tag{29}$$

meaning that a shape function is not equal to unity at the corresponding node and is non zero at other nodes, as it is the case for the FEM shape functions. For this reason, Lagrange multipliers were introduced in variational form (17) in order to enforce Dirichlet boundary conditions (7).
Fig. 2 represents a shape function as well as its first x-derivative, in the two-dimensional case, for an interior node of a regular distribution of nodes (the internodal spacing is called h and is constant). The linear basis (20) is used and the sizes of the domains of influence are chosen identical for all nodes (the value considered for Fig. 2 is $d_{infl} = 3h$). Note that for square domains and for the limit case

$$d_{infl} \to h \tag{30}$$

the EFGM shape functions tend to the standard FEM bilinear shape functions defined on a regular mesh (Fig. 3).

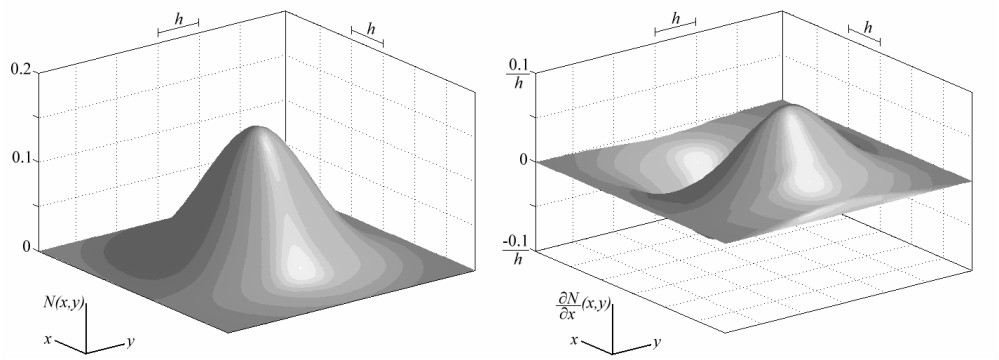

Fig. 2. EFGM 2D-shape function and its first x-derivative
(linear basis, regular distribution of nodes, square domains of influence with $d_{infl} = 3h$)

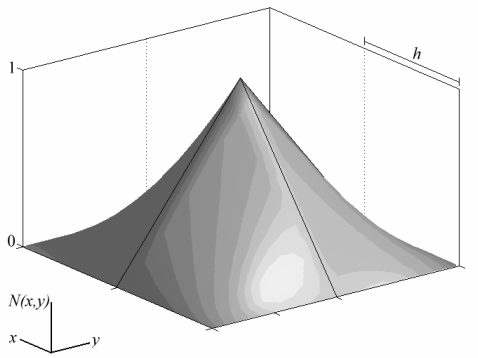

Fig. 3. With a linear basis, a regular distribution of nodes, square domains of influence with $d_{infl} \to h$,
the EFGM shape function tends to the standard FEM bilinear shape function

4.2. Application to the acoustic problem

The application of the EFGM to the acoustic problem formulated in Sections 2 and 3 is completely detailed in Reference [12]. We choose to approximate the acoustic pressure field and its variation by

$$p^h = \boldsymbol{N}\boldsymbol{p} \qquad \delta p^h = \boldsymbol{N}\delta\boldsymbol{p} \tag{31}$$

while the Lagrange multipliers and their variation are chosen to be

$$\lambda^h = \boldsymbol{\aleph}\boldsymbol{\Lambda} \qquad \delta\lambda^h = \boldsymbol{\aleph}\delta\boldsymbol{\Lambda} \tag{32}$$

where $\boldsymbol{\aleph}$ is a Lagrange interpolant.

Introducing (31)-(32) into variational form (17), we obtain a linear system of equations similar to the system obtained for a problem of structural dynamics

$$\begin{bmatrix} \boldsymbol{K} + j\rho ck\boldsymbol{C} - c^2k^2\boldsymbol{M} & \boldsymbol{K}_{p\lambda} \\ \boldsymbol{K}_{p\lambda}^t & 0 \end{bmatrix} \begin{Bmatrix} \boldsymbol{p} \\ \boldsymbol{\Lambda} \end{Bmatrix} = \begin{Bmatrix} -j\rho ck\boldsymbol{f} \\ \boldsymbol{b} \end{Bmatrix} \tag{33}$$

where the matrices and vectors are defined as follows

- the "stiffness" matrix $\boldsymbol{K}$

$$\boldsymbol{K} = \int_\Omega (\boldsymbol{\nabla N})^t (\boldsymbol{\nabla N})\, d\Omega \tag{34}$$

- the "damping" matrix $\boldsymbol{C}$ (Robin boundary conditions)

$$\boldsymbol{C} = \int_{\Gamma_R} \boldsymbol{N}^t \boldsymbol{N} A_n d\Gamma \tag{35}$$

- the "mass" matrix $\boldsymbol{M}$

$$\boldsymbol{M} = \frac{1}{c^2}\int_\Omega \boldsymbol{N}^t \boldsymbol{N} d\Omega \tag{36}$$

- the vector $\boldsymbol{p}$ of nodal pressure unknowns
- the vector $\boldsymbol{\Lambda}$ of nodal Lagrange multipliers unknowns
- the matrix $\boldsymbol{K}_{p\lambda}$, coupling the two kinds of unknowns

$$\boldsymbol{K}_{p\lambda} = \int_{\Gamma_D} \boldsymbol{N}^t \boldsymbol{\aleph} d\Gamma \tag{37}$$

- the vector $\boldsymbol{f}$, containing the prescribed normal velocities (Neumann boundary conditions)

$$\boldsymbol{f} = \int_{\Gamma_N} \boldsymbol{N}^t \bar{v}_n d\Gamma \tag{38}$$

- the vector $\boldsymbol{b}$, containing the prescribed values of the pressure (Dirichlet boundary conditions)

$$\boldsymbol{b} = \int_{\Gamma_D} \boldsymbol{\aleph}^t \bar{p} d\Gamma \tag{39}$$

5. Dispersion analysis for 2D Helmholtz equation

The numerical computation of waves always encounters a major problem: the dispersion effect. The numerical wave does not propagate at the same speed as the exact one, the dispersion can thus be observed as a difference of phase between both waves. For a given numerical method, the difference can be predicted, depending on the wavenumber k. This a priori computation of the dispersion has first been developped for standard FEM and other modified finite element methods (GLS, QSFEM, RFFEM…) in Reference [15]. It is also detailed in [16] for the one dimensional EFGM case, and is presented in this section for the two dimensional EFGM computations.

For the following computations, we will consider a regular distribution of nodes of internodal spacing h. All the domains of influence have the same size d_{infl} (defined in Section 3).
First of all, we will prove that if we assume an harmonic evolution of the nodal values, the MLSA derived from these values is also harmonic. This statement could a priori seem obvious, but it is not the case due to the fact that the MLSA does not interpolate the nodal values. As we will see, this property is only valid under some assumptions: h must be a constant value, and the domains of all nodes must be similar (theorem 1). The harmonic evolution of the MLSA is a requirement for theorem 2: the prediction of the discrete wavenumber k^h of the EFGM solution.

Those theorems are a generalization of the ones proposed in Reference [16] for the 1D dispersion analysis. For all the following developments, we will consider rectangular domains of influence, the square domains being a particular case. This assumption is in no case a restriction: the equations are also valid for circular domains of influence when replacing by zero the contribution of points located outside the circle but inside the square. Furthermore, all the nodes will be numbered using double indices.

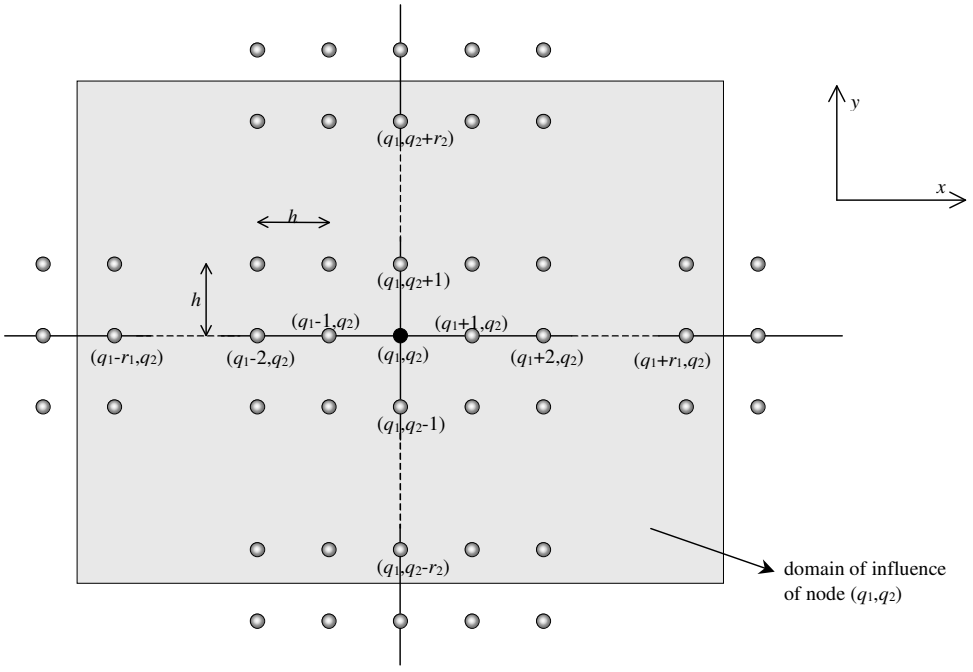

Fig. 4. Definition of parameters r_1 and r_2.

Theorem 1. *If the nodal values have an harmonic evolution with wavenumber k^h, the MLSA has also an harmonic evolution with the same wavenumber.*

Proof. We consider a regular 2D distribution of nodes, and we define integer parameters r_1 and r_2 such as one node influences r_1 nodes on each side along direction x, and r_2 nodes on each side along direction y. One domain contains then $(2r_1+1)(2r_2+1)$ nodes (see Fig. 4).

We assume that the nodal values follow an harmonic evolution of wavenumber k^h (plane wave propagating in the direction of the angle θ, measured from axis x), so the nodal value for node (i,j) is given by

$$p_{i_1,i_2} = A\exp(jk^h(x_{i_1}\cos\theta + y_{i_2}\sin\theta)) \tag{40}$$

After the moving least square approximation, the numerical solution for the acoustic pressure is, at an interior node (q_1,q_2)

$$\begin{aligned} p^h(x_{q_1},y_{q_2}) &= \sum_{i_1=q_1-r_1}^{q_1+r_1}\sum_{i_2=q_2-r_2}^{q_2+r_2} N_{i_1,i_2}(x_{q_1},y_{q_2})\,p_{i_1,i_2} \\ &= \sum_{i_1=q_1-r_1}^{q_1+r_1}\sum_{i_2=q_2-r_2}^{q_2+r_2} N_{i_1,i_2}(x_{q_1},y_{q_2})A\exp(jk^h(x_{i_1}\cos\theta + y_{i_2}\sin\theta)) \end{aligned} \tag{41}$$

and at another interior node $(q_1+\gamma_1,q_2+\gamma_2)$ $(\gamma_1,\gamma_2\in\mathbb{Z})$

$$\begin{aligned} p^h(x_{q_1+\gamma_1},y_{q_2+\gamma_2}) &= p^h(x_{q_1}+\gamma_1 h, y_{q_2}+\gamma_2 h) \\ &= \sum_{i_1=q_1+\gamma_1-r_1}^{q_1+\gamma_1+r_1}\sum_{i_2=q_2+\gamma_2-r_2}^{q_2+\gamma_2+r_2} N_{i_1,i_2}(x_{q_1+\gamma_1},y_{q_2+\gamma_2})A\exp(jk^h(x_{i_1}\cos\theta + y_{i_2}\sin\theta)) \end{aligned} \tag{42}$$

If we change the summation indices in (42) by choosing $i'_1 = i_1 - \gamma_1$ and $i'_2 = i_2 - \gamma_2$, we get

$$p^h(x_{q_1+\gamma_1},y_{q_2+\gamma_2}) = \sum_{i'_1=q_1-r_1}^{q_1+r_1}\sum_{i'_2=q_2-r_2}^{q_2+r_2}\begin{pmatrix} N_{i'_1+\gamma_1,i'_2+\gamma_2}(x_{q_1+\gamma_1},y_{q_2+\gamma_2}) \\ A\exp(jk^h((x_{i'_1}+\gamma_1 h)\cos\theta + (y_{i'_2}+\gamma_2 h)\sin\theta)) \end{pmatrix} \tag{43}$$

Due to the 2D periodicity of the distribution of nodes (h constant) and the fact that all the domains of influence are identical, there is also a repetitive sequence for the shape functions

$$N_{i'_1+\gamma_1,i'_2+\gamma_2}(x_{q_1+\gamma_1},y_{q_2+\gamma_2}) = N_{i'_1,i'_2}(x_{q_1},y_{q_2}) \tag{44}$$

and (43) becomes

$$\begin{aligned} &p^h(x_{q_1+\gamma_1},y_{q_2+\gamma_2}) \\ &= \sum_{i'_1=q_1-r_1}^{q_1+r_1}\sum_{i'_2=q_2-r_2}^{q_2+r_2} N_{i'_1,i'_2}(x_{q_1},y_{q_2})A\exp(jk^h((x_{i'_1}+\gamma_1 h)\cos\theta + (y_{i'_2}+\gamma_2 h)\sin\theta)) \end{aligned} \tag{45}$$

A comparison of (41) and (45) immediately leads to

$$p^h(x_{q_1+\gamma_1},y_{q_2+\gamma_2}) = p^h(x_{q_1},y_{q_2})\exp(jk^h(\gamma_1 h\cos\theta + \gamma_2 h\sin\theta)) \quad \forall\gamma_1,\gamma_2\in\mathbb{Z} \tag{46}$$

meaning that the MLSA solution at the nodes has also an harmonic evolution, with the same wavenumber k^h and the same angle θ of propagation as the nodal values. ■

Theorem 2. *On a 2D regular distribution of nodes, with a constant size for the domains of infuence, the wavenumber k^h of the numerical wave propagating in the direction θ can be a priori determined and is solution of the following equation*

$$\sum_{I=0}^{s_1}\sum_{J=0}^{s_2}\beta_I\beta_J\cos(Ik^h h\cos\theta)\cos(Jk^h h\sin\theta)X_{I,J} = 0$$

The coefficients β_I, β_J and $X_{I,J}$ of the cosine terms will be defined in the proof.

This theorem is the generalization of Reference [16].

Proof. As mentioned above, we consider a uniform distribution of nodes and identical domains of influence for all nodes. We define here two new parameters s_1 and s_2 such as domains of influence of nodes (q_1,q_2) and (q_1+s_1,q_2+s_2) intersect, while neither nodes (q_1,q_2) and (q_1+s_1+1,q_2+s_2), neither nodes (q_1,q_2) and (q_1+s_1,q_2+s_2+1) are connected. Parameters s_1 and s_2 represent the connectivities between nodes along directions x and y (see Fig. 5).

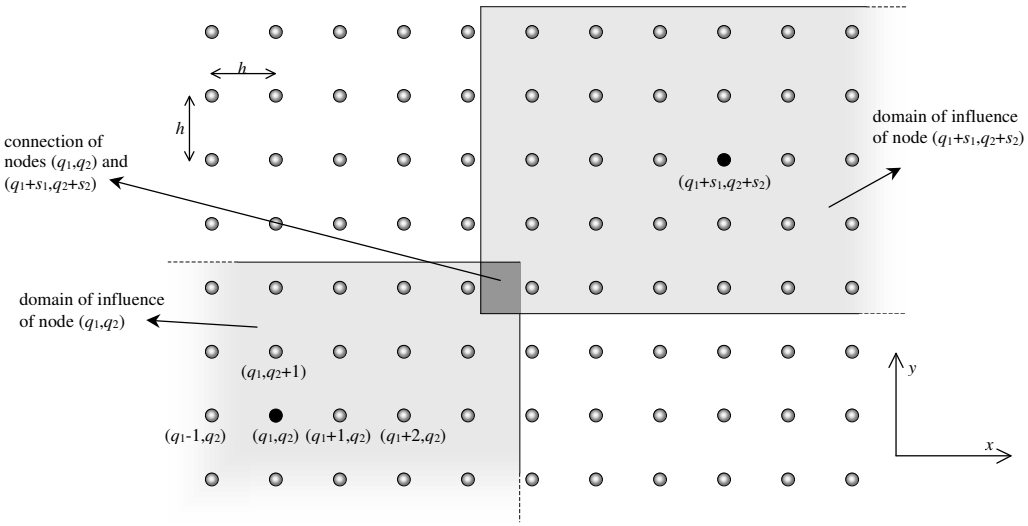

Fig. 5. Definition of parameters s_1 and s_2.

If we consider only interior nodes, not concerned by any boundary condition, meaning that the corresponding terms of $\boldsymbol{C}$ and $\boldsymbol{f}$ are zero, system (33) has the following banded form

$$\begin{bmatrix} \ddots & \ddots & \ddots & \ddots & & \ddots & \ddots & \ddots & \ddots & \ddots & & \ddots & \ddots & \ddots & \ddots & \ddots & \\ X_{s_1,s_2} & \cdots & X_{s_1,0} & \cdots & X_{s_1,s_2} & \cdots & X_{0,s_2} & \cdots & X_{0,0} & \cdots & X_{0,s_2} & \cdots & X_{s_1,s_2} & \cdots & X_{s_1,0} & \cdots & X_{s_1,s_2} & \\ & X_{s_1,s_2} & \cdots & X_{s_1,0} & \cdots & X_{s_1,s_2} & \cdots & X_{0,s_2} & \cdots & X_{0,0} & \cdots & X_{0,s_2} & \cdots & X_{s_1,s_2} & \cdots & X_{s_1,0} & \cdots & X_{s_1,s_2} & \\ & & X_{s_1,s_2} & \cdots & X_{s_1,0} & \cdots & X_{s_1,s_2} & \cdots & X_{0,s_2} & \cdots & X_{0,0} & \cdots & X_{0,s_2} & \cdots & X_{s_1,s_2} & \cdots & X_{s_1,0} & \cdots & X_{s_1,s_2} \\ & & & \ddots & \ddots & \ddots & \ddots & \ddots & & \ddots & \ddots & \ddots & \ddots & \ddots & & \ddots & \ddots & \ddots & \ddots \end{bmatrix} \begin{Bmatrix} \vdots \\ p_{i_1,i_2-1} \\ p_{i_1,i_2} \\ p_{i_1,i_2+1} \\ \vdots \end{Bmatrix} = \begin{Bmatrix} \vdots \\ 0 \\ 0 \\ 0 \\ \vdots \end{Bmatrix} \tag{47}$$

where we have defined

$$X_{I,J} = K_{I,J} - \omega^2 M_{I,J} \tag{48}$$

the term of $\boldsymbol{K} - \omega^2 \boldsymbol{M}$ connecting node (i_1,i_2) and (i_1+I,i_2+J), $\forall$ i_1, i_2. We consider here only shape functions that are both x- and y-symmetric, having for consequence that each node has equal connections in directions $-x$ and $+x$, as well as for $-y$ and $+y$. This leads to the fact that terms $X_{I,J}$, $X_{-I,-J}$, $X_{-I,J}$ and $X_{I,-J}$ are all eqal and will be from now noted $X_{|I|,|J|}$.

If we isolate equation corresponding to node (i_1,i_2), we get

$$\sum_{I=-s_1}^{+s_1} \sum_{J=-s_2}^{+s_2} X_{|I|,|J|} p_{i_1+I,i_2+J} = 0 \tag{49}$$

If we assume that the nodal values of the acoustic pressure have an harmonic evolution (40) with wavenumber k^h and angle θ of propagation, meaning that the MLSA solution if a plane wave propagating in the direction θ (theorem 1), (49) becomes

$$\sum_{I=-s_1}^{+s_1}\sum_{J=-s_2}^{+s_2} X_{|I|,|J|} A\exp(jk^h(x_{I_1}+Ih)\cos\theta)\exp(jk^h(y_{I_2}+Jh)\sin\theta)=0 \tag{50}$$

or

$$\sum_{I=-s_1}^{+s_1}\sum_{J=-s_2}^{+s_2} X_{|I|,|J|} A\exp(jk^h Ih\cos\theta)\exp(jk^h Jh\sin\theta)=0 \tag{51}$$

We define the following notation

$$\beta_I=\begin{cases}1 \ \ if\ I=0\\ 2 \ \ if\ I\in\ \square_0\end{cases} \tag{52}$$

Equation (51) becomes

$$\sum_{I=0}^{s_1}\sum_{J=0}^{s_2}\beta_I\beta_J\cos(Ik^h h\cos\theta)\cos(Jk^h h\sin\theta)X_{I,J}=0 \tag{53}$$

This last equation has for unknown k^h (or $k^h h$, which is the non dimensional version of the wavenumber). After computation of the stiffness and mass coefficients (48), we will be able to a priori determine the discrete wavenumber k^h, for given values of k and the angle of propagation θ. ■

Dispersion error. In all the following computations, we will measure the dispersion by

$$\varepsilon=\frac{k-k^h}{k}=\frac{kh-k^h h}{kh} \tag{54}$$

defined as the relative phase difference between the exact and numerical waves.

6. Numerical results for the dispersion

We present here the two-dimensional results of dispersion obtained for EFGM, obtained by solving Equation (53), for a regular distribution of nodes (internodal spacing h). After having chosen a value of k (or the non-dimensional wavenumber kh) in the Helmholtz equation, we can compute coefficients $X_{I,J}$ (48) of the matrix of linear system (47). A value of the angle θ must also be chosen. Then, through a numerical resolution of (53), k^h (or $k^h h$) can be obtained as a function of k (or kh) and θ.

In Section 6.1., we present the dispersion results when a polynomial basis is used to build the EFGM shape functions. Section 6.2. goes further, presenting dispersion results for special bases, leading to frequency-dependant shape functions, enabling us to obtain an improved accuracy for the numerical solution.

6.1. Study of EFGM dispersion with a polynomial basis

Throughout this whole section, we will focus on the EFGM built with polynomial bases. Some results are plotted in Fig. 6. For three different values of θ, the computed value of $k^h h$ is presented as a function of kh, and compared to kh. The computations were performed for several values of d_{infl}, using a linear basis (20) and square domains of influence. Note that the case $d_{infl} = h$ corresponds to the Finite Element Method (bilinear shape functions defined on square elements, see Fig. 3).

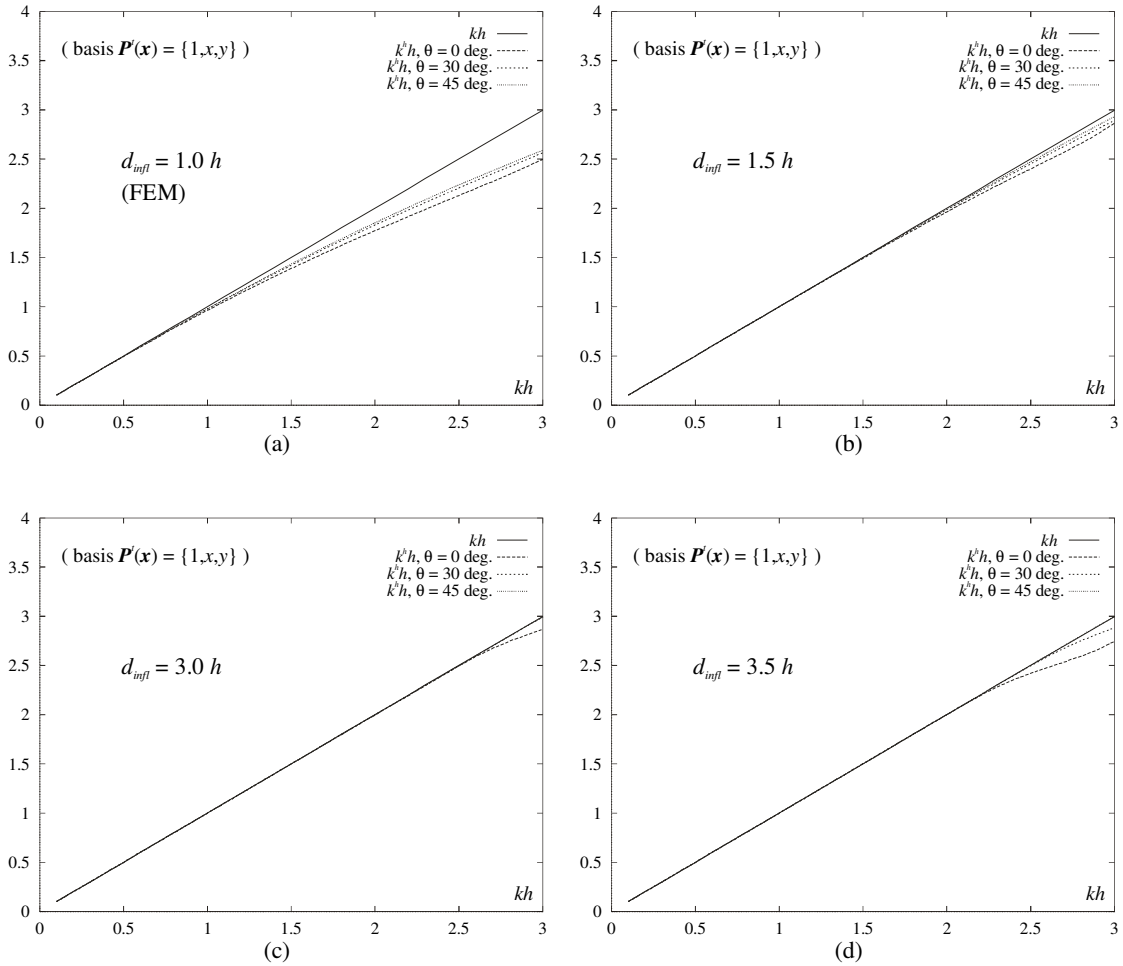

Fig. 6. Dispersion wavenumber of the EFGM wave, for $\theta = 0°, 30°, 45°$
(a) $d_{infl} = 1.0\ h$ (FEM) (b) $d_{infl} = 1.5\ h$ (c) $d_{infl} = 3.0\ h$ (d) $d_{infl} = 3.5\ h$

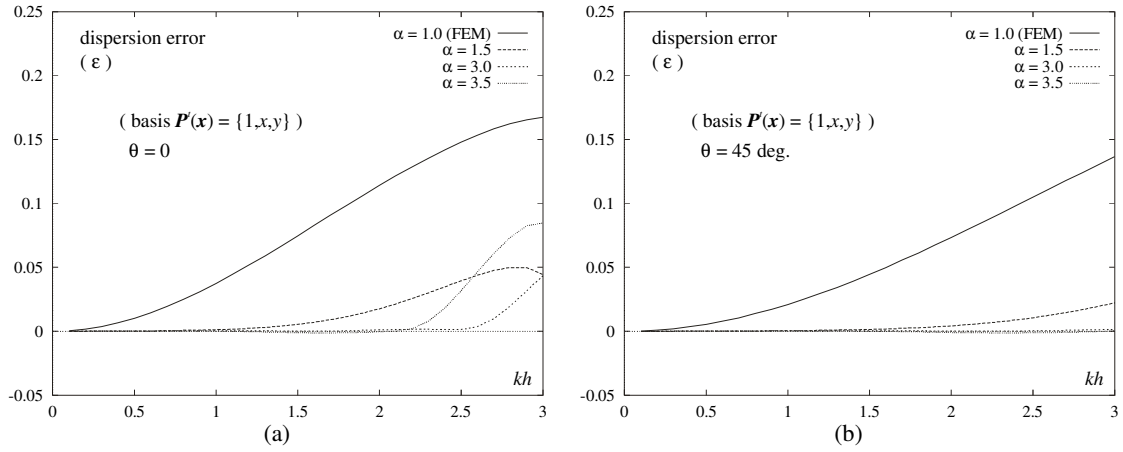

Fig. 7. Dispersion error ε of the EFGM wave for several values of the size of the domains of influence ($\alpha = d_{infl}/h$)
(a) angle of propagation $\theta = 0°$. (b) $\theta = 45°$.

Fig. 7 summarizes the dispersion results of Fig. 6: the dispersion error ε defined by Equation (54) is given as a function of kh, for $\theta = 0$ and $\theta = 45°$. It can be seen, from Fig.s 6 and 7, that the dispersion error increases when kh increases. But it has to be noticed that EFGM with $d_{infl} = 1.5\ h$ or $d_{infl} = 3.0\ h$ has a better behaviour than FEM ($d_{infl} = h$). For larger domains of influence (3.5 h), the dispersion increases, while still remaining smaller than FEM. There is thus an optimal range for the size of the domains of influence.

As the size of the domains of influence is a major parameter of the EFGM, its effect on the dispersion error is investigated here. The dispersion error has been computed for two values of the wavenumber ($kh = 1.0$ and $kh = 2.5$) as a function of the size d_{infl}, for a range of the angle of propagation varying from 0 up to 90° (Fig. 8 and 9). The representations of Fig. 8 and 9 start from the value $d_{infl}/h = 1.0$, which is the FEM case.

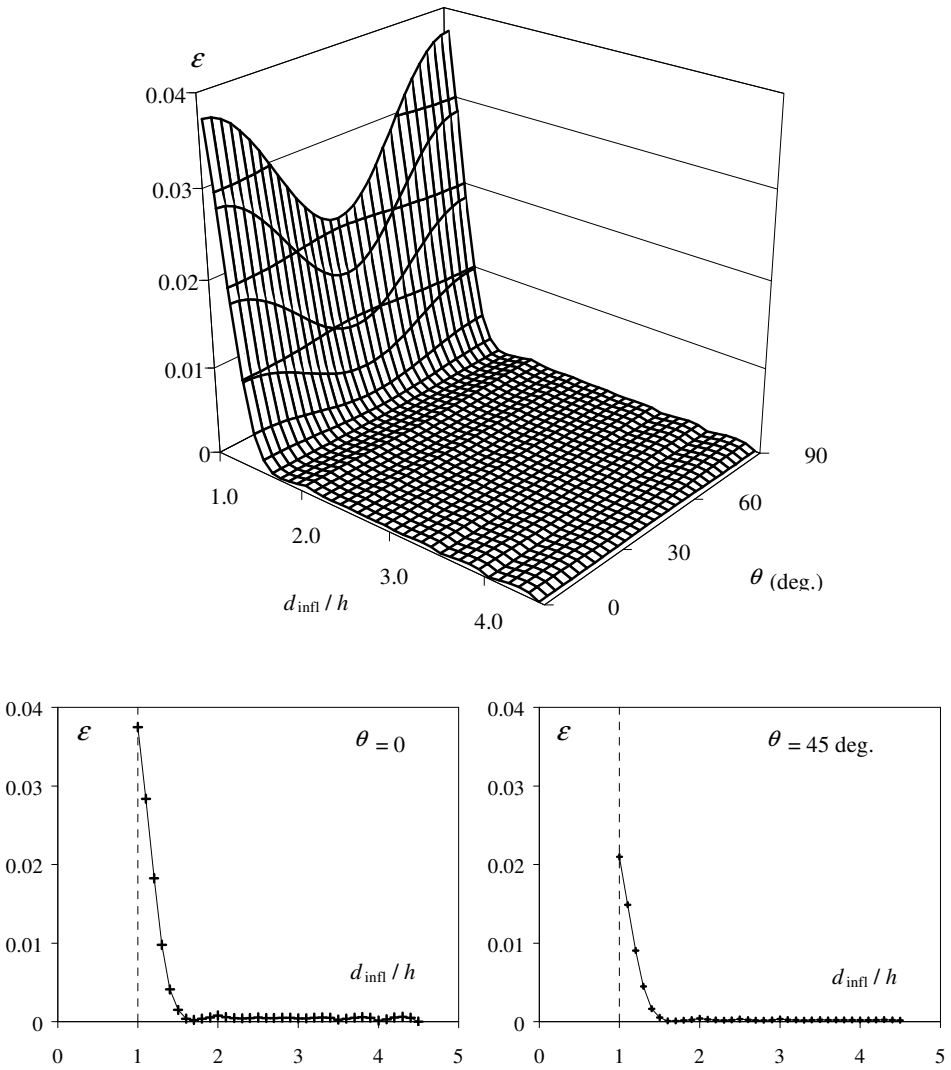

Fig. 8. Dispersion error ε of the EFGM as a function of the size of the domains of influence and of the direction of propagation θ (computed for $kh = 1.0$)

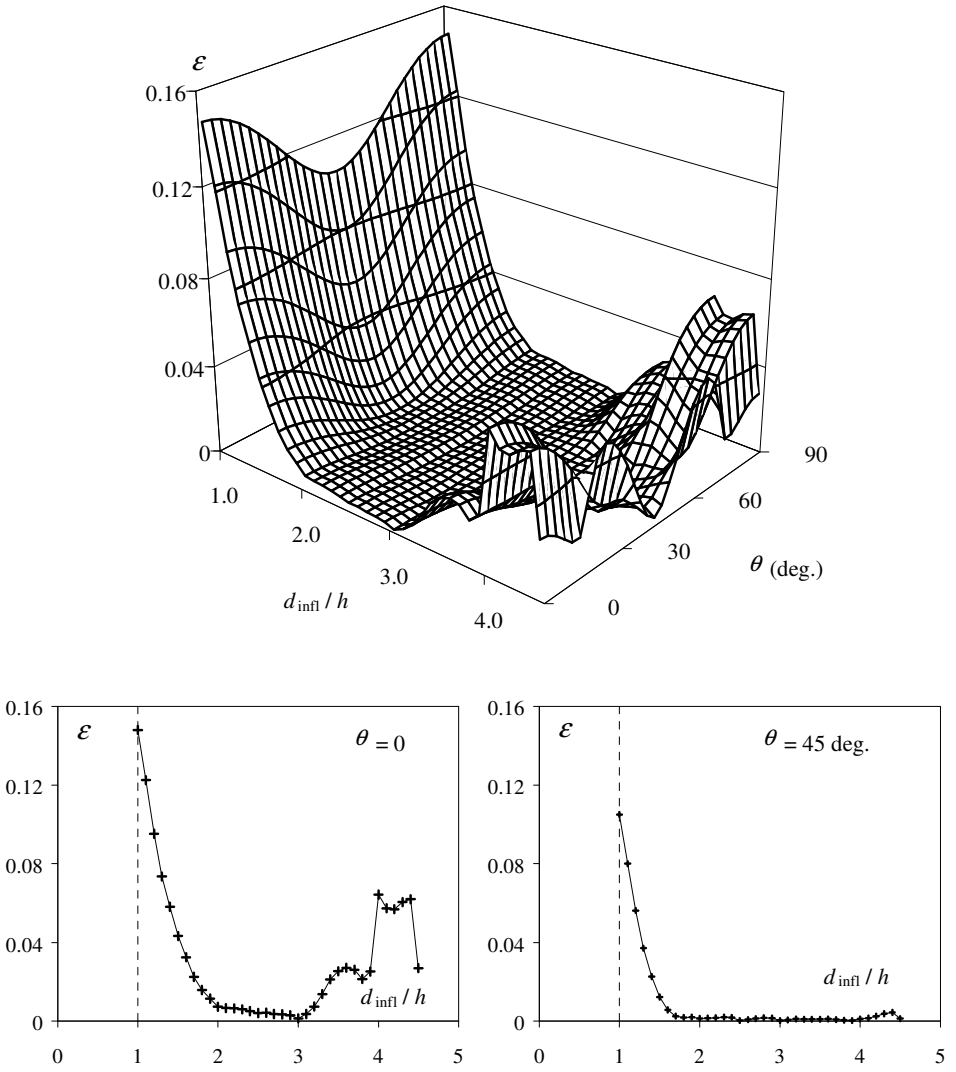

Fig. 9. Dispersion error ε of the EFGM as a function of the size of the domains of influence and of the direction of propagation θ (computed for $kh = 2.5$)

These results show the advantages of EFGM compared to standard FEM when it is applied to the resolution of the Helmholtz equation. When d_{infl}/h increases from its minimum value 1 (bilinear FEM on square elements), the dispersion error decreases. But for very large domains, especially when kh is also large, the quality of EFGM becomes poor. As for previous one-dimensional studies, there seems to be an optimal range given by $2h < d_{infl} < 3h$.

We will now examine the evolution of the dispersion error with the angle of propagation θ of the plane wave. This is done on Fig. 10, where we compare FEM and EFGM ($d_{infl} = 2.5\ h$, linear basis), for two values of the non-dimensional wavenumber ($kh = 1.0$ and $kh = 2.5$). We can note that for both methods, the dispersion is maximum for $\theta = 0$, while a minimum for the dispersion is reached when the angle is equal to 45°. We can also already notice the significant improvement of switching from standard FEM to EFGM in terms of dispersion: it it reduced by a factor around 50, even much more for some values of θ. Further comparisons will be presented in Section 7, including comparisons with other modified Finite Element Methods.

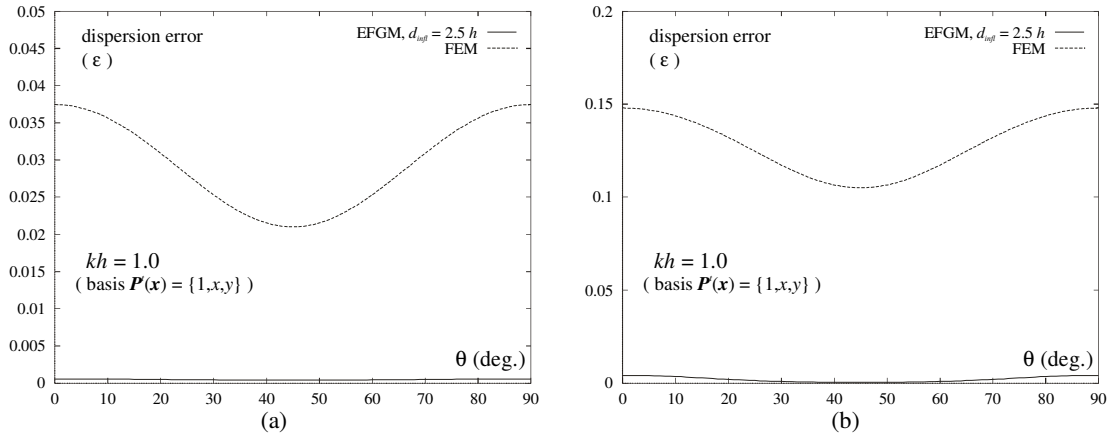

Fig. 10. Dispersion error as a function of θ. Comparison of standard FEM and EFGM with d_{infl} = 2.5 h.
(a) kh = 1.0 (b) kh = 2.5

6.2. Further reduction of the dispersion: frequency-dependant shape functions

As it has already been done in the 1D case (Reference [16]), it is possible to construct shape functions that are better suited for the wave representation, especially for the high wavenumbers. These shape functions include an oscillatory behaviour and are frequency-dependent: they make use of a basis including sine and cosine terms.

We remember that the 1D basis used in Reference [16] was given by

$$\boldsymbol{P}^t(x) = \{1, \cos(kx), \sin(kx)\} \tag{55}$$

enabling us to completely eliminate the dispersion in 1D: the waves of wavenumber k can be exactly represented by the basis functions, and the EFGM solution is exact everywhere.

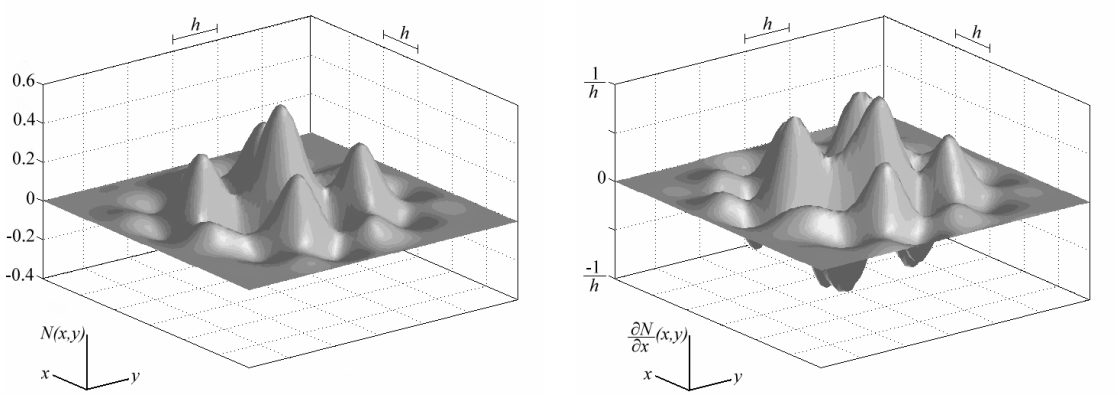

Fig. 11. Frequency-dependent shape function and its first x-derivative, built form basis (56), with kh = 4.0, $\tilde{\theta}$ =30°.

For the 2D case, it is not possible to completely eliminate the dispersion for every θ by the use of a numerical method, as it can be theoretically proved (Reference [15]). But it is possible to eliminate it for some values of θ, and minimize it for the close values. Consider for example the use of the following basis

$$\boldsymbol{P}^t(x) = \begin{Bmatrix} 1, \cos(kx\cos\tilde{\theta} + ky\sin\tilde{\theta}), \sin(kx\cos\tilde{\theta} + ky\sin\tilde{\theta}), \\ \cos(-kx\sin\tilde{\theta} + ky\cos\tilde{\theta}), \cos(-kx\sin\tilde{\theta} + ky\cos\tilde{\theta}) \end{Bmatrix} \tag{56}$$

The MLSA built from basis (56) is able to exactly reproduce plane waves of wavenumber k, propagating in directions $\tilde{\theta}$ and $\tilde{\theta} + \pi/2$. The corresponding shape function and its first x-derivative are represented at Fig. 11, for the particular case $kh = 4.0$ and $\tilde{\theta} = 30°$.

As the EFGM leads to the exact solution for $\tilde{\theta}$ and $\tilde{\theta} + \pi/2$, the dispersion for these directions is zero. The dispersion error can be computed as a function of θ, by numerically solving Equation (53). As mentioned in Section 5.2, this equation is only valid for shape functions that are x and y-symmetric, so we have made the computations for $\tilde{\theta} = 0°$ (Fig. 12a) and $\tilde{\theta} = 45°$ (Fig. 12b).

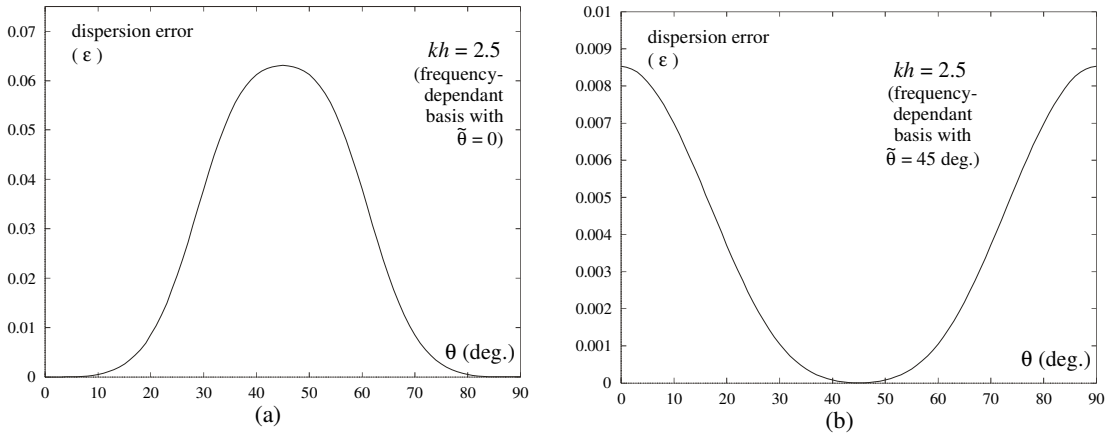

Fig. 12. Dispersion error $\varepsilon(kh = 2.5)$ for the frequency-dependent shape functions built from basis (56).
(a) $\tilde{\theta} = 0°$ (b) $\tilde{\theta} = 45°$.

As expected, we can observe on Figs. 12a and 12b that the dispersion error is zero when $\theta = \tilde{\theta}$ and $\theta = \tilde{\theta} + \pi/2$, because the EFGM shape functions are able to exactly reproduce the plane waves propagating in those directions. The error for angles close to these ones is relatively low. However, the dispersion for the wave of angle $\theta = \tilde{\theta} + \pi/4$ is rather high, and higher than the corresponding one obtained with a linear basis (refer to Fig. 10b): this is obviously due to the fact that the basis and the corresponding shape functions are not well suited for this angle of propagation.

The remedy to this last problem can be easily found. The frequency dependent basis can be enriched with other basis functions, corresponding to other angles of propagation. Consider for example the following basis

$$\begin{aligned} \boldsymbol{P}^t(x) = \{ \; & 1, \cos(kx\cos\tilde{\theta}_1 + ky\sin\tilde{\theta}_1), \sin(kx\cos\tilde{\theta}_1 + ky\sin\tilde{\theta}_1), \\ & \cos(-kx\sin\tilde{\theta}_1 + ky\cos\tilde{\theta}_1), \cos(-kx\sin\tilde{\theta}_1 + ky\cos\tilde{\theta}_1), \\ & \cos(kx\cos\tilde{\theta}_2 + ky\sin\tilde{\theta}_2), \sin(kx\cos\tilde{\theta}_2 + ky\sin\tilde{\theta}_2), \\ & \cos(-kx\sin\tilde{\theta}_2 + ky\cos\tilde{\theta}_2), \cos(-kx\sin\tilde{\theta}_2 + ky\cos\tilde{\theta}_2) \; \} \end{aligned} \tag{57}$$

It leads to the exact solution for $\tilde{\theta}_1$, $\tilde{\theta}_2$, $\tilde{\theta}_1 + \pi/2$ and $\tilde{\theta}_2 + \pi/2$. Fig. 13 shows the dispersion results obtained with $kh = 2.5$, the two angles chosen are $\tilde{\theta}_1 = 0°$ and $\tilde{\theta}_2 = 45°$. The dispersion error is zero for the directions of propagation contained in the basis, and it is kept at a very low level for other directions (inferior to 0.002 for $kh = 2.5$, while the corresponding error for standard FEM is in the range 0.10 to 0.15 (Fig. 10b)). However, we have to keep in mind that adding functions to the basis implies increasing the size of the domains of influence, and so the number of computations.

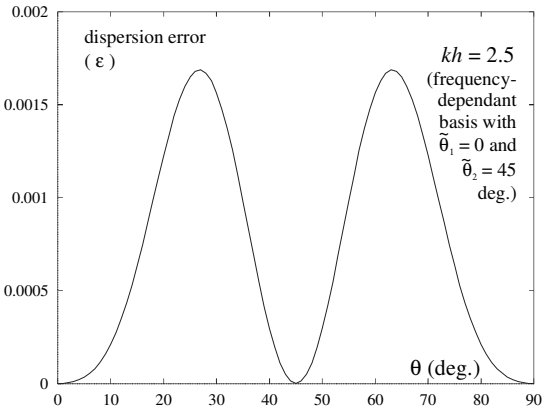

Fig. 13. Dispersion error ε (kh = 2.5) for the frequency-dependent shape functions built from basis (57). $\tilde{\theta}_1 = 0°$ and $\tilde{\theta}_2 = 45°$.

7. Comparison with other numerical methods

In this section, we will compare the EFGM dispersion results with the ones obtained from FEM and other methods derived from it:

- the standard linear Finite Element Method, defined on square elements (FEM);
- the Generalized Least-Squares finite element method (GLS) (Reference [5]);
- the Quasi-Sabilized Finite Element Method (QSFEM) (Reference [6]);
- the Residual-Free Finite Element Method (RFFEM), where the standard FEM shape functions are enhanced with a residual-free bubble constructed on the element. The bubble is the exact local solution of the Helmholtz equation, it is an infinite sum that has been restricted to 200 terms (Reference [7]).

Two versions of the EFGM will be taken into account: the EFGM built with a linear basis (20) presented in Section 6.1, and the frequency-dependent EFGM built from basis (57) optimized for two angles of propagation $\tilde{\theta}_1 = 0°$ and $\tilde{\theta}_2 = 45°$, presented in Section 6.2.

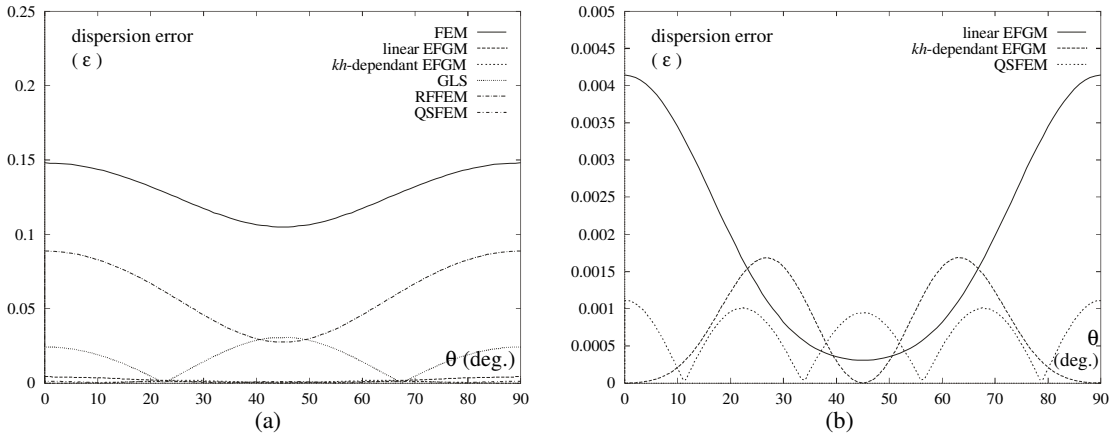

Fig. 14. (a) Comparison of EFGM with other numerical methods in terms of dispersion (b) idem (detail)

The results for the dispersion error ε as a function of angle θ are presented in Fig. 14 for a given value of the wavenumber (kh = 2.5).

Considering Fig. 14, it appears that EFGM is far superior to GLS and RFFEM, even in its standard form built from the linear basis. In its *kh*-dependent form optimized for some values of the propagation angle, the EFGM leads to dispersion results comparable to those obtained with QSFEM.

We can say that EFGM has a good behaviour in terms of dispersion and has a good ranking when a classification is made amongst all numerical methods. But another advantage of EFGM is that it does not require a regular distribution of nodes, as it is the case for some of the other methods, which can only be defined on a regular grid. EFGM is far more general, and can be applied to real life problems as will be shown in Section 8.

8. Numerical tests on a model problem

We consider a real-life problem in order to show that the EFGM is really efficient and contributes to the reduction of the dispersion in cases where the solutions are no more plane waves. The problem (see Fig. 15a) is a 2D-section in the bodywork of a car (Reference [17]). The air inside the cabin is excited by the vibrations due to the engine through the front panel (Neumann boundary conditions). The roof is covered with an absorbant material (Robin boundary conditions). We study the acoustic response inside the car at a frequency of 500 Hz.

Three computations have been performed. We first consider a FEM discretization of linear elements and 279 nodes (Fig. 15b). The EFGM computation with a linear basis is performed on the same distribution of nodes as FEM. In order to compare both methods, we use as reference the FEM solution on a highly refined mesh (17859 nodes).

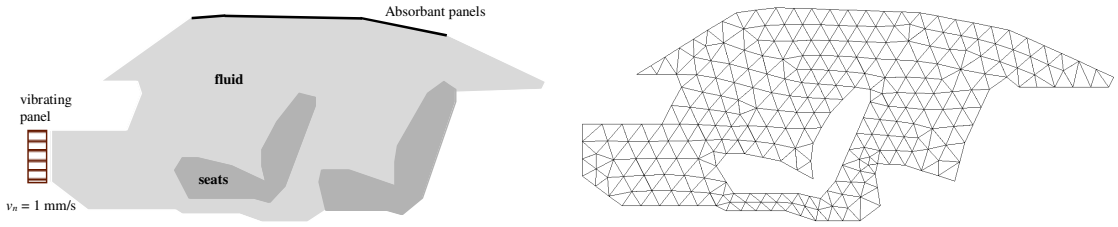

(a) (b)

Fig. 15. (a) Model problem (b) FEM mesh (279 nodes).

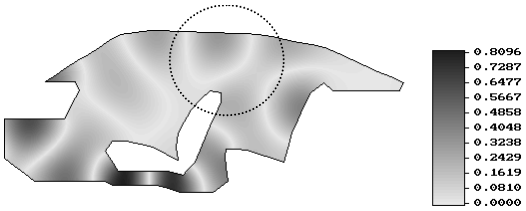

(a)

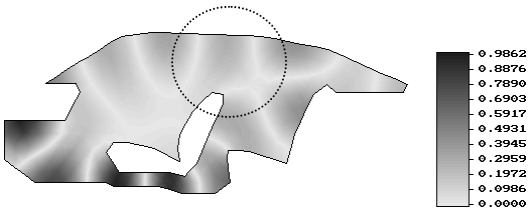

(b)

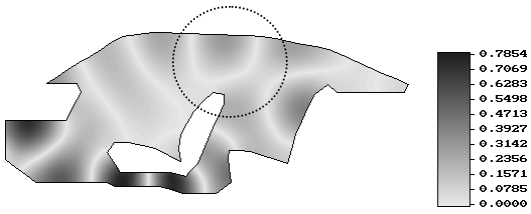

(c)

Fig. 16. Distribution of the real part of the acoustic pressure at 500 Hz. (a) reference solution (FEM 17859 nodes) (b) FEM solution (279 nodes) (c) EFGM solution (279 nodes).

Fig. 16 presents the results of the three computations for the distribution of the real part of the acoustic pressure inside the car at a frequency of 500 Hz. The graph of Fig. 17a presents the same results, computed along the straight line defined in Fig. 17b.

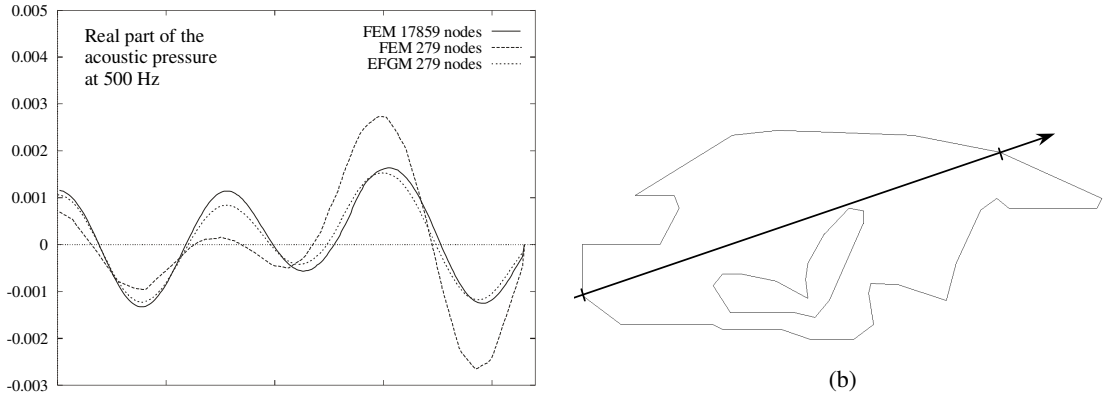

Fig. 17. (a) Distribution of the real part of the acoustic pressure at 500 Hz along the straight line (b) definition of the straight line.

These Fig. show the advantages of the EFGM compared to FEM, for the numerical wavenumber as well as for the amplitude of the wave. Considering the plots of Fig. 16, we can easily observe the wavefronts, especially in the region above the seat. The EFGM solution exhibits a good behaviour, while the FEM wave presents an important phase lag, when compared to the reference solution. This is confirmed in the cut view of Fig. 17a, where we can also see that the amplitude of the EFGM wave is really better than the FEM one.

We can conclude from this that EFGM is applicable to real-life acoustic problems, and in this case, when compared to standard FEM with the same number of nodes, EFGM is really more efficient than FEM, leading to a lower error in terms of wavenumber and amplitude. As it has already been said in Section 7, EFGM combines two advantages: it is very efficient in terms of reduction of the dispersion, and its formulation is general and easily applicable to real life problems, where its behaviour reveals to be very good.

9. Conclusions

In the present computations, the interest is dedicated in one part of the error which is the pollution error. Because the control of the pollution error leads to uneconomical meshes, we are looking for a method for which the pollution error is very small compared to the local error so that it can be neglected. We show that a meshless approach, based on the Element-Free Galerkin method, gives very accurate results. In comparison with the stabilized finite element methods, it is shown that EFGM is almost as accurate as QSFEM. However, it has to be noticed that QSFEM not adapted to non uniform meshes and irregular boundaries, which is not the case to the present formulation. This is further illustrated by a 2D industrial computation. Moreover, we observe, just like I. Babuška and J. Melenk [8], that it is possible to use a basis containing the exact solution of the Helmholtz equation. This allows us to completely cancel the pollution effect for some particular directions of propagation. Further work will be dedicated to the use of local frequency and angular dependent basis functions.

References

[1] F. Ihlenburg and I. Babuška, 'Finite Element Solution of the Helmholtz Equation with High Wave Number. Part 1: The h-Version of the FEM', *Computers Math. Applic.*, **38**(9), 9-37 (1995)

[2] Ph. Bouillard and F. Ihlenburg, 'Error estimation and adaptivity for the finite element solution in acoustics', in *Advances in Adaptive Computational Methods in Mechanics*, P. Ladevèze & J. T. Oden (Eds.), Elsevier (1998)
[3] F. Ihlenburg and I. Babuška, 'Dispersion Analysis and Error Estimation of Galerkin Finite Element Methods for the Helmholtz Equation', *Int. j. numer. methods eng.*, **38**, 3745-3774 (1995)
[4] I. Babuška, F. Ihlenburg, T. Strouboulis and S. K. Gangaraj, '*A posteriori* Error Estimation for Finite Element Solutions of Helmholtz' Equation. Part I: the Quality of Local Indicators and Estimators', *Int. j. numer. methods eng.*, **40,** 3443-3462 (1997)
[5] I. Harari, K. Grosh, T. J. R. Hughes, M. Malhotra, P. M. Pinsky, J. R. Stewart, L. L. Thompson, 'Recent Developments in Finite Element Methods for Structural Acoustics', *Arch. of Comp. Meth. Eng.*, **3**, 131-311 (1996)
[6] I. Babuška, F. Ihlenburg, E. Paik and S. Sauter, 'A Generalized Finite Element Method for solving the Helmholtz equation in two dimensions with minimal pollution', *Comput. Methods Appl. Mech. Eng.*, **128**, 325-359 (1995)
[7] L. Franca, C. Farhat, A. Macedo and M. Lessoine, 'Residual-Free Bubbles for the Helmholtz Equation', *Int. j. numer. methods eng.*, **40**, 4003-4009 (1997)
[8] I. Babuška and J. M. Melenk, 'The partition of unity method', *Int. j. numer. methods eng.*, **40**, 727-758 (1997)
[9] P. Lancaster and K. Salkausas, 'Surfaces generated by moving least squares methods', *Math. Comput.*, **37**, 141-158 (1981)
[10] T. Belytschko, Y. Y. Lu and L. Gu, 'Element-Free Galerkin Methods', *Int. j. numer. methods eng.*, **37**, 229-256 (1994)
[11] T. Belytschko, Y. Krongauz, D. Organ, M. Fleming and P. Krysl, 'Meshless methods: An overview and recent developments', *Comput. Methods Appl. Mech. Eng.*, **139**, 3-47 (1996)
[12] Ph. Bouillard and S. Suleau, 'Element-free Galerkin solutions for Helmholtz problems: formulation and numerical assessment of the pollution effect', to appear in *Comput. Methods Appl. Mech. Eng.* (1998)
[13] I. Kaljevic and S. Saigal, 'An Improved Element Free Galerkin Formulation', *Int. j. numer. methods eng.*, **40**, 2953-2974 (1997)
[14] Y. Krongauz and T. Belytschko, 'Enforcement of essential boundary conditions in meshless approximations using finite elements', to appear in *Comput. Methods Appl. Mech. Eng.*
[15] A. Deramaeker, I. Babuška and Ph. Bouillard, 'Dispersion and pollution of the FEM sloution for the Helmholtz equation in one, two and three dimensions', accepted in *Int. j. numer. methods eng.*
[16] S. Suleau and Ph. Bouillard, '1D Dispersion analysis for the element-free Galerkin method for the Helmholtz equation', submitted to *Int. j. numer. methods eng.*
[17] D. J. Nefske, 'Sound in small enclosures' in *Noise and Vibration Control Engineering. Principles and Applications*, L. Beranek and I. Vér (Editors), 1st edition, J. Wiley & Sons, ISBN 0-471-61751-2, London, 1992

2.4 La méthode EFGM itérative

La méthode EFGM permet de placer dans la base ***P(x)*** (2.1) n'importe quelle fonction. Dans les espaces à une dimension, il est évident que considérer les fonctions *sin(kx)* et *cos(kx)* conduit immédiatement à une solution numérique exacte. Pour des espaces à deux ou trois dimensions, ce n'est plus le cas en général car une solution acoustique peut être vue en chaque point comme une superposition d'une infinité d'ondes planes.

Toutefois, la pression acoustique $p(\boldsymbol{x})$ étant une variable complexe, nous pouvons toujours l'écrire, en distinguant parties réelle et imaginaire, sous la forme

$$p(\boldsymbol{x}) = p_r(\boldsymbol{x}) + jp_i(\boldsymbol{x}) \tag{2.17}$$

ou encore, en faisant apparaître l'amplitude et la phase,

$$p(\boldsymbol{x}) = \bar{P}(\boldsymbol{x})\left[\cos\theta(\boldsymbol{x}) + \mathrm{j}\sin\theta(\boldsymbol{x})\right] \tag{2.18}$$

avec $\theta(\boldsymbol{x})$ la phase de l'onde, reliée aux parties réelle et imaginaire par (2.19), et $\bar{P}(\boldsymbol{x})$ son amplitude

$$\cos\theta(\boldsymbol{x}) = \frac{p_r(\boldsymbol{x})}{\sqrt{p_r^2(\boldsymbol{x}) + p_i^2(\boldsymbol{x})}} \quad \text{et} \quad \sin\theta(\boldsymbol{x}) = \frac{p_i(\boldsymbol{x})}{\sqrt{p_r^2(\boldsymbol{x}) + p_i^2(\boldsymbol{x})}} \tag{2.19}$$

Dès lors, s'il nous est possible de calculer exactement la phase de l'onde en tout point ($\boldsymbol{x}$) du domaine considéré, l'utilisation d'une base *meshless* telle que définie en (2.18)

$$\boldsymbol{P}^t(\boldsymbol{x}) = \left\{1, \cos\theta(\boldsymbol{x}), \sin\theta(\boldsymbol{x})\right\} \tag{2.20}$$

nous fournirait une solution numérique EFGM exacte et sans dispersion, aux erreurs d'arrondis près.

Il est évidemment impossible de déterminer de façon exacte la distribution de la phase pour tout problème de propagation acoustique. Nous allons, par conséquent, travailler avec une base de type (2.20) pour laquelle la distribution $\theta(\boldsymbol{x})$ sera évaluée par une première approximation du champ de pression $p^{\mathrm{h}}(\boldsymbol{x})$ obtenue par une base *meshless* polynomiale linéaire classique (2.21)

$$\boldsymbol{P}^t(\boldsymbol{x}) = \{1, x, y, z\} \tag{2.21}$$

et à l'aide des relations (2.19) qui deviennent

$$\cos\theta^{\mathrm{h}} = \frac{p_r^{\mathrm{h}}}{\sqrt{(p_r^{\mathrm{h}})^2 + (p_i^{\mathrm{h}})^2}} \quad \text{et} \quad \sin\theta^{\mathrm{h}} = \frac{p_r^{\mathrm{h}}}{\sqrt{(p_r^{\mathrm{h}})^2 + (p_i^{\mathrm{h}})^2}} \tag{2.22}$$

où,

$$p_{\mathrm{I}}^{\mathrm{h}}(\boldsymbol{x}) = p_{r\mathrm{I}}^{\mathrm{h}}(\boldsymbol{x}) + jp_{i\mathrm{I}}^{\mathrm{h}}(\boldsymbol{x}) \tag{2.23}$$

La nouvelle base *meshless* ainsi construite sera donc

$$\boldsymbol{P}^{t}(\boldsymbol{x}) = \left\{1, \cos\theta_{\mathrm{I}}^{\mathrm{h}}(\boldsymbol{x}), \sin\theta_{\mathrm{I}}^{\mathrm{h}}(\boldsymbol{x})\right\} \tag{2.24}$$

Elle nous permet de calculer une deuxième approximation $p_{\mathrm{II}}^{\mathrm{h}}(\boldsymbol{x})$ du champ de pression acoustique.

En suivant ce formalisme, une troisième approximation du champ de pression peut être calculée en construisant une base de type (2.24) avec les équations (2.22) mais en utilisant cette fois $p_{\mathrm{II}}^{\mathrm{h}}(\boldsymbol{x})$ au lieu de $p_{\mathrm{I}}^{\mathrm{h}}(\boldsymbol{x})$ et ainsi de suite jusqu'à l'obtention d'une convergence ou d'une erreur prescrite. En général, une itération suffit pour améliorer déjà nettement la solution. Du point de vue du temps de calcul, cette solution est plus économique qu'une augmentation du degré des bases polynomiales.

L'article qui suit explicite cette approche itérative. Il s'agit d'un reprint de V. Lacroix, P. Villon, Ph. Bouillard, 'An iterative defect-correction type meshless method for acoustics', Reprint Int. j. numer. methods eng. 2003; **57**:2131-2146.

INTERNATIONAL JOURNAL FOR NUMERICAL METHODS IN ENGINEERING
Int. j. numer. methods eng. 2003; **57**:2131-2146 (DOI: 10.1002/nme.757)

An iterative defect-correction type meshless method for acoustics

V. Lacroix[1], Ph. Bouillard[1,*] and P. Villon[2]

[1]*Université Libre de Bruxelles, Continuum Mechanics Dept. CP 194/5, F.D. Roosevelt Av. 50, B-1050 Brussels, Belgium*
[2]*Centre de Recherche de Royallieu, Génie des Systèmes Mécaniques BP 20529 60205 Compiègne Cédex, France*

SUMMARY

Accurate numerical simulation of acoustic wave propagation is still an open problem, particularly for medium frequencies. We have then formulated a new numerical method better suited to the acoustical problem: Element-Free Galerkin Method (EFGM) improved by appropriate basis functions computed by a defect correction approach.

One of the EFGM advantages is that the shape functions are customizable. Indeed, we can construct the basis of the approximation with terms that are suited to the problem which has to be solved. Acoustical problems, in cavities Ω with boundary Γ, are governed by the Helmholtz equation completed with appropriate boundary conditions.

As the pressure $p(x,y)$ is a complex variable, it can always be expressed as a function of $\cos\theta(x,y)$ and $\sin\theta(x,y)$ where $\theta(x,y)$ is the phase of the wave in each point (x,y).

If the exact distribution $\theta(x,y)$ of the phase is known and if a *meshless* basis $\{1, \cos\theta(x,y), \sin\theta(x,y)\}$ is used, then the exact solution of the acoustic problem can be obtained.

Obviously, in real-life cases, the distribution of the phase is unknown. The idea of our work is to resolve, as a first step, the acoustic problem by using a polynomial basis to obtain a first approximation of the pressure field $p_I^h(x,y)$. As a second step, from $p_I^h(x,y)$ we compute the distribution of the phase $\theta_I^h(x,y)$ and we introduce it in the *meshless* basis in order to compute a second approximated pressure field $p_{II}^h(x,y)$. From $p_{II}^h(x,y)$ a new distribution of the phase is computed in order to obtain a third approximated pressure field and so on until a convergence criterion, concerning the pressure or the phase, is obtained. So, an iterative defect-correction type *meshless* method has been developed to compute the pressure field in Ω.

This work will show the efficiency of this *meshless* method in terms of accuracy and in terms of computational time. We will also compare the performance of this method with the classical finite element method.

KEY WORDS: acoustics, Helmholtz equation, dispersion error, element-free Galerkin method, meshless method

1. INTRODUCTION

The numerical solution of the Helmholtz equation, governing the wave propagation, is one of the main problems that has not yet been properly addressed because of spurious phenomena inherent to this differential operator. To compute the acoustic response several numerical methods are used like the finite element method (FEM) and the boundary element method (BEM). Nevertheless, these methods present some disadvantages: the FEM suffers from pollution (error on the amplitude) and dispersion (error on the phase) phenomena widely studied a.o. by I. Babuška, F. Ihlenburg and Ph. Bouillard [1-4] (figure 1); the BEM needs significant computational time because it works with full, complex and non-symmetrical

* Correspondence to: Ph. Bouillard, Université Libre de Bruxelles, Structural and Material Computational Mechanics Dept. CP 194/5, F.D. Roosevelt Av. 50, B-1050 Brussels, Belgium. E-mail: pbouilla@smc.ulb.ac.be

matrices. More recently, O.C. Zienkiewicz [5] has classified the short wave acoustic problems amongst the still unsolved problem of the finite element method (FEM)

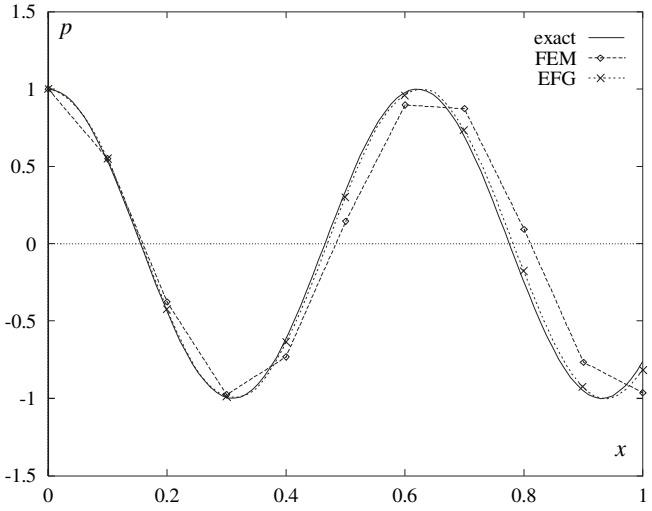

Figure 1. Illustration of the dispersion

Several authors have then suggested methods to stabilize the finite element method: the Galerkin Least Square (GLS) [6],proposed by I. Harari, T. J. R. Hughes and *al*., consists of a modification of the variational problem in order to minimize the dispersion, the Quasi-Stabilized Finite Element Method (QSFEM) [7], by I. Babuška and F. Ihlenburg, modifies the system matrix with the same goal, but is restricted to regular meshes of square elements, and more recently a Residual-Free Finite Element Method (RFFEM)[8] was implemented for the Helmholtz equation by L. Franca, Ch. Farhat and *al*., etc. However, none of these methods eliminates the dispersion in a general two-dimensional case, see Reference 9 for a complete analysis.

Moreover, one the one hand T. J. R. Hughes has proposed another alternative to solve acoustic problems by formulating a multiscale FEM [10] which seems to give good results and on the other hand A. Brandt and I. Livshits have formulated a multigrid method to solve the Helmholtz equation [30].

In order to decrease dispersion and pollution, several high order formulations have also been developed. Amongst them, the *hp*-FEM by L. Demkowicz and K. Gerdes [11], the Reproducing Kernel Particle Method (RKPM) by W. K. Liu and M. Christon [12,13] and, simultaneously, S. Suleau and Ph. Bouillard applied classical EFGM to acoustics [17,18].

Nevertheless, everybody seems to agree that it is very advantageous to use a set of plane wave solutions of the homogenized Helmholtz equation as the local function basis. A natural and very efficient way to achieve this is to use a meshless formulation. I. Babuška and J. M. Melenk [14] have developed the Partition of Unity Method (PUM), E. Chadwick and P. Bettes suggest the using of a set of plane wave to build the basis of the subspace [15], Ch. Farhat, I. Harari and L. P. Franca have proposed a Discontinuous Generalized FEM [16] while V. Lacroix, Ph. Bouillard and P. Villon formulate a new Element Free Galerkin Method (EFGM) approach showing very accurate results [28].

The EFGM is based on the Moving Least Square Approximation (MLSA), first introduced by P. Lancaster *et al.* [19] in the field of surface and function smoothing. Then, the MLSA has been extended by B. Nayroles, G. Touzot and P. Villon to develop the Diffuse Element Method [20]. Recently, the EFGM has been extensively investigated by T. Belystchko et *al.* in the fields of elasticity and crack propagation problems [21-22]. The main advantages of the formulation are well known (no connections by nodes, easy pre- and postprocessing tasks). For the particular case of the Helmholtz equation, we also take advantage of the fact that the shape functions are non rational and the local basis can naturally contain terms which are solution of the Helmholtz equation [23].

In our work, as the pressure is a complex variable, terms in $\cos\theta(x,y)$ and $\sin\theta(x,y)$ are introduced in the *meshless* basis, where $\theta(x,y)$ is the value of the phase of the pressure field in each point (x,y). Seeing that $\theta(x,y)$ is *a priori* unknown, it has first to be evaluated by a first computation of the pressure field with

a classical polynomial basis. In this way, with this new *meshless* basis a second evaluation of $\theta(x,y)$ can be obtained and so until convergence.

The paper is organized as follows. Sections 2 and 3 present the strong and variational forms of the acoustic problem. In section 4, the EFGM shape functions are defined and the method is applied to acoustics. Principles and details of the Iterative Defect-Correction Type Meshless Method (I2M) are presented in section 5. Section 6 deals with numerical results showing performances of the method.

2. STRONG FORMULATION OF THE ACOUSTIC PROBLEM

Consider a fluid inside a domain Ω with boundary Γ, let c be the speed of sound in the fluid and ρ the specific mass of the fluid. If p' denotes the field of acoustic pressure (small perturbations around a steady uniform state), the equation of wave propagation (1) is derived from the fundamental equations of continuum mechanics [2].

$$\Delta p' = \frac{1}{c^2}\frac{\partial^2 p'}{\partial t^2} \tag{1}$$

If the phenomena are assumed to be steady harmonic, e.g.

$$p' = p \exp(j \omega t) \tag{2}$$

where ω is the angular frequency, thus the spatial distribution p of the acoustic pressure (which now is a complex variable) inside Ω, is solution of Helmholtz equation

$$\Delta p + k^2 p = 0 \tag{3}$$

where the wave number k is defined by the ratio between the angular frequency and the speed of sound

$$k = \frac{\omega}{c} \tag{4}$$

Another important quantity of the acoustic analysis is the particle velocity (vector $\boldsymbol{v}$) linked to the gradient of the acoustic pressure through the equation of motion

$$j \rho c k \boldsymbol{v} + \nabla p = 0 \tag{5}$$

In order to completely address the acoustic problem, Helmholtz equation (3) is associated with boundary conditions on Γ. The boundary can be split for interior problems into three parts

$$\Gamma = \Gamma_D \cup \Gamma_N \cup \Gamma_R \tag{6}$$

corresponding to different types of boundary conditions

- Dirichlet boundary conditions

$$p = \bar{p} \quad \text{on } \Gamma_D \tag{7}$$

- Neumann boundary conditions

$$v_n = \bar{v}_n \quad \text{or} \quad \boldsymbol{n}^t \nabla p = -j \rho c k \bar{v}_n \quad \text{on } \Gamma_N \tag{8}$$

- Robin boundary conditions

$$\boldsymbol{n}^t \nabla p = -j \rho c k A_n p \quad \text{on } \Gamma_R \tag{9}$$

where A_n is the admittance coefficient modelling the damping.

Neumann boundary conditions correspond to vibrating panels while Robin boundary conditions correspond to absorbant panels. Conditions (7)-(9) have been defined for interior and exterior problems. For an infinite medium, a non reflecting wave is considered at infinity by the so-called Sommerfeld boundary condition.

*Reprint de Int. j. numer. methods eng. 2003; **57**:2131-2146.*

3. VARIATIONAL FORMULATION OF THE ACOUSTIC PROBLEM

The variational formulation corresponding to the strong form presented in Section 2 is well known and in the following, only the main aspects will be emphasized. For more details, see Reference 12.
The space of admissible trial functions p is defined as

$$H_D^1(\Omega) = \{\ p \in H^1(\Omega) \,|\, p = \bar{p} \text{ on } \Gamma_D\ \} \tag{10}$$

and the space of homogeneous test functions w is

$$H_0^1(\Omega) = \{\ w \in H^1(\Omega) \,|\, w = 0 \text{ on } \Gamma_D\ \} \tag{11}$$

Both of them are subspaces of $H^1(\Omega)$, the Sobolev space of functions square-integrable together with their first derivatives. Consider the functional Π

$$\Pi = \frac{1}{2} a(p, \tilde{p}) - \varphi(\tilde{p}) \tag{12}$$

with

$$a(p, \tilde{p}) : H_D^1 \times H_D^1 \to \mathrm{C} \;|\; a(p, \tilde{p}) = \int_\Omega (\nabla p \nabla \tilde{p} - k^2 p\, \tilde{p})\, d\Omega + \int_{\Gamma_R} j \rho c k A_n\, p\, \tilde{p}\; d\Gamma \tag{13}$$

$$\varphi(\tilde{p}) : H_D^1 \to \mathrm{C} \;|\; \varphi(\tilde{p}) = -\int_{\Gamma_N} j \rho c k \bar{v}_n\, \tilde{p}\, d\Gamma \tag{14}$$

where the notation $\tilde{\bullet}$ stands for the complex conjugate.

The variational form corresponding to Helmholtz equation (3) and boundary conditions (7)-(9) is expressed by

$$\text{Find} \quad p \in H_D^1 \;|\; \delta\Pi = 0 \quad \forall \delta p \in H_0^1 \tag{15}$$

It will be shown in Section 4 that, in the case of the Element-Free Galerkin Method, the approximation does not interpolate the nodal values. The variational formulation has to be accordingly modified to take into account Dirichlet boundary conditions (7) for instance by introducing any penalty method like Lagrange multipliers λ in functional (12)

$$\Pi^* = \Pi + \int_{\Gamma_D} \lambda (p - \tilde{\tilde{p}})\, d\Gamma \tag{16}$$

and variational form (15) is reformulated as

$$\text{Find} \quad p \in H^1 \;|\; \delta\Pi^* = 0 \quad \forall \delta p \in H_0^1, \delta\lambda \in H^0 \tag{17}$$

Note that Dirichlet boundary conditions and their treatment by Lagrange multipliers have only been mentioned for completeness. In real-life acoustic problems, this kind of boundary conditions seldom appears. This method of introducing the Dirichlet boundary conditions has been developed in previous papers [32-33] but more recent techniques and more efficient than Lagrange multipliers exist for EFG [24-25].

4. ELEMENT-FREE GALERKIN METHOD APPLIED TO ACOUSTICS

4.1. Element-Free shape functions: the Moving Least Square Approximation (MLSA)

A complete report on the construction of the shape functions defining the EFGM can be found in References 21,22,26. This paragraph only gives a brief overview of the main steps.

The MLSA is defined on a cloud of n nodes, which are not connected by elements as it is required for the Finite Element Method (FEM). The nodes are located at $\boldsymbol{x}_I$ inside Ω ($I = 1,\ldots,n$). For each node I, we define a domain of influence characterized by a typical dimension size d_{infl} (in 1D, the domain is a

segment and d_{infl} is its half length while in 2D, the domain is a disc of radius d_{infl} or a square of half lengthside d_{infl}). These domains are defined to connect the nodes: two nodes are connected if their domains of influence intersect.

A weight function w_I is also defined for each node to represent the influence of the node $\boldsymbol{x}_I$ at a given point $\boldsymbol{x}$. This weight function is equal to unity at the node, decreasing when the distance to the node increases and zero outside the domain of influence of the node. For all the computations reported in this paper, we have used an exponential weight function, that can be defined either on a square domain of influence as the product of two one-dimensional weight functions

$$\begin{aligned} w_I(x,y) &= \left(\frac{e^{-\left(2\frac{x-x_I}{d_{infl,I}}\right)^2} - e^{-4}}{1-e^{-4}} \right)\left(\frac{e^{-\left(2\frac{y-y_I}{d_{infl,I}}\right)^2} - e^{-4}}{1-e^{-4}} \right) \qquad & (x \le d_{infl,I} \text{ and } y \le d_{infl,I}) \\ &= 0 & (x > d_{infl,I} \text{ or } y > d_{infl,I}) \end{aligned} \tag{18}$$

or on a circular domain as a function of d, the distance between point $\boldsymbol{x}$ and node $\boldsymbol{x}_I$

$$\begin{aligned} w_I(x,y) &= \frac{e^{-\left(2\frac{d}{d_{infl,I}}\right)^2} - e^{-4}}{1-e^{-4}} \qquad & (d \le d_{infl,I}) \\ &= 0 & (d > d_{infl,I}) \end{aligned} \tag{19}$$

The construction of the MLSA and the corresponding shape functions is based on the choice of a basis $\boldsymbol{P}(x)$ (dimension m) of functions which, in the case of 1D polynomials, are

$$\boldsymbol{P}^t(x) = \{1, x\} \quad (\text{linear basis, } m = 2) \tag{20}$$

$$\boldsymbol{P}^t(x) = \{1, x, x^2\} \quad (\text{quadratic basis, } m = 3) \tag{21}$$

Polynomial bases are not the only choice: non-polynomial bases can also be chosen, introducing better suited functions for solving the Helmholtz equation as it will be seen further.
The unknown p^h (acoustic pressure, the upper h standing for numerical solution) of the problem is interpolated from

$$p^h(\boldsymbol{x}) = \boldsymbol{P}^t(\boldsymbol{x})\boldsymbol{a}(\boldsymbol{x}) \tag{22}$$

where the $\boldsymbol{a}(\boldsymbol{x})$ coefficients are non constant and are determined by minimizing a L^2 norm (see References 20 and 21), leading to

$$\boldsymbol{a}(\boldsymbol{x}) = \boldsymbol{A}^{-1}(\boldsymbol{x})\boldsymbol{B}(\boldsymbol{x})\boldsymbol{p} \tag{23}$$

where $\boldsymbol{p}$ is the array of the nodal values p_I. $\boldsymbol{A}(\boldsymbol{x})$ and $\boldsymbol{B}(\boldsymbol{x})$ are the matrices defined by

$$\boldsymbol{A}(\boldsymbol{x}) = \sum_{I=1}^{n(x)} w_I(\boldsymbol{x})\boldsymbol{P}(\boldsymbol{x}_I)\boldsymbol{P}^t(\boldsymbol{x}_I) \tag{24}$$

$$\boldsymbol{B}(\boldsymbol{x}) = [\, w_1(\boldsymbol{x})\boldsymbol{P}(\boldsymbol{x}_I), ..., w_n(\boldsymbol{x})\boldsymbol{P}(\boldsymbol{x}_n) \,] \tag{25}$$

where $n(\boldsymbol{x})$ is the number of nodes influencing the point $(\boldsymbol{x})$. Equation (21) can then be written as

$$p^h(\boldsymbol{x}) = \boldsymbol{N}(\boldsymbol{x})\boldsymbol{p} \tag{26}$$

where $\boldsymbol{N}(\boldsymbol{x})$ contains the shape functions and is defined by

$$\boldsymbol{N}(\boldsymbol{x}) = \boldsymbol{P}^t(\boldsymbol{x})\boldsymbol{A}^{-1}(\boldsymbol{x})\boldsymbol{B}(\boldsymbol{x}) \tag{27}$$

At this point, we have to underline the fact that the $m*m$ matrix $\boldsymbol{A}(\boldsymbol{x})$ is the sum of matrices of rank 1. As $w_I(\boldsymbol{x})$ is zero for all nodes that do not influence point $\boldsymbol{x}$, $\boldsymbol{A}(\boldsymbol{x})$ is the sum of only $n(\boldsymbol{x})$ matrices of rank 1, where $n(\boldsymbol{x})$ is the number of nodes influencing $\boldsymbol{x}$. The rank of $\boldsymbol{A}(x)$ must be equal to m since (27) needs the computation of $\boldsymbol{A}^{-1}(x)$. This leads to the necessary (but not sufficient) condition of existence of the MLSA: $n(\boldsymbol{x}) \geq m$, i.e. each point of Ω has to be influenced by at least as many nodes as there are functions in the basis $\boldsymbol{P}(\boldsymbol{x})$.

4.2. Application to the acoustic problem

The application of the EFG to the acoustic problem formulated in sections 2 and 3 is completely detailed in Reference 26. We choose to approximate the acoustic pressure field and its variation by

$$p^h = \boldsymbol{N}\,\boldsymbol{p} \qquad \delta p^h = \boldsymbol{N}\,\boldsymbol{\delta p} \tag{28}$$

while the Lagrange multipliers and their variation are chosen to be

$$\lambda^h = \boldsymbol{N}_\lambda \boldsymbol{\Lambda} \qquad \delta\lambda^h = \boldsymbol{N}_\lambda \boldsymbol{\delta\Lambda} \tag{29}$$

where $\boldsymbol{N}_\lambda$ is a Lagrange interpolant defined on the boundary.
Introducing (28)-(29) into variational form (17), a linear system of equations, similar to the system obtained for a problem of structural dynamics, is obtained

$$\begin{bmatrix} \boldsymbol{K} + j\,\rho\,c\,k\,\boldsymbol{C} - c^2k^2\boldsymbol{M} & \boldsymbol{K}_{p\lambda} \\ \boldsymbol{K}_{p\lambda}^t & 0 \end{bmatrix} \begin{Bmatrix} \boldsymbol{p} \\ \boldsymbol{\Lambda} \end{Bmatrix} = \begin{Bmatrix} -j\,\rho\,c\,k\,\boldsymbol{f} \\ \boldsymbol{b} \end{Bmatrix} \tag{30}$$

where the matrices and vectors are defined as follows

- the "stiffness" matrix $\boldsymbol{K}$

$$\boldsymbol{K} = \int_\Omega (\nabla \boldsymbol{N})^t (\nabla \boldsymbol{N})\, d\,\Omega \tag{31}$$

- the "damping" matrix $\boldsymbol{C}$ (Robin boundary conditions)

$$\boldsymbol{C} = \int_{\Gamma_R} \boldsymbol{N}^t\,\boldsymbol{N}\,A_n\,d\,\Gamma \tag{32}$$

- the "mass" matrix $\boldsymbol{M}$

$$\boldsymbol{M} = \frac{1}{c^2}\int_\Omega \boldsymbol{N}^t\,\boldsymbol{N}\,d\,\Omega \tag{33}$$

- the vector $\boldsymbol{p}$ of nodal pressure unknowns
- the vector $\boldsymbol{\Lambda}$ of nodal Lagrange multipliers unknowns
- the matrix $\boldsymbol{K}_{p\lambda}$, coupling both kind of unknowns

$$\boldsymbol{K}_{p\lambda} = \int_{\Gamma_D} \boldsymbol{N}^t\,\boldsymbol{N}_\lambda\,d\,\Gamma \tag{34}$$

- the vector $\boldsymbol{f}$, containing the prescribed normal velocities (Neumann boundary conditions)

$$\boldsymbol{f} = \int_{\Gamma_N} \boldsymbol{N}^t\,\bar{\boldsymbol{v}}_{\boldsymbol{n}}\,d\,\Gamma \tag{35}$$

- the vector $\boldsymbol{b}$, containing the prescribed values of the pressure (Dirichlet boundary conditions)

$$\boldsymbol{b} = \int_{\Gamma_D} \boldsymbol{N}_\lambda{}^t\,\bar{p}\,d\,\Gamma \tag{36}$$

*Reprint de Int. j. numer. methods eng. 2003; **57**:2131-2146.*

5. ITERATIVE DEFECT-CORRECTION TYPE MESHLESS METHOD

5.1. Introduction of the phase in the meshless basis

As mentioned in the introduction, the purpose of our work is to take the phase of the wave into account to build the *meshless* basis. As the pressure is a complex variable, we can always write in each point *(x,y)*

$$p(x, y) = \overline{P}(x, y)\ [\cos\theta(x, y) + j\ \sin\theta(\mathrm{x}, \mathrm{y})\ ] \tag{37}$$

where $\overline{P}(x, y)$ is the amplitude of the wave and $\theta(x,y)$ the phase.

Therefore, if the distribution of the phase is exactly known over the whole domain and if the basis

$$\boldsymbol{P}^t(x, y) = \{1, \cos\theta(x, y), \sin\theta(x, y)\} \tag{38}$$

is used, the obtained *meshless* solution is dispersion-free if the errors due to the numerical integration are not considered.

Obviously, for real-life cases, the distribution of $\theta(x,y)$ is *a priori* unknown. Thus, in the latter, $\theta(x,y)$ will be approximated by a distribution $\theta^h(x,y)$ obtained by a first computation of the pressure field using, for instance, a linear polynomial *meshless* basis.

5.2. Iterative computations : principle

In this section, the acoustic problem iterative resolution based on a θ-adaptive *meshless* basis is presented step by step.

5.2.1 First step: computation of $\theta^h(x,y)$. To introduce $\theta(x,y)$ in the meshless basis we compute a first approximation $p_I^h(x,y)$ of the pressure field by using, for instance a classical linear meshless basis

$$\boldsymbol{P}^t(x, y) = \{1, x, y\} \tag{39}$$

because this solution is already very accurate [26] and needs a small CPU time.

Thus we obtain in each point of the domain, by splitting the real and imaginary parts of the pressure

$$p_{\mathrm{I}}^{\mathrm{h}}(x, y) = p_{\mathrm{I},r}^{\mathrm{h}}(x, y) + j\ p_{\mathrm{I},i}^{\mathrm{h}}(x, y) \tag{40}$$

From the general expression of the pressure given in (37) it immediately comes

$$p_{\mathrm{I}}^{\mathrm{h}}(x, y) = \overline{P}_{\mathrm{I}}^{\mathrm{h}}(x, y)\left[\cos\theta_{\mathrm{I}}^{\mathrm{h}}(x,y) + \mathrm{j}\sin\theta_{\mathrm{I}}^{\mathrm{h}}(x, y)\ \right] \tag{41}$$

where

$$\cos\theta_{\mathrm{I}}^{\mathrm{h}} = \frac{p_{\mathrm{I},r}^{\mathrm{h}}}{\sqrt{(p_{\mathrm{I},r}^{\mathrm{h}})^2 + (p_{\mathrm{I},i}^{\mathrm{h}})^2}} \quad \text{and} \quad \sin\theta_{\mathrm{I}}^{\mathrm{h}} = \frac{p_{\mathrm{I},i}^{\mathrm{h}}}{\sqrt{(p_{\mathrm{I},r}^{\mathrm{h}})^2 + (p_{\mathrm{I},i}^{\mathrm{h}})^2}} \tag{42}$$

5.2.2 Second step: EFGM resolution with local basis. *Consider now the* meshless *basis defined by*

$$\boldsymbol{P}^t(x, y) = \left\{1, \cos\theta_{\mathrm{I}}^{\mathrm{h}}(x,y), \sin\theta_{\mathrm{I}}^{\mathrm{h}}(x, y)\right\} \tag{43}$$

with $\cos\theta_{\mathrm{I}}^{\mathrm{h}}(x,y)$ and $\sin\theta_{\mathrm{I}}^{\mathrm{h}}(x,y)$ coming from the first computation.

A new approximated pressure field $p_{\mathrm{II}}^{\mathrm{h}}(x,y)$ is computed by a EFGM with local basis (43). Of course, this method can be iterated: a third approximation of the pressure can be computed by building a basis of type (43) with equation (42) but by using $p_{\mathrm{II}}^{\mathrm{h}}(x,y)$ instead of $p_{\mathrm{I}}^{\mathrm{h}}(x,y)$ and so on until a convergence criterion is obtained, for instance at iteration *i*

$$\sqrt{\frac{\int_\Omega\ (p_{\mathrm{i}} - p_{\mathrm{i-1}})\,(\tilde{p}_{\mathrm{i}} - \tilde{p}_{\mathrm{i-1}})\mathrm{d}\Omega}{\int_\Omega\ p_{\mathrm{i-1}}\tilde{p}_{\mathrm{i-1}}\mathrm{d}\Omega}} \le \varepsilon \tag{44}$$

or, if the convergence of $\theta(x,y)$ is preferred, the following criterion is used

$$\sqrt{\frac{\int_\Omega (\theta_i - \theta_{i-1})^2 \, d\Omega}{\int_\Omega \theta_{i-1}^2 \, d\Omega}} \leq \varepsilon \tag{45}$$

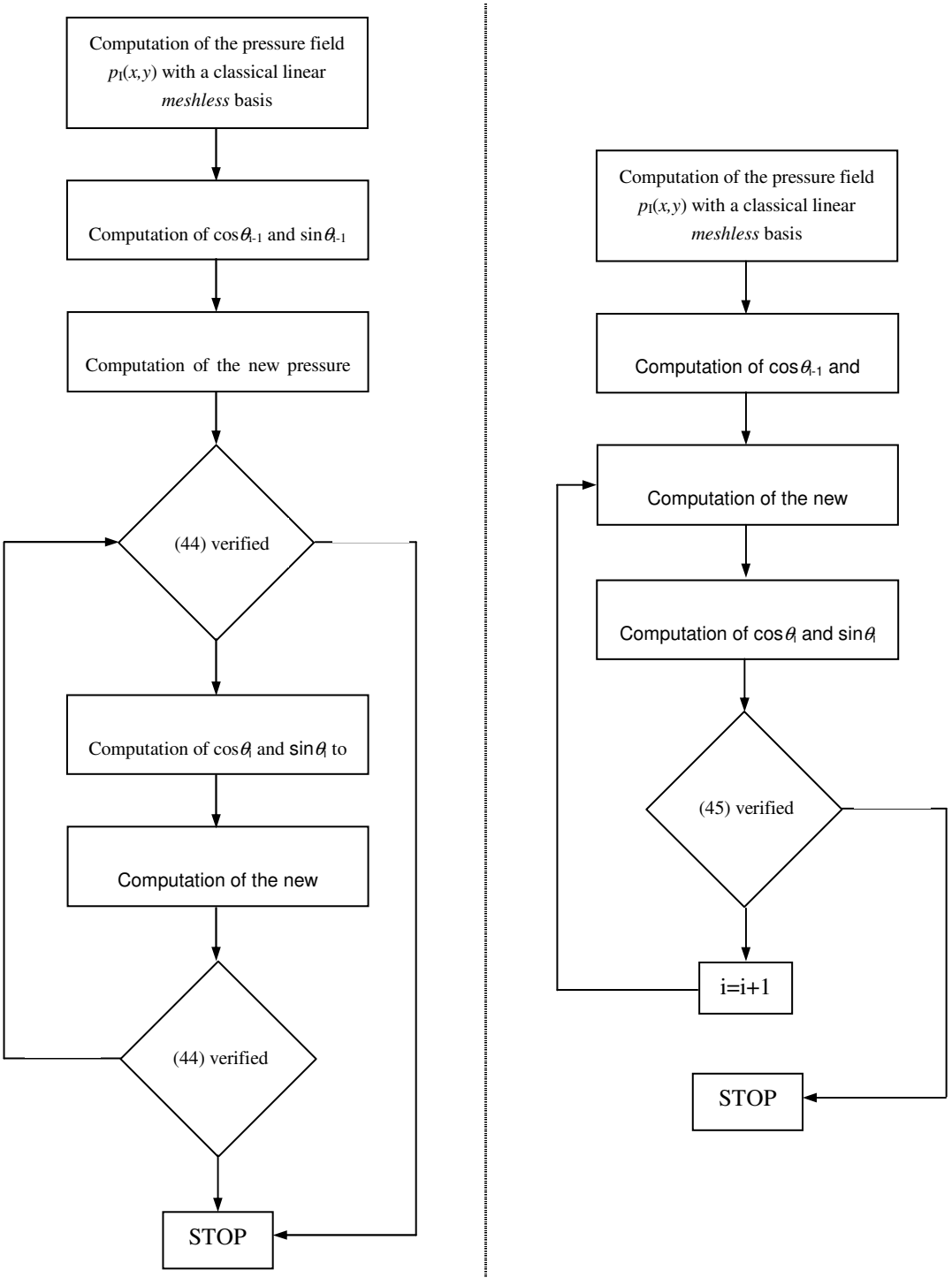

Figure 2.
(a) Iterative algorithm using convergence criterion (44) (b) Iterative algorithm using convergence criterion (45)

5.2.3 I2M algorithm. So, an iterative defect-correction type meshless method (I2M) has been developed to compute the pressure field in Ω. Figures 2(a-b) illustrate this method by its algorithm according to the convergence criterion (44) or (45).

6. NUMERICAL RESULTS

In this section, I2M is compared from the accuracy point of view with other methods already used to solve acoustic problem like FEM, classical EFGM, …. The behaviour of this new method in relation to the acoustic dispersion phenomenon is also studied. But first, one has to demonstrate that the iterative scheme of the method is well-founded.

6.1. Square cavity

This first numerical test deals with a square cavity (figure 3) which a plane wave propagates in. The analytical solution of this problem is known and given by (46)

$$p(x, y) = \cos k(x\cos\alpha + y\sin\alpha) + j\sin k(x\cos\alpha + y\sin\alpha) \tag{46}$$

where α is the propagation angle. For information, the linear system (30) is solved here with a Gauss-Jordan algorithm because of the Dirichlet b.c. enforced by Lagrangian multipliers.

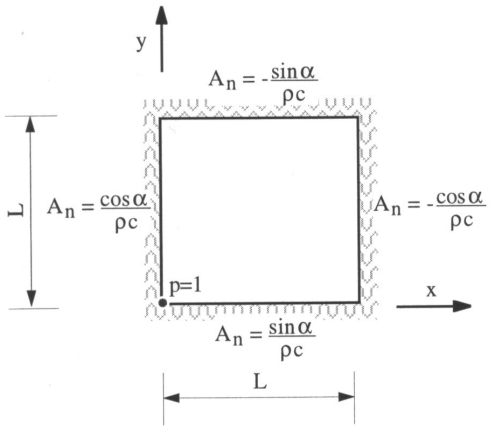

Figure 3. Square cavity : plane wave propagation

6.1.1 Behaviour of the error with iterations. For this result, two discretizations are considered: 441 nodes (21 by 21) and 1681 nodes (41 by 41). Moreover, in order to analyse the influence of the numerical integration error, two quadrature schemes will be used for the first discretisation: integration cells with 3 by 3 Gauss points and with 10 by 10 Gauss points (size of the cells = h). The evolution of the L^2 norm in relation to the number of iterations (frequency=550 Hz) is represented in figure 4.

*Reprint de Int. j. numer. methods eng. 2003; **57**:2131-2146.*

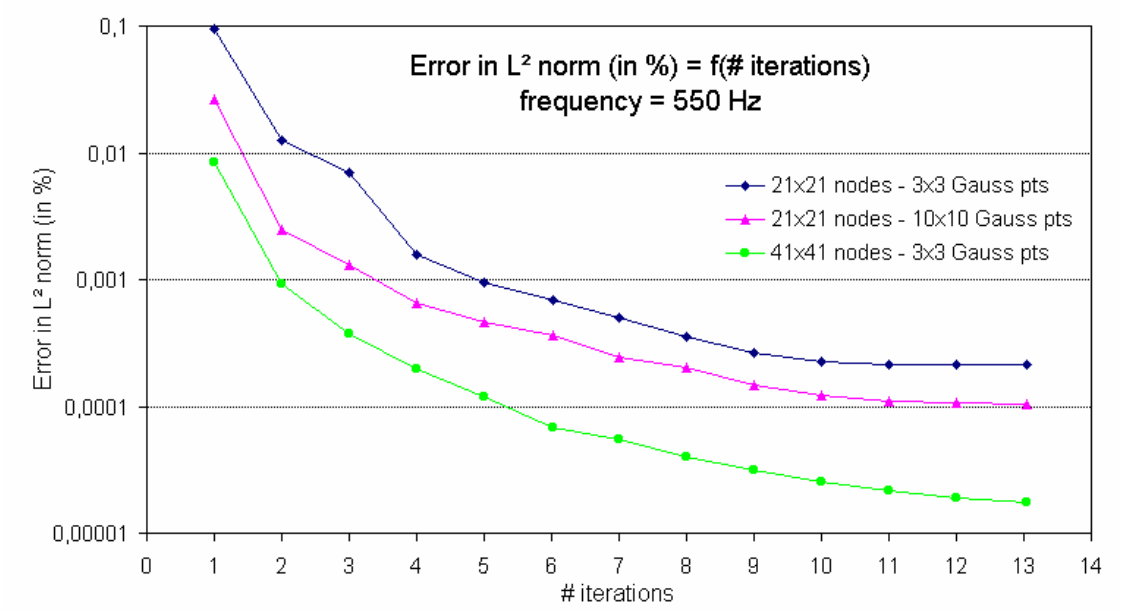

Figure 4. Error in L² norm in relation to the number of iterations

One can observe that for a given discretization the error decreases with the number of iterations until a saturation value depending to the considered discretization and the quality of the quadrature scheme. Therefore, this example shows that the iterative principle of the method is well-founded. Moreover, the error decreases when a refined discretisation is used i.e. I2M converges when $h \to 0$.

6.1.2 Frequency response function. The second numerical test on the square cavity deals with the frequency response function (FRF) in the middle of the square cavity. The FRF is computed with linear FEM, linear basis *meshless* method and I2M limited to one iteration. The analytical FRF is also represented. These curves are shown in figure 5 for the real part of the pressure. The lower and upper bounds of the frequencies are 100 Hz and 1500 Hz. The response is given in dBA (ref. $2\ 10^{-5}$).

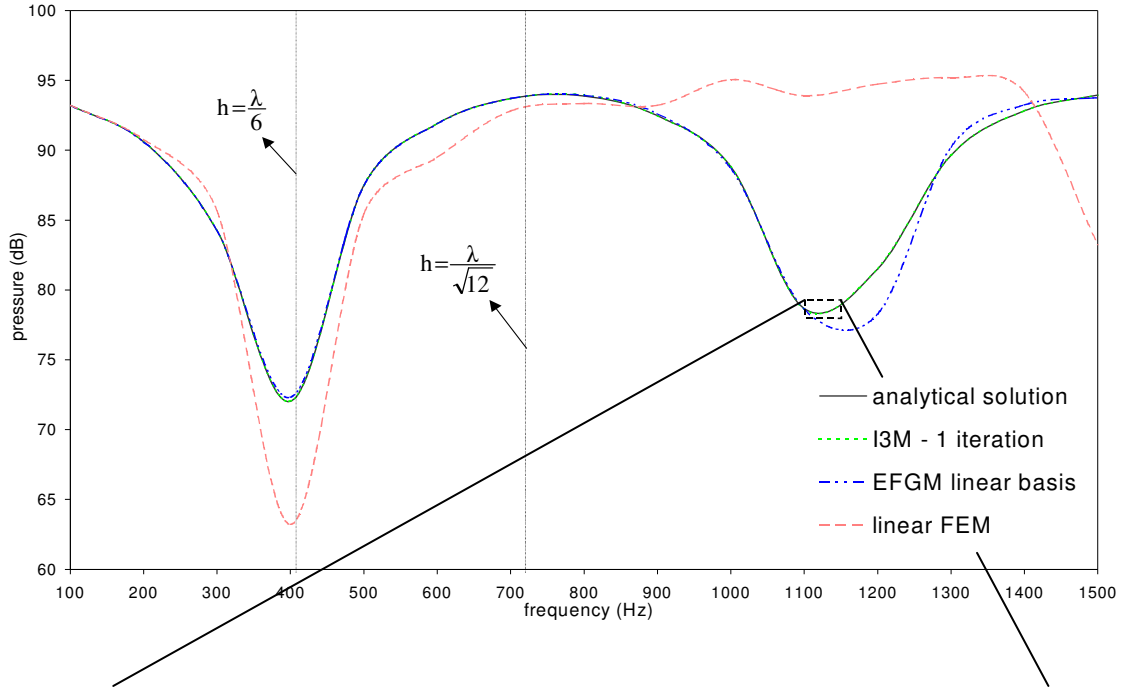

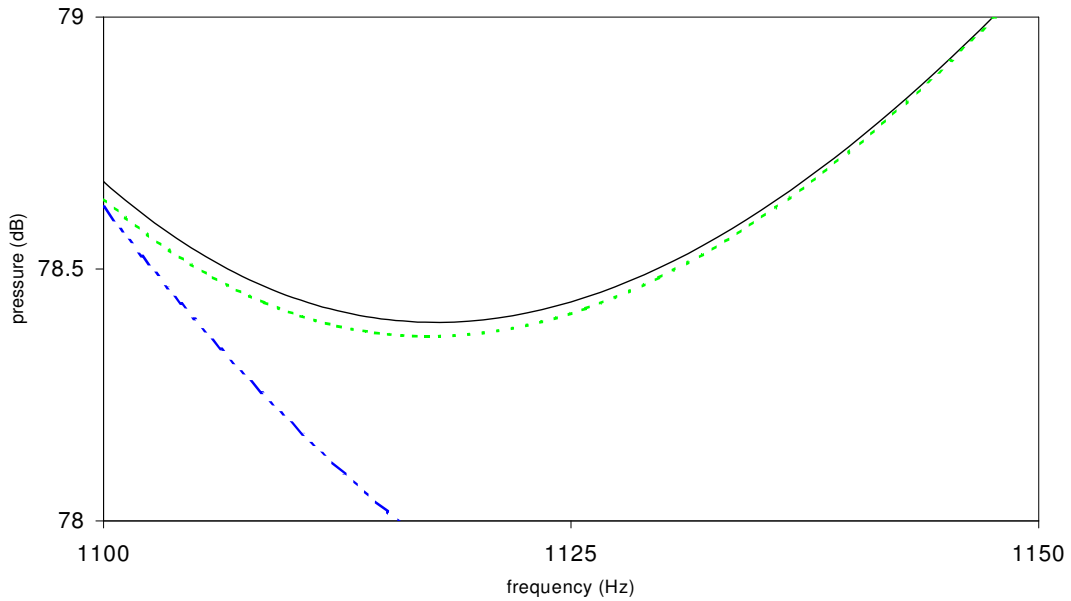

Figure 5. FRF for the real part of the pressure in the middle of the square and zoom

One can notice that I2M present a good behaviour when the frequency increases over the numerical description limit of the wave with linear FEM [2] i.e. $h=\lambda/\sqrt{12}$. For information the frequency corresponding to the classicalrule of the thumb for linear FEM [27] has also been plotted i.e. $h=\lambda/6$.

6.2. Bidimensional section of a car

The second numerical example deals with a real-life problem in order to show the efficiency of I2M in cases where the solutions are no more plane but common waves. The problem (figure 6a) is a 2D-section in the bodywork of a car [29]. The air inside the cabin is excited by the vibrations due to the engine through the front panel (Neumann boundary conditions). The roof is covered with an absorbent material (Robin boundary conditions). The acoustic response inside the car is studied at a frequency of 200 Hz with a discretization of 777 nodes (figure 6b). For this example, to solve the linear system (30), a QMR-type algorithm is used which is more suited for an efficient resolution.

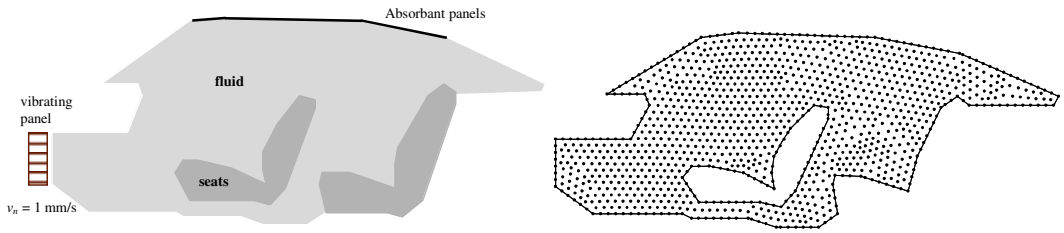

Figure 6. (a) Model problem (b) Distribution of nodes

6.2.1 Analysis of dispersion phenomenon. In order to analyse the behavior of I2M in relation to the dispersion phenomenon, four computations have been performed on this distribution of nodes: two classical *meshless* computations with linear basis and cubic basis, I2M with one iteration and a linear FEM computation. In order to compare the results, we use as reference a FEM solution on a highly refined mesh (17859 nodes).

Figure 8 presents of the three computations for the distribution of the real part of the acoustic pressure inside the car at a frequency of 200 Hz. The results are along the straight line defined in figure 7.

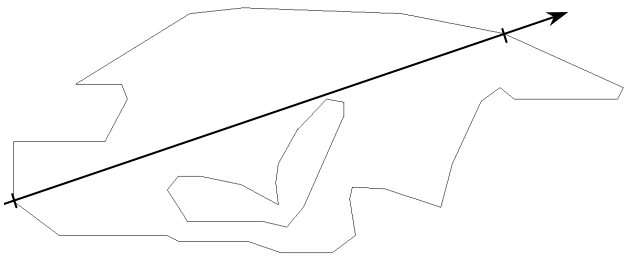

Figure 7. Definition of the straight line

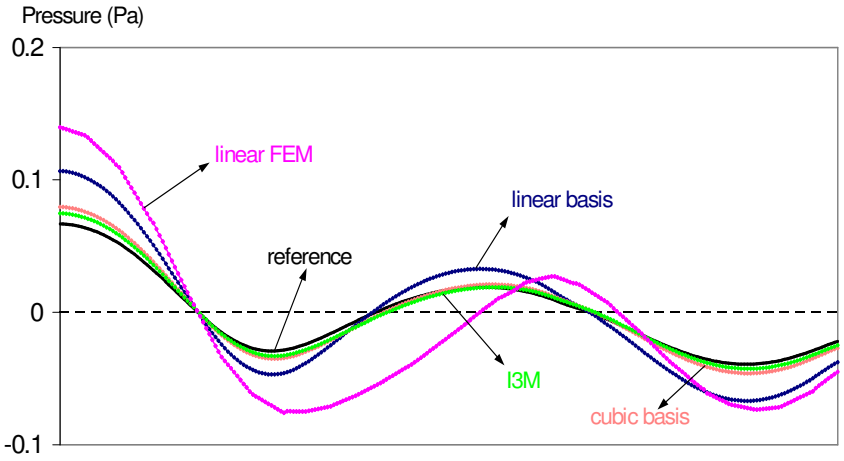

Figure 8. Real part of the pressure at 200 Hz along the straight line

First, one can immediately notice that the linear FEM result is subject to the dispersion whereas this phenomenon is hardly reduced by *meshless* computations.

Moreover, one can observe that the I2M solution is more close by the reference than the others i.e. I2M presents less pollution error with only one iteration. Nevertheless, the gain of accuracy between the cubic basis and the I2M seems to be not very significant in comparison with all the intermediate steps and computations to obtain an I2M solution. To justify the using of I2M, the computational time of I2M has to be analysed.

6.2.2 Computational time of I2M. Finally, the total computational time of the I2M solution (computational time of linear basis solution added to the computational time of the second solution with the new basis) is lower than the one of the cubic basis solution as illustrated on figure 9.

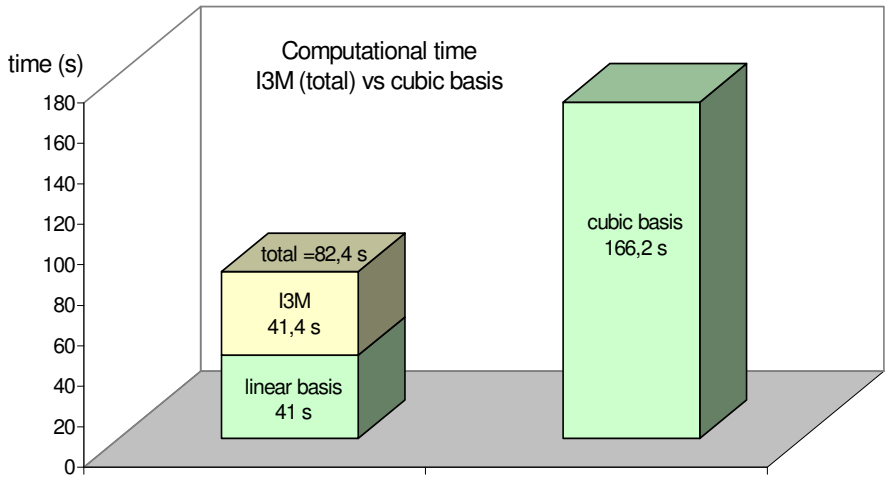

Figure 9. Comparison of the computational time between I3M and cubic basis

One can explain that fact by considering that we work with Lagrangian polynomial subspaces. Thus, the used cubic basis contains ten monomial terms whereas both linear basis and I2M-basis defined in (38) contain only three terms. Hence the domains of influence of the cubic basis method will be much more large than those of I2M to ensure the existence of the shape function matrix as mentioned in section 4.1. It implicates that the time needed to compute the stiffness and the mass matrices and to solve (30) (larger bandwidth) will be much more important for the cubic basis than the one of I2M.

On this example, I2M presents better performances in terms of accuracy and computational time than the classical polynomial *meshless* method.

7. CONCLUDING REMARKS

This paper has presented the research and the development of an iterative defect-correction type *meshless* method (I2M) to solve acoustic problems governed by the Helmholtz equation.

The idea of the I2M consists in introducing in the *meshless* basis the local phase of the wave which is an intrinsic property of this acoustic wave. The way to build this new basis can be extended to an iterative algorithm in order to compute more accurately the distribution of the phase and the pressure field.

The efficiency of I2M has been demonstrated on a square cavity model example and on a real-life case problem.

The first example has demonstrate that the iterative principle of the method is well-founded i.e. improvement of the solution with iteration. The FRF computed on this example has shown a very good behaviour of I2M when the frequency increases and a weak sensitivity to the first approximation of the pressure field needed to compute the distribution of the phase. Indeed, one can notice that the error on the first evaluation of the pressure field does not prevent to obtain a better approximation with the new basis.

The I2M presents very accurate solution in terms of dispersion and pollution error as presented by the bidimensional section of a car example. And, in terms of computational time, for a prescribed accuracy, I2M resolution is faster than classical *meshless* resolution using polynomial basis.

Finally, one must emphasize that the I2M can be easily extended to the resolution of 3D problems because it is only based on the fact that the acoustic pressure is a complex variable.

ACKNOWLEDGMENTS

The first author is supported by the Région Wallonne under grant SIVA and by the Commissariat général aux Relations internationales (CGRI – Communauté française de Belgique). Free Field Technologies (FFT) is gratefully acknowledged for its collaboration.

REFERENCES

[1] A. Deraemaeker, I. Babuška and Ph. Bouillard. 'Dispersion and pollution of the FEM solution for the Helmholtz equation in one, two and three dimensions'. *Int. j. numer. methods eng.* 1999; **46**: 471-500.
[2] Ph. Bouillard, *Méthodes de contrôle de la qualité de solutions éléments finis (application à l'acoustique)*, Thèse de doctorat, Service des Milieux Continus, Université Libre de Bruxelles, 1997.
[3] Ph. Bouillard, F. Ihlenburg. 'Error estimation and adaptivity for the finite element method in acoustics'. *Advances in Adaptive Computational Methods in Mechanics*. 1998; 477-492.
[4] F. Ihlenburg, I. Babuška. 'Dispersion analysis and error estimation of Galerkin Finite Element Methods for the Helmholtz equation'. *Int. j. numer. methods eng.* 1995; **38**: 3745-3774.
[5] O.C. Zienkiewicz. ,Achievements and some unsolved problems of the finite element method'. *Int. j. numer. methods eng.* 2000; **47**: 9-28.
[6] I. Harari, T.J.R. Hughes. 'Galerkin/least-squares finite element methods for the reduced wave equation with non-reflecting boundary conditions in unbounded domains'. *Comput. Methods Appl. Mech. Eng.* 1992; **98**(3): 411-454.
[7] I. Babuška, F. Ihlenburg, E. Paik. 'A Generalized Finite Element Method for solving the Helmholtz equation in two dimension with minimal pollution'. *Comput. Methods Appl. Mech. Eng.* 1995; **128**: 325-359.
[8] L. Franca, C. Farhat, A. Macedo. 'Residual-Free Bubbles for the Helmholtz equation'. *Int. j. numer. methods eng.* 1997; **40**: 4003-4009.
[9] A. Deraemaeker, I. Babuška and Ph. Bouillard. 'Dispersion and pollution of the FEM solution for the Helmholtz equation in one, two and three dimensions'. *Int. j. numer. methods eng.* 1999; **46**: 471-500.
[10] T.J.R. Hughes, 'Multiscale phenomena: Green's functions, the Dirichlet-to-Neumann formulation, subgrid-scale models, bubbles and the origins of stabilized methods'. *Comput. Methods Appl. Mech. Eng*. 1995; **l27**: 387-401.
[11] K. Gerdes and L. Demkowicz, 'Solution of the 3D Helmholtz equation in arbitrary exterior domains using hp-FEM and IFEM'. *Comput. Methods Appl. Mech. Eng.* 1996; **137**: 239-273.
[12] R. A. Uras, C. T. Chang, Y. Chen and W. K. Liu, 'Multiresolution Reproducing Kernel Particle Methods in Acoustics'. *Journal of Computational Acoustics*. 1997; **5**(1): 71-94.
[13] Th. E. Voth and Mark A. Christon, 'Discretization Errors Associated with Reproducing Kernel Methods: One-Dimensional Domains'. *Comput. Methods Appl. Mech. Eng.* 2001; **190**(18-19): 2429-2446.
[14] I. Babuška, J. Melenk. 'The partition of unity method'. *Int. j. numer. methods eng.* 1997; **40**: 727-758.
[15] E. Chadwick, P. Bettes. 'Modelling of progressive short waves using wave envelopes'. *Int. j. numer. methods eng.* 1997; **40**: 3229-3245.
[16] C. Farhat, I. Harari and L. P. Franca, 'A Discontinuous Finite Element Method for the Helmholtz Equation'. Proceedings of the European Congress on Computational Methods in Applied Sciences and Engineering (ECCOMAS) 2000, Barcelona, Spain, September 11-14 (2000).
[17] S. Suleau and Ph. Bouillard. '1D Dispersion analysis for the element-free Galerkin method for the Helmholtz equation'. *Int. j. numer. methods eng.* **47**: 1169-1188, 2000.
[18] S. Suleau, A. Deraemaeker and Ph. Bouillard. 'Dispersion and pollution of meshless solutions for the Helmholtz equation'. *Comput. Methods Appl. Mech. Eng,* 2000; **190**: 639-657.
[19] P. Lancaster and K. Salkausas. 'Surfaces generated by moving least squares methods'. *Math. Comput.* 1981; **37**: 141-158.
[20] B. Nayroles, G. Touzot and P. Villon, 'Generalizing the FEM : diffuse approximation and diffuse elements', *Comp. Mech.* 1992; **10**: 307-318.
[21] T. Belytschko, Y. Y. Lu and L. Gu, 'Element-Free Galerkin Methods', *Int. j. numer. methods eng.*, 1994; **37**: 229-256.
[22] T. Belytschko, Y. Krongauz, D. Organ, M. Fleming and P. Krysl, 'Meshless methods: An overview and recent developments', *Comput. Methods Appl. Mech. Eng.* 1996; **139**: 3-47.
[23] St. Suleau and Ph. Bouillard, 'Accurate acoustic computations using a meshless method', *Comp. Assist. Mech. and Eng. Sc.* 2001; **8**: 445-468.
[24] I. Kaljevic and S. Saigal, 'An Improved Element Free Galerkin Formulation', *Int. j. numer. methods eng.*, 1997; **40**: 2953-2974.
[25] Y. Krongauz and T. Belytschko, 'Enforcement of essential boundary conditions in meshless approximations using finite elements'. *Comput. Methods Appl. Mech. Eng.* 1996; **131**: 133-145.
[26] Ph. Bouillard, S. Suleau. 'Element-Free Galerkin solutions for Helmholtz problems: formulation and numerical assessment of the pollution effect'. *Comput. Methods Appl. Mech. Eng.* 1998; **162**: 317-335.
[27] SYSNOISE User manual, LMS INTERNATIONAL, Researchpark Z1, Interleuvenlaan, 68, 3001 Leuven, Belgium
[28] V. Lacroix, Ph. Bouillard and P. Villon, 'Iterative multilevel meshless method for acoustics'. Proceedings of the Sixth U.S. National Congress on Computational Mechanics (USNCCM) 2001, Dearborn, Michigan, USA, August 1-4 (2001).
[29] D. J. Nefske, 'Sound in small enclosures'. In L. Beranek and I. Vér (Editors), *Noise and Vibration Control Engineering. Principles and Applications*, 1st edition, J. Wiley & Sons, ISBN 0-471-61751-2, London, 1992.

[30] A. Brandt and I. Livshits. 'Wave-ray multigrid method for standjng wave equation'. *Electronic Trans. Num. An.* 1997; **6**: 162-181.